THE UNIVERSITY OF QUEENSLAND

DEPARTMENT OF CIVIL ENGINEERING

REPORT CH54/04

A STUDY OF DAM BREAK WAVE OF THIXOTROPIC FLUID: BENTONITE SURGES DOWN AN INCLINED PLANE

AUTHORS: H. CHANSON, P. COUSSOT, S. JARNY, L. TOQUER

A STUDY OF DAM BREAK WAVE OF THIXOTROPIC FLUID: BENTONITE SURGES DOWN AN INCLINED PLANE

by

Hubert CHANSON
Dept of Civil Engineering, The University of Queensland, Brisbane QLD 4072, Australia
Email: h.chanson@uq.edu.au
Url : http://www.uq.edu.au/~e2hchans/

Philippe COUSSOT, Sébastien JARNY and Laurent TOCQUER
Laboratoire des Matériaux et Structures du Génie Civil, Unité Mixte de Recherche (LCPC-ENPC-CNRS), 2 allée Kepler, 77420 Champs-sur-Marne, France
Email: philippe.coussot@lcpc.fr

REPORT No. CH 54/04
ISBN 1864997710
Department of Civil Engineering, The University of Queensland
June, 2004

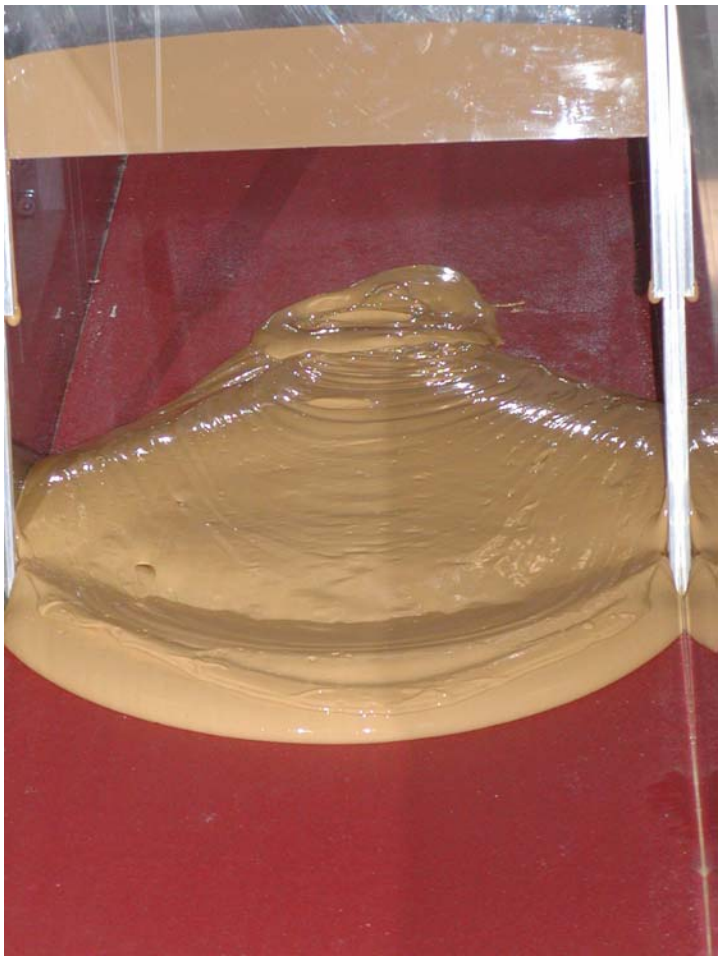

Dam break wave of bentonite suspension (17% mass concentration) down 15º slope

ABSTRACT

Thixotropic fluids are commonly used in the construction industry (e.g. liquid cements, liquid concrete, drilling fluids), industrial applications (e.g. muds, paints) and the food industry (e.g. liquid dairy products, ketchup). Related applications include some forms of mud flows and debris flows, pasty sewage sludges and some wastewater treatment residues. Thixotropy is the characteristic of a fluid to form a gelled structure over time when it is not subjected to shearing and to liquefy when agitated. A thixotropic fluid is a non-Newtonian fluid with a viscosity that is a function of both shear rate $\partial V/\partial y$ and instantaneous state(s) of structure of the material. Such a fluid exhibits a reversible time-dependent decrease in apparent viscosity under shear rate and a gradual recovery when the shear stress is removed. This report describes a basic study of dam break wave with thixotropic fluid. A dam break wave is a sudden release of a mass of fluid in a channel. This type of flows has not been studied to date with thixotropic fluid, despite its practical applications : e.g., mudflow release, concrete tests including L-Box and J-Ring for self-consolidating concrete testing, paint applications.

Theoretical considerations were developed based upon a kinematic wave approximation of the Saint-Venant equations for a thixotropic fluid down a prismatic sloping channel. The thixotropic fluid model of COUSSOT et al. (2002a) was used since it describes the instantaneous state of fluid structure by a single parameter. The analytical solution of the basic flow motion and rheology equations predict three basic flow regimes depending upon the fluid properties and flow conditions, including the initial degree of jamming of the fluid : (1) a short motion with relatively-rapid flow stoppage for relatively small mass of fluid, (2) a fast flow motion for a large mass of fluid, or (3) an intermediate motion initially rapid before final fluid stoppage for intermediate mass of fluid and intermediate initial rest period T_o. Physical experiments were performed with bentonite suspensions. Systematic experiments showed four types of flows. For small bentonite mass concentrations and short relaxation times T_o, the fluid flowed rapidly down the slope and spilled into the overflow container (Flow Type I). For intermediate concentrations and rest periods, the suspension flowed rapidly initially, decelerated relatively suddenly, continued to flow slowly for sometimes before complete stoppage (Flow Type II). For large mass concentrations and long rest periods, the mass of fluid stretched down the slope, until the head separated from the tail (Flow Type III). The last flow pattern (Type IV) corresponded to an absence of flow for large bentonite concentrations and long rest times. Quantitative informations were documented in terms of the final fluid thickness, wave front position, wave front curvature, side profile of the wave front during motion and after stoppage, as well as the flow motion immediately after gate opening. Some free-surface instabilities are also discussed and illustrated.

It is believed that the present study is the first theoretical analysis combining successfully the basic principles of unsteady flow motion (i.e. Saint-Venant equations) with a thixotropic fluid model, which was validated with large-size systematic laboratory experiments. It is the belief of the writers that, for such complex systems this kind of approach, combining both rheology and fluid dynamics, is necessary to gain new insights of these complicated flow motions.

RÉSUMÉ

Les fluides thixotropes sont couramment utilisés dans le génie civil (bétons frais, pâtes de ciment liquides, boues de forage), ou d'autres industries (argiles, peintures, ketchup, mayonnaise, etc). On trouve également de tels fluides dans l'environnement : laves torrentielles, boues résiduaires. La thixotropie est la propriété qu'on certains fluides à se "gélifier" au repos et à se liquéfier en cours d'écoulement. Ces évolutions de la viscosité apparente sont réversibles. Ce rapport décrit une étude de la rupture d'un barrage contenant un fluide thixotrope. En dépit de son intérêt pratique

(glissement de terrain boueux, mise en oeuvre du béton, tests rhéométriques pratiques pour le béton (L-box, J-Ring), étalement des peintures, ce type d'étude n'a jamais été réalisée.
Des considérations théoriques ont été développées dans le cadre de l'approximation des longues ondes pour les équations de St-Venant appliquées à un fluide thixotrope en écoulement dans un canal incliné prismatique. Le modèle de comportement thixotrope proposé par COUSSOT et al. (2002a) est utilisé pour décrire les évolutions de l'état du matériau au cours du temps, avec l'aide d'un seul paramètre. La solution analytique du système d'équations prédit trois régimes d'écoulements fondamentaux selon les caractéristiques du fluide et les conditions d'écoulement, en particulier le degré de restructuration initial du matériau : (1) faible déplacement et arrêt rapide pour une masse de fluide relativement petite, (2) mouvement rapide pour une masse de fluide importante, ou (3) mouvement intermédiaire initialement rapide puis arrêt pour une masse de fluide et un temps de restructuration intermédiaire. Des expériences ont été réalisées, en plus, avec des suspensions de bentonite. Quatre régimes d'écoulement sont apparus. Aux faibles concentrations solides et temps de restructuration (repos initial avant la rupture du barrage), le fluide coule rapidement et sort du canal à l'aval. Pour des concentrations et des temps de repos intermédiaires, le fluide coule rapidement au début puis décélère rapidement, continue de couler lentement puis s'arrête complètement. Pour des concentrations fortes et des temps de repos longs, le fluide s'étire sur le canal jusqu'à ce que le front se détache du reste du fluide. Dans le quatrième régime le fluide ne s'écoule pas du tout. Des informations quantitatives ont été obtenues concernant l'épaisseur finale, la position du front, la courbure du front, le profil de coté en cours d'écoulement et après l'arrêt, ainsi que pour l'écoulement juste après l'ouverture de la porte. Des instabilités de l'écoulement ont également été observées et discutées.
La présente étude constitue la première analyse théorique combinant les principes de base pour décrire les écoulements transitoires avec un fluide thixotrope, et des expériences systématiques à grande échelle. Ces approches complémentaires semblent nécessaires pour progresser dans la compréhension de ces systèmes complexes.

TABLE OF CONTENTS

NOTATION

The following symbols are used in this report :

A	flow cross-section area (m^2);
B	free-surface width (m);
C	celerity (m/s) of a small disturbance for an observer travelling with the flow;
C_m	bentonite mass concentration;
C_S	wave front celerity (m/s);
$(C_S)_{max}$	maximum shock celerity (m/s);
D_H	hydraulic diameter : $D_H = 4*A/P_W$;
d	flow depth (m) measured normal to the invert;
d_s	dam break wave front thickness (m);
d_o	initial reservoir height (m) measured normal to the chute invert;
f	Darcy-Weisbach friction factor;
g	gravity constant (m/s^2); g = 9.81 m/s^2;
H_{dam}	vertical reservoir height (m) at the gate;
h_c	characteristic fluid thickness (m) (paragraph 2);
L	reservoir length (m);
M	initial mass of fluid (kg)
m, n	exponents;
P	pressure (Pa);
P_W	wetted perimeter (m);
Q	volume flow rate (m^3/s);
S_f	friction slope;
S_o	bed slope : $S_o = \sin\theta_b$;
t	time (s);
t_c	characteristic time (s);
t_{max}	instant (s) at which the shock celerity is maximum : $C_S(t=t_{max}) = (C_S)_{max}$;
T	characteristic time (s) when the initial characteristic C2 reaches the reservoir upstream end;
T_o	fluid rest time (s);
U	free-stream celerity (m/s) (paragraph 3);
u, v	integration parameters;
V	velocity (m/s);
V_H	uniform equilibrium flow velocity (m/s) for a water depth H_{dam};
V_x	velocity component (m/s) in the x-direction;
W	channel width (m);
X	relative longitudinal position (m) : $X = X_S - x$;
X_S	wave front position (m);
$(X_S)_{end}$	wave front position (m) at the end of experiment (i.e. after stoppage);
x	longitudinal distance (m) measured from the gate;
y	distance (m) normal to the invert;
Z	transverse distance (m) measured from the centreline;
z	vertical coordinate (m);

Greek symbols

α	characteristic time of evolution of the fluid structure, assumed constant for a given fluid;
λ	degree of jamming of the thixotropic fluid;
λ_c	characteristic degree of jamming of the fluid;
λ_1, λ_2	characteristic degrees of jamming of the fluid;
λ_o	initial degree of jamming of the fluid;

μ	1- dynamic viscosity (Pa.s); 2- apparent viscosity (Pa/s);
μ'	Herschel-Bulkley fluid parameter (Pa.s);
μ_o	characteristic viscosity (Pa.s) of destructured thixotropic fluid;
ν	kinematic viscosity (m^2/s) : $\nu = \mu/\rho$;
π	$\pi = 3.14159265358979323846264 3$;
θ	characteristic restructuration time (s);
θ_b	bed slope angle;
ρ	fluid density (kg/m^3);
ρ_b	bentonite density (kg/m^3);
ρ_s	bentonite suspension density (kg/m^3);
ρ_w	water density (kg/m^3);
τ	shear stress (Pa);
τ_c	1- yield stress (Pa); 2- critical shear stress (Pa);
τ_o	boundary shear stress (Pa);

Abbreviations

D/S (or d/s)	downstream;
U/S (or u/s)	upstream;

Notation

$\frac{D}{Dt}$	absolute differential;
$\frac{\partial}{\partial y}$	partial differentiation with respect to y.

ABOUT THE CONTRIBUTORS

HUBERT CHANSON

Hubert Chanson received a degree of 'Ingénieur Hydraulicien' from the Ecole Nationale Supérieure d'Hydraulique et de Mécanique de Grenoble (France) in 1983 and a degree of 'Ingénieur Génie Atomique' from the 'Institut National des Sciences et Techniques Nucléaires' in 1984. He worked for the industry in France as a R&D engineer at the Atomic Energy Commission from 1984 to 1986, and as a computer professional in fluid mechanics for Thomson-CSF between 1989 and 1990. From 1986 to 1988, he studied at the University of Canterbury (New Zealand) as part of a Ph.D. project. He was awarded a Doctor of Engineering from the University of Queensland in 1999 for outstanding research achievements in gas-liquid bubbly flows. In 2003, the International Association for Hydraulic engineering and Research (IAHR) presented him the 13th Arthur Ippen award for outstanding achievements in hydraulic engineering.

Hubert Chanson is a Reader in environmental fluid mechanics and water engineering at the University of Queensland since 1990. His research interests include design of hydraulic structures, experimental investigations of two-phase flows, coastal hydrodynamics, water quality modelling, environmental management and natural resources. He is the author of six books : "Hydraulic Design of Stepped Cascades, Channels, Weirs and Spillways" (*Pergamon*, 1995), "Air Bubble Entrainment in Free-Surface Turbulent Shear Flows" (*Academic Press*, 1997), "The Hydraulics of Open Channel Flows : An Introduction" (*Butterworth-Heinemann*, 1999; *Elsevier*, 2004), "The Hydraulics of Stepped Chutes and Spillways" (*Balkema*, 2001) and "Environmental Hydraulics of Open Channel Flows" (*Elsevier*, 2004). He further co-authored the book "Fluid Mechanics for Ecologists" (*IPC Press*, 2002). His textbook "The Hydraulics of Open Channel Flows : An Introduction" has already been translated into Chinese (*Hydrology Bureau of Yellow River Conservancy Committee*) and Spanish (*McGraw Hill Interamericana*), and it was re-edited in 2004 (*Elsevier*, 2nd edition, 2004). His publication record includes over 250 international refereed papers and his work was cited over 1,000 times since 1990. Hubert Chanson has been active also as consultant for both governmental agencies and private organisations.

He has been awarded six fellowships from the Australian Academy of Science. In 1995 he was a Visiting Associate Professor at National Cheng Kung University (Taiwan R.O.C.). He was Visiting Research Fellow at Toyohashi University of Technology (Japan) in 1999 and 2001. In 2004, he was a Visiting Professorial Fellow at Université de Bretagne Occidentale (France), and a Visiting Research Fellow at Laboratoire Central des Ponts et Chaussées (France) and at McGill University (Canada).

Hubert Chanson was invited to deliver keynote lectures at the 1998 ASME Fluids Engineering Symposium on Flow Aeration (Washington DC), at the Workshop on Flow Characteristics around Hydraulic Structures (Nihon University, Japan 1998), at the first International Conference of the International Federation for Environmental Management System IFEMS'01 (Tsurugi, Japan 2001), at the 6th International Conference on Civil Engineering (Isfahan, Iran 2003), at the 2003 IAHR Biennial Congress (Thessaloniki, Greece), at the International Conference on Hydraulic Design of Dams and River Structures HDRS'04 (Tehran, Iran 2004) and at the 9th International Symposium on River Sedimentation (Yichang, China 2004). He gave an invited lecture at the International Workshop on Hydraulics of Stepped Spillways (ETH-Zürich, 2000) and at the 2001 IAHR Biennial Congress (Beijing, China). He lectured several short courses in Australia and overseas (e.g. Taiwan, Japan, Italy).

His Internet home page is http://www.uq.edu.au/~e2hchans. He also developed a gallery of photographs website {http://www.uq.edu.au/~e2hchans/photo.html}.

PHILIPPE COUSSOT

Philippe COUSSOT graduated from Ecole Polytechnique (France) in 1987 and from the Ecole Nationale du Génie Rural des Eaux et Forêts (ENGREF) in 1989. He obtained a Ph.D. from the University of Grenoble (France) in 1992.

He was the MRI project manager at the Laboratory of Materials and Structures for Civil Engineering (L.M.S.G.C.) in Marne la Vallée from 1996 to 2001. He was Scientific Head of research on natural hazards at Laboratoire Central des Ponts et Chaussées (L.C.P.C.), and Researcher at L.M.S.G.C. between 2001 and 2002. Since he is the Head of the Laboratoire des Matériaux et Structures en Génie Civil (L.M.S.G.C.). The L.M.S.G.C. is a joint research laboratory between the Laboratoire Central des Ponts de Chaussées (L.C.P.C.) and the Centre National de la Recherche Scientifique (C.N.R.S.), based at Champs-sur-Marne (France).

Philippe COUSSOT's research interests include rheophysics and rheometry of pastes (suspensions, granular materials, foams, emulsions, etc), physics of drying, Saffman-Taylor instability in yield stress fluids, and mudflows and debris flows. His publication record includes 6 books, a video-documentary, over 90 journal articles and more than 70 international refereed conference papers.

He was awarded the Henri Milon award of the French Society of Hydraulics (SHF) in 1994 for his outstanding Ph.D. thesis work, the Schoemaker award from the International Association of Hydraulic engineering and Research (I.A.H.R.) for the most outstanding paper in Journal of Hydraulic Research from 1994 to 1996, and the Roberval award (special mention) for his remarkable educational book in French language ("Understanding Rheology - From Blood Circulation to Concrete Hardening", *EDP Sciences* co-edited by J.L. GROSSIORD, 2002). He is the president of the French Society of Rheology, an associate-editor of the Journal of Hydraulic Engineering, American Society of Civil Engineers, the founder and editor-in-chief of the Journal of the French Society of Rheology "Rhéologie" and member of the Editorial Board of Applied Rheology. His email address is {mailto:philippe.coussot@lcpc.fr}.

SÉBASTIEN JARNY

Sébastien JARNY graduated from the University of Poitiers, France. He is currently a Ph.D. student at the Laboratoire des Matériaux et Structures du Génie Civil (L.M.S.G.C.), Champs-sur-Marne (France).

LAURENT TOCQUER

Laurent TOCQUER graduated from the University of Toulon, France. He is currently a research officer at the Laboratoire des Matériaux et Structures du Génie Civil (L.M.S.G.C.), Champs-sur-Marne (France).

1. INTRODUCTION

1.1 PRESENTATION

Thixotropic fluids are commonly used in the construction industry for drilling and tunnelling : e.g., liquid cements, drilling fluids, muds (e.g. BESQ 2000) (Fig. 1-1). Other industrial applications include liquid concrete, some paints, the food industry (e.g. liquid dairy products, ketchup) and clay-water mixtures used by the beauty industry for skin treatment. Related applications cover some forms of mud flows and debris flows, pasty sewage sludges and some wastewater treatment residues (e.g. COUSSOT 1997, TABUTEAU et al. 2004) (Fig. 1-1).

Thixotropy is the characteristic of a fluid to form a gelled structure over time when it is not subjected to shearing and to liquefy when agitated. A thixotropic fluid is a non-Newtonian fluid with generally exhibits an apparent yield stress, and an apparent viscosity that is a function of both the shear intensity and the current state(s) of structure of the material, sometimes also called degree(s) of jamming of the fluid, where V is the velocity and y is the distance normal to the flow direction. The apparent viscosity of a thixotropic fluid changes with time under constant shear rate until reaching equilibrium. In other words, such fluids exhibit a reversible time-dependent decrease in apparent viscosity under shear rate and a gradual recovery when the shear stress is removed.

Fig. 1-1 - Examples of thixotropic fluid flows and applications
(A) Flow of self-compacting concrete (S.C.C.)
(A1) Initial installation (Courtesy of Dr Nicolas ROUSSEL) - Flow from top left to bottom right

(A2) The thixotropic nature of modern concrete is illustrated by the localisation of fluid flow in the centre of the photograph, while concrete appears gelled elsewhere (Courtesy of Dr Nicolas ROUSSEL) - Flow from bottom foreground to top background

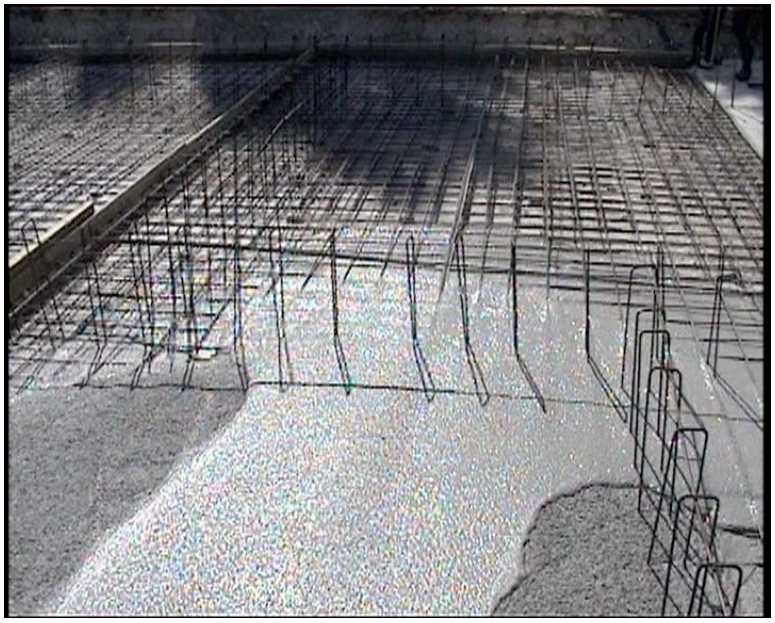

(B) Dry sewage sludges with a solid content about 20% in weight (Courtesy of Dr Bill CLARKE)

(C) Debris flow control structure along Ruisseau Saint Bernard, Saint-Martin-de-la-Porte, in Vallée de la Maurienne (France) on 11 Feb. 2004 - Slit check dam in foreground and sediment retention basin behind - Note that the upstream concrete walls were reinforced by thick steel plates

(D) River training on Ravin de Saint Julien, Saint-Julien-Mont-Denis, Vallée de la Maurienne (France) on 11 Feb. 2004 - Note the slit check dam in background

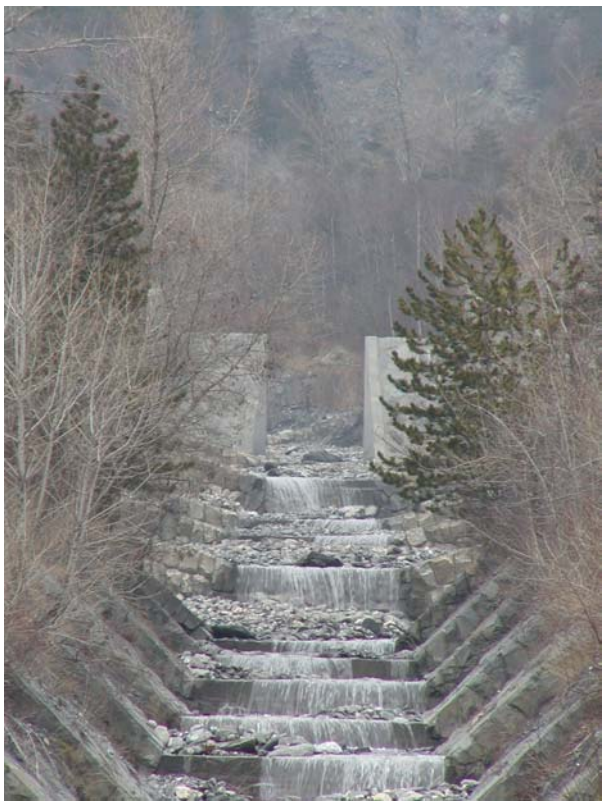

1.2 FLUID RHEOLOGY

For a Newtonian fluid (e.g. clear-water, liquid honey), the shear stress acting in a direction (e.g. x-direction) is proportional to the velocity gradient in the normal direction (e.g. y-direction). For a laminar flow, this gives Newton's law of viscosity which postulates that, for the straight parallel motion of a given fluid, the tangential stress between two adjacent layers of fluid equals :

$$\tau = \mu * \frac{\partial V}{\partial y} \qquad (1\text{-}1)$$

where τ is the shear stress, μ is the dynamic viscosity of the fluid, V is the velocity and y is the direction perpendicular to the fluid motion. Fluids that obey Newton's law of viscosity are called Newtonian fluids.

For homogenous suspension of fine particles, the constitutive law of the fluid becomes :

$$\tau = \tau_c + \mu * \frac{\partial V}{\partial y} \qquad (1\text{-}2)$$

where μ is the apparent viscosity of the fluid mixture and τ_c is a constant called the yield stress. Fluids satisfying Equation (1-2) are called Bingham plastic fluids. They are non-Newtonian fluids since they do not satisfy Equation (1-1). The Bingham plastic model is well suited to some sediment-laden flows with large concentrations of fine particles (e.g. WAN and WANG 1994, JULIEN 1995). A more advanced rheological model is the Herschel-Bulkley fluid. The relationship between shear stress and shear rate is assumed to be :

$$\tau = \tau_c + \mu' * \left(\frac{\partial V}{\partial y}\right)^m \qquad (1\text{-}3)$$

where $0 < m \leq 1$ (e.g. HUANG and GARCIA 1998, WILSON and BURGESS 1998). For $m = 1$, Equation (1-3) yields the Bingham fluid behaviour and μ' is a material parameter.

Various models have been proposed to describe the behaviour of thixotropic fluids (e.g. MEWIS 1979, USUI 1995, TOORMAN 1997). Most have a similar structure consisting of an apparent viscosity function of the shear rate $\partial V/\partial y$ and of some structure parameter(s) associated with some kinetic equation(s) giving the time evolution of the(se) structure parameter(s) as function(s) of time and shear rate.

1.3 THE RHEOLOGICAL MODEL

COUSSOT et al. (2002a) proposed a simple model to describe the rheological properties of a thixotropic fluid:

$$\mu = \mu_o * (1 + \lambda^n) \qquad (1\text{-}4)$$

$$\frac{\partial \lambda}{\partial t} = \frac{1}{\theta} - \alpha * \frac{\partial V}{\partial y} * \lambda \qquad (1\text{-}5)$$

where V is the velocity, y is the distance normal to the flow direction, μ_o, n, θ and α are four constant parameters for a given fluid, and μ is the apparent viscosity of the thixotropic fluid defined as :

$$\mu = \frac{\tau}{\frac{\partial V}{\partial y}} \qquad (1\text{-}6)$$

with τ being the shear stress. In Equations (1-4) and (1-5), it is assumed that the degree of jamming of the thixotropic fluid can be represented by a single parameter λ which describes the instantaneous state of fluid structure. λ is also called the degree of jamming of the fluid. This single parameter could represent the degree of flocculation of clays, a measure of free energy landscape

for glasses or the fraction of particles in potential wells for colloidal suspensions (COUSSOT et al. 2002a).
For a fluid at rest ($\partial V/\partial y = 0$), the rheological model (Eq. (1-4) & (1-5)) gives an increase in degree of jamming λ at a constant rate $1/\theta$, where θ is the characteristic time of evolution of the fluid structure. Under shear ($\partial V/\partial y > 0$), the rate of decrease of λ is proportional to both shear rate $\partial V/\partial y$ and degree of jamming λ. At the limit, when the fluid structure is completely destroyed ($\lambda \rightarrow 0$), the viscosity μ tends to an asymptotic value μ_o.
One advantage of this model is that flow simulations do not require the determination of a solid-liquid limit like other yield stress models. This simple model is capable to predict qualitatively the trends of fluid behaviours, as well as quantitative properties under steady and unsteady states (ROUSSEL et al. 2004). It has been successfully applied to a wide range of thixotropic fluid situations (e.g. TABUTEAU et al. 2004, FERROIR et al. 2004).

Discussion

In Equations (1-4) and (1-5), the apparent viscosity μ is a function of the rate of change of the degree of jamming $\partial\lambda/\partial t$ and of the initial conditions : e.g., the initial degree of jamming $\lambda_o = \lambda(t=0)$. For a constant shear stress τ, the variations in viscosity are driven by the relative values of the two terms on the right handside of Equation (1-5). For $n > 0$, the viscosity tends either to infinity or to a small asymptotic value μ_o depending upon the shear stress τ being larger or smaller than a critical value τ_c defined as:

$$\tau_c = \frac{\mu_o * (1 + \lambda_o^n)}{\alpha * \lambda_o * \theta} \qquad (1\text{-}7)$$

where λ_o is the initial degree of jamming. (For $\tau > \tau_c$, the apparent viscosity μ tends to μ_o.) While the model of COUSSOT et al. (2002a) did not introduce explicitly a yield stress, the critical shear stress τ_c (Eq. (1-7)) may be seen as an apparent yield stress. In particular, its increase with the time of rest well agrees with current observations of yielding of thixotropic pastes.

1.4 STRUCTURE OF THE REPORT

This report describes a basic study of dam break wave with thixotropic fluid. A dam break wave is a sudden release of a mass of fluid in a channel. This type of flows has not been studied to date with thixotropic fluid, despite its practical applications : e.g., mudflow release, concrete tests, including L-Box and J-Ring for self-consolidating concrete testing, paint applications. Basically, this project is a study of highly-unsteady open channel flow of thixotropic fluid under controlled conditions. The results will show that the thixotropic nature of the flow has a strong influence on the flow motion, while the fluid properties are closely linked with the instantaneous flow conditions. In the next section, one-dimensional equations are developed yielding analytical solutions of the problem. In section 3, the two-dimensional flow motion at the shock front are discussed. Section 4 introduces new experimental works, and the results are presented in sections 5, 6 and 7.

2. THEORETICAL ANALYSIS (1) DAM BREAK WAVE

A dam break wave is the flow resulting from a sudden release of a mass of fluid in a channel. In this section, the basic equations for unsteady open channel flow are first described. Then these equations are applied to a turbulent dam break wave down a sloping channel with Newtonian fluids. Later, the theory is extended to thixotropic fluids and a complete solution dam break wave of thixotropic is presented.

2.1 BASIC UNSTEADY OPEN CHANNEL FLOW EQUATIONS

In unsteady open channel flows, the velocities and fluid depths change with time and longitudinal position. For one-dimensional applications, basic unsteady open channel flow equations, called Saint-Venant equations, may be developed. The basic assumptions of the development are : [H1] the flow is one-dimensional, [H2] the streamline curvature is very small and the pressure distributions are hydrostatic, [H3] the flow resistance are the same as for a steady uniform flow for the same depth and velocity, [H4] the bed slope is small enough to satisfy : $\cos\theta_b \approx 1$ and $\sin\theta_b \approx \tan\theta$; [H5] the water density is a constant; and [H6] sediment transport is neglected. With these basic hypotheses, the flow can be characterised at any point and any time by two variables: e.g., Q and d, where Q is the volume flow rate and d is the flow depth; or V and d, where V is the flow velocity.

The unsteady flow properties are described by a system of two partial differential equations :

$$\frac{\partial A}{\partial t} + \frac{\partial Q}{\partial x} = 0 \qquad \text{Continuity equation (2-1)}$$

$$\frac{1}{g} * \left(\frac{\partial V}{\partial t} + V * \frac{\partial V}{\partial x} \right) + \frac{\partial d}{\partial x} + S_f - S_o = 0 \qquad \text{Dynamic equation (2-2)}$$

where A is the cross-section area, t is the time, V is the flow velocity, S_o is the bed slope ($S_o = \sin\theta_b$), S_f is the friction slope and x is the longitudinal distance.

The Saint-Venant equations (Eq. (2-1) & (2-2)) may be transformed to yield a characteristic system of equations :

$$\frac{D}{Dt}(V + 2 * C) = - g * (S_f - S_o) \qquad \text{forward characteristic}$$

$$\frac{D}{Dt}(V - 2 * C) = - g * (S_f - S_o) \qquad \text{backward characteristic}$$

along :

$$\frac{dx}{dt} = V + C \qquad \text{forward characteristic C1}$$

$$\frac{dx}{dt} = V - C \qquad \text{backward characteristic C2}$$

where C is celerity of a small disturbance for an observer travelling with the flow: $C = \sqrt{g*d}$ (e.g. HENDERSON 1966, MONTES 1988, CHANSON 2004a,b).

Simplification of the dynamic wave equation

In the general case of unsteady flows, the dynamic equation (Eq. (2-2)) may be simplified under some conditions, if the acceleration term $\partial V/\partial t$ and the inertial term $V*\partial V/\partial x$ become small. For example, during a river flood, when the flow velocity increases from 1 to 2 m/s in three hours (i.e. a rapid variation), the dimensionless acceleration term $1/g*\partial V/\partial x$ equals 9.4 E-6; when the velocity increases from 1.0 m/s to 1.4 m/s along a 10 km reach (e.g. reduction in channel width), the longitudinal slope of the kinetic energy line $1/g*V*\partial V/\partial x$ is equals to 4.9 E-6. For comparison, the

average bed slope S_o of the Rhône river between Lyon and Avignon is about 0.7 E-3 and the friction slope is of the same order of magnitude. Basically, the dynamic equation may be simplified when one or more terms become negligible.
In a kinematic wave model, the differential form of the Saint-Venant equations is simplified as :

$$B * \frac{\partial d}{\partial t} + \frac{\partial Q}{\partial x} = 0 \qquad \text{Continuity equation (2-3)}$$

$$S_f - S_o = 0 \qquad \text{Kinematic wave equation (2-4)}$$

where B is the free-surface width. That is, the acceleration and inertial terms are neglected in the dynamic wave equation, and the free-surface is assumed parallel to the channel bottom (CHANSON 2004a,b). The kinematic wave equation may be rewritten as :

$$V = \sqrt{\frac{8 * g}{f}} * \sqrt{\frac{D_H}{4}} * \sqrt{S_o} \qquad (2\text{-}5)$$

where f is the Darcy-Weisbach friction factor, and D_H is the hydraulic diameter ([1]). Equation (2-5) expresses an unique relationship between the velocity V and the water depth d, hence the cross-section area at a given location x by continuity.
Note that the boundary shear stress is defined as :

$$\tau_o = \frac{f}{8} * \rho * V^2 \qquad (2\text{-}6)$$

where ρ is the fluid density. The friction slope S_f equals :

$$S_f = \frac{4 * \tau_o}{\rho * g * D_H} \qquad (2\text{-}7)$$

Application to a dam break wave in an initially-dry channel is developed in Appendix A.

Fig. 2-1 - Dam break wave down a sloping channel
(A) Definition sketch

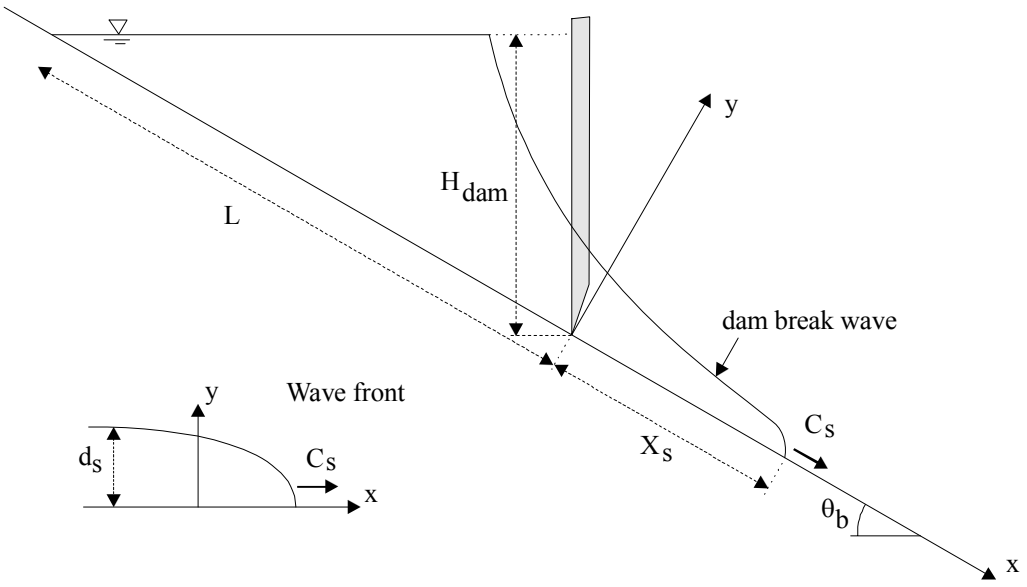

[1]For a wide rectangular channel, the hydraulic diameter or equivalent pipe diameter equals : D_H = 4*d where d is the flow depth.

(B) Characteristics and dam break wave front path in the (x, t) plane

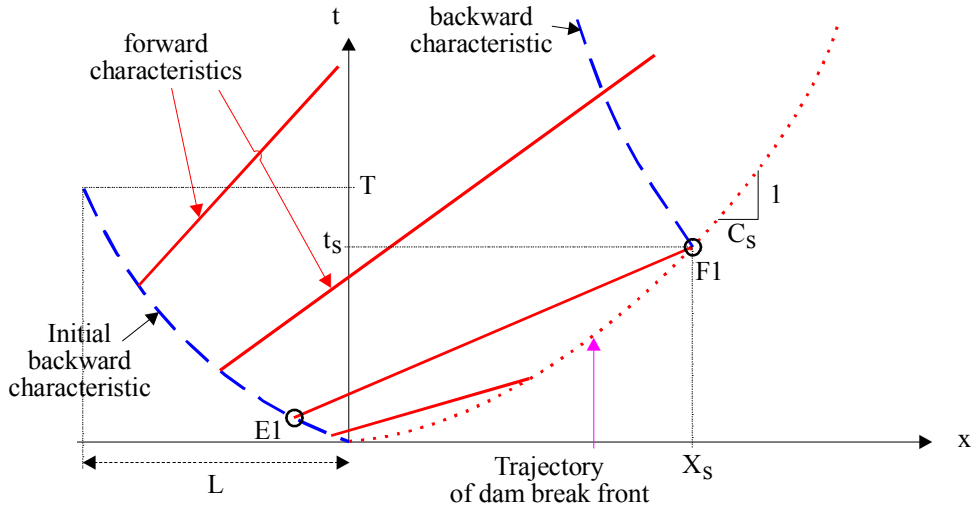

2.2 DAM BREAK WAVE DOWN A SLOPING CHANNEL

2.2.1 Basic equations

The above equations may be applied to a turbulent dam break wave down a sloping, prismatic, two-dimensional channel (Fig. 2-1). HUNT (1982) developed a complete kinematic wave solution for which the basic equations are :

$$\frac{\partial d}{\partial t} + \frac{\partial (V * d)}{\partial x} = 0 \qquad \text{Continuity equation (2-3)}$$

$$S_f = S_o \qquad \text{Kinematic wave equation (2-4)}$$

For a wide rectangular channel, the combination of the continuity and momentum equations yields :

$$\frac{\partial d}{\partial t} + \frac{3}{2} * \sqrt{\frac{8 * g}{f} * S_o * d} * \frac{\partial d}{\partial x} = 0 \qquad (2\text{-}8)$$

Equation (2-8) maybe rewritten as :

$$\frac{D d}{Dt} = 0 \qquad (2\text{-}9a)$$

along the characteristic trajectory :

$$\frac{d x}{dt} = \frac{3}{2} * \sqrt{\frac{8 * g}{f} * S_o * d} \qquad \text{Characteristic trajectory (2-9b)}$$

where D/Dt characterises the absolute differentiation operator.
Assuming a constant Darcy friction factor, the integration of Equations (2-9a) and (2-9b) gives :

$$d = \text{constant} \qquad (2\text{-}10a)$$

along

$$x = \frac{3}{2} * \sqrt{\frac{8 * g}{f} * S_o} * \sqrt{d} * t + \text{constant} \qquad (2\text{-}10b)$$

Equation (2-10b) shows that the forward characteristic is a straight line since d and f are constants, as sketched in Figure 2-1B.
The boundary conditions include the conservation of mass :

$$\int_{x=-L}^{X_s} d * dx = \frac{1}{2} * H_{dam} * L * \cos\theta = \frac{1}{2} * d_o * L \qquad (2\text{-}11)$$

where L is the reservoir length, H_{dam} is the dam height, d_o is the initial reservoir height measured normal to the chute invert and X_S is the wave front position (Fig. 2-1). Considering the forward characteristic d = constant issued from the initial backward characteristic, its trajectory is :

$$x = \frac{3}{2} * \sqrt{\frac{8 * g}{f} * S_o} * \sqrt{d} * t \qquad (2\text{-}12)$$

Combining Equations (2-12) and (2-11), it yields the location X_S of the shock (i.e. dam break wave front) and its celerity C_S as sketched in Figure 2-1B.

Complete solution for turbulent flows

HUNT's analysis yields a system of three equations :

$$\frac{V_H * t}{L} = \frac{1 - \left(\frac{d_S}{H_{dam}}\right)^2}{\left(\frac{d_S}{H_{dam}}\right)^{3/2}} \qquad (2\text{-}13)$$

$$\frac{X_S}{L} = \frac{\frac{3}{2}}{\frac{d_S}{H_{dam}}} - \frac{1}{2} * \frac{d_S}{H_{dam}} - 1 \qquad (2\text{-}14)$$

$$\frac{C_S}{V_H} = -\frac{3}{4} * \frac{V_H * t}{L} + \sqrt{\frac{X_S + L}{L} + \left(\frac{3}{4} * \frac{V_H * t}{L}\right)^2} \qquad (2\text{-}15)$$

where t is the time with t = 0 at dam break, d_S is the dam break wave front thickness, X_S is the dam break wave front position measured from the dam site, C_S is the wave front celerity, H_{dam} is the reservoir height at dam site, L is the reservoir length, and S_o is the bed slope, $S_o = H_{dam}/L$ (Fig. 2-1). The velocity V_H is the uniform equilibrium flow velocity for a water depth H_{dam} :

$$V_H = \sqrt{\frac{8*g}{f} * H_{dam} * S_o} \qquad (2\text{-}16)$$

where f is the Darcy friction factor which is assumed constant. Equations (2-13), (2-14) and (2-15) are valid for $S_o = S_f$ where S_f is the friction slope, and when the free-surface is parallel to the bottom of the sloping channel. Equation (2-14) may be transformed :

$$\frac{d_S}{H_{dam}} = \frac{3}{2} * \frac{L}{x_S - L} \qquad \text{for } x_S/L > 4 \quad (2\text{-}14b)$$

HUNT (1984, 1988) developed an analytical expression of the shock front shape :

$$\frac{x - X_S}{L} = \frac{d_S}{H_{dam}} * \left(\frac{d}{d_S} + \mathrm{Ln}\left(1 - \frac{d}{d_S}\right) + \frac{1}{2}\right) \qquad (2\text{-}17)$$

where d is the depth (or thickness) measured normal to the bottom, and d_S and X_S are functions of time which may be calculated using Equations (2-13) and (2-14) respectively. Note that Equation (2-17) applies only to the rounded nose of the shock.

Remarks

The dynamic wave equation is simplified by neglecting acceleration and inertial terms, and the free-surface is assumed parallel to the channel bottom ($S_o \approx S_f$). The kinematic wave approximation gives the relationship between the velocity and the water depth :

$$V = V_H * \sqrt{\frac{d}{H_{dam}}} \qquad (2\text{-}18)$$

Once the flood wave has travelled approximately four lengths of reservoir downstream of the dam site, the free-surface profile of the dam break wave follows :

$$\frac{x + L}{L} = \frac{d}{H_{dam}} + \frac{3}{2} * \frac{V_H * t}{L} * \sqrt{\frac{d}{H_{dam}}} \qquad \text{for } x \leq x_S \text{ and } x_S/L > 4 \quad (2\text{-}19)$$

The above development is valid for turbulent dam break waves. HUNT (1994) presented a similar development for laminar dam break waves.

For turbulent flows, HUNT (1982) showed that the assumption is valid after the wave front travelled approximately four reservoir lengths downstream of the gate : i.e., $X_S/L > 4$ where X_S is the wave front location and L is the reservoir length. The assumption is not valid in the initial instants after dam break nor until the free-surface becomes parallel to the chute invert. HUNT (1984) commented however that his approach could be adapted for $X_S/L < 4$: "*it is possible that an approach similar [...] could be used to route the flood downstream and that the result might be valid even for relatively small distance downstream*".

2.2.2 Negative wave

The dam removal is associated with the dam break wave propagation, as well as a backward characteristic C2 propagating upstream into the reservoir initially at rest (Fig. 2-1B). Since the propagation of the initial negative (backward) wave is relatively rapid, the kinematic wave approximation is improper and the complete equations of St Venant (i.e. dynamic wave equation) must be considered (paragraph 2.1).

The initial backward characteristic propagates in a fluid at rest ($V = 0$, $S_f = 0$). Its upstream extent is:

$$x_{C2} = -\frac{1}{4} * g * \sin\theta_b * t^2 \qquad \text{initial backward characteristic} \quad (2\text{-}20)$$

where t is the time from dam removal. For a two-dimensional triangular reservoir, the initial characteristic C2 reaches the reservoir upstream end for :

$$T = \sqrt{\frac{4 * L}{g * \sin\theta_b}} \qquad (2\text{-}21)$$

and T is shown in Figure 2-1B.

2.3 APPLICATION TO THIXOTROPIC FLUIDS

HUNT's (1982) kinematic wave solution for dam break wave down a sloping, prismatic, two-dimensional channel may be extended to a thixotropic fluid. The basic kinematic equations are:

$$\frac{D\,d}{Dt} = 0 \qquad (2\text{-}9a)$$

along the characteristic trajectory :

$$\frac{d\,x}{dt} = \frac{3}{2} * \sqrt{\frac{8 * g}{f} * S_o * d} \qquad \text{forward characteristic} \quad (2\text{-}9b)$$

where D/Dt characterises the absolute differentiation operator. For the rheological model of COUSSOT et al. (2002a) (paragraph 1.3), the basic equations of the thixotropic fluid may be approximated as:

$$\tau_o \approx \mu * \frac{V}{d} \qquad (2\text{-}22)$$

$$\mu = \mu_o * (1 + \lambda^n) \qquad (2\text{-}23)$$

$$\frac{d\lambda}{dt} \approx \frac{1}{\theta} - \alpha * \frac{V}{d} * \lambda \qquad (2\text{-}24)$$

assuming that $\partial V/\partial y \approx V/d$ where τ_o is the boundary shear stress, μ is the apparent fluid viscosity, V is the depth-averaged velocity and d is the flow depth (or fluid thickness) measured normal to the flow direction.
The kinematic wave approximation ($S_o = S_f$) yields :

$$V = \frac{\rho * g * S_o * d^2}{\mu_o * (1 + \lambda^n)} \qquad \text{Kinematic wave approximation} \quad (2\text{-}25)$$

That is, along the characteristic trajectory, the degree of jamming of the material satisfies :

$$\frac{d\lambda}{dt} + \alpha * \frac{\rho * g * d * S_o}{\mu_o} * \frac{\lambda}{1 + \lambda^n} = \frac{1}{\theta} \qquad (2\text{-}26)$$

with d = constant along the forward characteristic (Eq. (2-9a)). Combining Equations (2-9) and (2-25), the equation of the forward characteristic trajectory becomes:

$$\frac{dx}{dt} = \frac{3}{2} * \frac{\rho * g * S_o * d^2}{\mu_o * (1 + \lambda^n)} \qquad \text{forward characteristic trajectory} \quad (2\text{-}27)$$

The trajectory is not a straight line since λ is a function of time and space (Fig. 2-2).
Along a forward trajectory where Dd/Dt = 0, the boundary shear stress equals :

$$\tau_o = \rho * g * d * S_o$$

The result derives from the kinematic wave approximation for a wide channel. It is independent of the initial degree of jamming.

Fig. 2-2 - Dam break wave of thixotropic fluid down a sloping channel: characteristics and dam break wave front path in the (x, t) plane

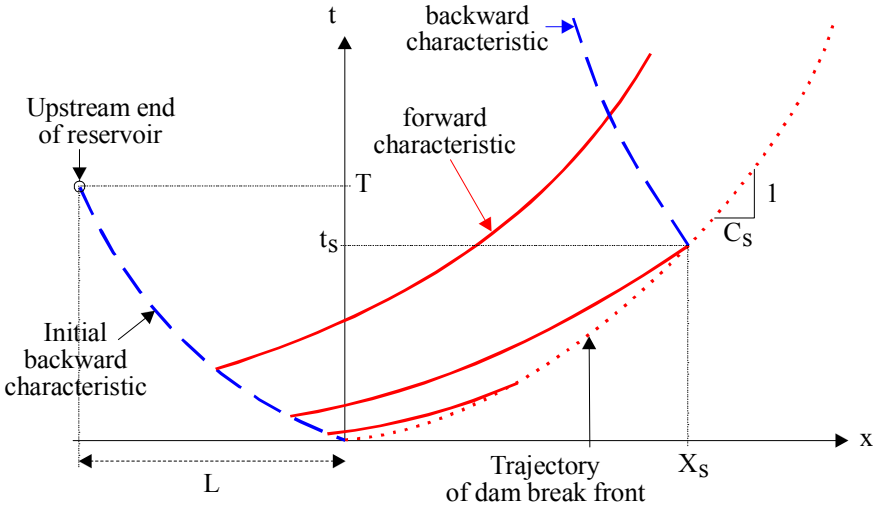

2.3.1 Basic application

Several analytical developments may be derived in particular cases including for $\theta \rightarrow +\infty$ or for integer values of n. Further developments are available when the exponent n is a real value greater than unity. These are detailed in Appendix B.
Equation (2-26) may be rewritten as :

$$\frac{d\lambda}{dt} = \frac{1}{\theta} - \alpha * \frac{\rho * g * d * S_o}{\mu_o} * \frac{\lambda}{1 + \lambda^n} \qquad (2\text{-}26)$$

while the trajectory of the forward characteristic is given by Equation (2-27). Considering a fluid with an initial degree of jamming $\lambda(t=0) = \lambda_o$ and for $n > 1$, Equation (2-26) predicts different behaviours along a forward characteristic depending upon the sign of $d\lambda/dt$. Considering the case $d\lambda/dt = 0$, Equation (2-26) yields :

$$0 = \frac{1}{\theta} - \alpha * \frac{\rho * g * d * S_o}{\mu_o} * \frac{\lambda}{1 + \lambda^n} \qquad (2\text{-}29)$$

Note that the function $\lambda/(1+\lambda^n)$ tends to zero for $\lambda \to 0$ and $\lambda \to +\infty$ (for $n > 1$). The function has a maximum for $\lambda = \lambda_c$ where

$$\lambda_c = \left(\frac{1}{n - 1}\right)^{1/n} \qquad (2\text{-}28)$$

The maximum value of the function $\lambda/(1+\lambda^n)$ is:

$$\frac{(n - 1)^{(n-1)/n}}{n}$$

Basically, Equation (2-29) has zero real solution, one solution λ_c or two solutions λ_1 and λ_2 depending upon the value of the dimensionless viscosity :

$$\frac{\mu_o}{\theta * \alpha * \rho * g * d * S_o}.$$

Considering a dam break down a sloping channel, Equation (2-26) gives at the time origin ($t = 0$) :

$$\left(\frac{d\lambda}{dt}\right)_{t=0} = \alpha * \frac{\rho * g * d * S_o}{\mu_o} * \left(\frac{\mu_o}{\theta * \alpha * \rho * g * d * S_o} - \frac{\lambda_o}{1 + \lambda_o^n}\right)$$

along the forward characteristic where d is constant and λ_o is the initial degree of fluid jamming. Consider the flow situation :

$$\frac{\mu_o}{\theta * \alpha * \rho * g * d * S_o} > \left(\frac{1}{n - 1}\right)^{1/n} \qquad \text{(Case 1)}$$

Initially ($t = 0$), $d\lambda/dt$ is positive and $\lambda(t=0+) > \lambda(t=0) = \lambda_o$. More generally, for $t \geq 0$, $d\lambda/dt > 0$ everywhere along the characteristic trajectory and λ increases monotically towards the wave front. For large times ($t >> 1$), $d\lambda/dt$ tends to $1/\theta$ and the degree of jamming λ tends to an infinite value. That is, complete stoppage. Note that the result is independent of the initial degree of jamming λ_o. The forward characteristics form a series of convex curves in the (x,t) plane ([2]).
Consider the flow situation :

$$\frac{\mu_o}{\theta * \alpha * \rho * g * d * S_o} = \left(\frac{1}{n - 1}\right)^{1/n} \qquad \text{(Case 2)}$$

three flow situations may occur depending upon the sign of $(\lambda_o - \lambda_c)$. For $\lambda_o > \lambda_c$ (Case 2.1), $d\lambda/dt$ is positive for $t \geq 0$ everywhere along the characteristic trajectory and λ increases monotically. The fluid flow tends to complete stoppage. The forward characteristics form a series of convex curves. For $\lambda_o = \lambda_c$ (Case 2.2), $d\lambda/dt$ is zero and $\lambda(t) = \lambda_o = \lambda_c$ everywhere along the forward characteristic which is a straight line. The fluid flow has a constant apparent viscosity $\mu = \mu_o*(1+\lambda_c^n) =$

[2]Remember. In the (x,t) plane, the slope of the characteristics is dt/dx.

$\mu_o*(1+\lambda_o^n)$. For $\lambda_o < \lambda_c$ (Case 2.3), $d\lambda/dt$ is positive initially. The degree of jamming tends to $\lambda = \lambda_c$ for large times, and the fluid flow tends to a constant viscosity fluid behaviour ($\mu \rightarrow \mu_o*(1+\lambda_c^n)$) for large times t. In the (x,t) plane, the forward characteristics form a series of convex curves which tend to straight lines for large times t.
Lastly, considering the flow condition :

$$\frac{\mu_o}{\theta * \alpha * \rho * g * d * S_o} < \left(\frac{1}{n - 1}\right)^{1/n} \qquad \text{(Case 3)}$$

five flow situations may occur depending upon the signs of $(\lambda_o - \lambda_1)$ and $(\lambda_o - \lambda_2)$, where λ_1 and λ_2 are the solutions of Equation (2-29) with $\lambda_1 < \lambda_2$ ([3]). For $(\lambda_o > \lambda_2)$ (Case 3.1), $d\lambda/dt$ is positive at $t = 0$ and $\lambda(t=0+) > \lambda_o$. More generally, for $t \geq 0$, $d\lambda/dt$ is positive everywhere along the characteristic trajectory and λ increases monotically until complete flow stoppage. The forward characteristics form a series of convex curves in the (x,t) plane. For $(\lambda_o = \lambda_2)$ (Case 3.2), $d\lambda/dt$ is zero and $\lambda(t) = \lambda_2$ everywhere along the forward characteristic which is a straight line. The fluid flow has constant viscosity $\mu = \mu_o*(1+\lambda_2^n)$. For $(\lambda_1 < \lambda_o < \lambda_2)$ (Case 3.3), $d\lambda/dt < 0$ at $t = 0$. More generally, $d\lambda/dt \leq 0$ at $t \geq 0$, although $d\lambda/dt$ tends to zero and λ tends to λ_1 for large times ($t >> 1$). Along a forward characteristic, the fluid flow tends to a constant viscosity behaviour ($\mu = \mu_o*(1+\lambda_1^n)$). The forward characteristics form a series of concave curves which tend to straight lines for large times t. For $(\lambda_o = \lambda_1)$ (Case 3.4), $d\lambda/dt$ is zero and $\lambda(t) = \lambda_1$ everywhere along a forward characteristic which is a straight line. The fluid flow has a constant viscosity. For $(\lambda_o < \lambda_1)$ (Case 3.5), $d\lambda/dt > 0$ initially. More generally, $d\lambda/dt \geq 0$ at $t \geq 0$. $d\lambda/dt$ tends to zero and λ tends to λ_1 for large times ($t >> 1$). The fluid flow tends to a constant viscosity fluid behaviour ($\mu = \mu_o*(1+\lambda_1^n)$). The forward characteristics form a series of convex curves which tend to straight lines for large times.
All the trends are summarised in Table 2-1.

2.3.2 Application to a dam break wave down a sloping channel

The above development was performed along a forward characteristic on which the flow depth d was a constant (Eq. (2-9a)). It may be extended to a series of characteristics issued from the initial negative characteristic with different flow depths. For a dam break wave down a sloping channel (e.g. Fig. 2-2), the flow depths d must satisfy : $0 \leq d \leq d_o = H_{dam}*\cos\theta$ where H_{dam} is the vertical reservoir height at gate (e.g. Fig. 2-1).
A characteristic flow depth h_c may be defined as :

$$h_c = \frac{\mu_o * (n - 1)^{1/n}}{\theta * \alpha * \rho * g * S_o} \qquad \text{(2-30)}$$

[3]For very small values of $\lambda/(1+\lambda^n)$, it can be shown that :

$$\lambda_1 \approx \frac{1 + \sqrt{1 - 4 * n * \frac{\mu_o}{\theta * \alpha * \rho * g * d * S_o}}}{2 * n}$$

$$\lambda_2 \approx \left(\frac{\theta * \alpha * \rho * g * d * S_o}{\mu_o}\right)^{1/(n-1)}$$

Table 2-1 - Summary of possible flow situations along a forward characteristic

Condition	λ	$\frac{d\lambda}{dt}$	Forward characteristics	Remarks
(1)	(2)	(3)	(4)	(5)
(1) $\frac{\mu_o}{\theta * \alpha * \rho * g * d * S_o} > \left(\frac{1}{n-1}\right)^{1/n}$	$\rightarrow +\infty$ for $t \rightarrow +\infty$	> 0 for $t \geq 0$	Series of convex curves	Evolution towards complete stoppage.
(2) $\frac{\mu_o}{\theta * \alpha * \rho * g * d * S_o} = \left(\frac{1}{n-1}\right)^{1/n}$				
(2.1) $\lambda_o > \lambda_c$	$\rightarrow +\infty$ for $t \rightarrow +\infty$	> 0 for $t \geq 0$ $\rightarrow 1/\theta$ for $t \rightarrow +\infty$	Series of convex curves	Evolution towards complete stoppage.
(2.2) $\lambda_o = \lambda_c$	$\lambda(t) = \lambda_c$ for $t \geq 0$	0 for $t \geq 0$	Straight line	Constant viscosity fluid.
(2.3) $\lambda_o < \lambda_c$	$\rightarrow \lambda_c$ for $t \rightarrow +\infty$	≥ 0 for $t \geq 0$ $\rightarrow 0$ for $t \rightarrow +\infty$	Series of convex curves tending to straight lines	Evolution towards constant viscosity fluid.
(3) $\frac{\mu_o}{\theta * \alpha * \rho * g * d * S_o} < \left(\frac{1}{n-1}\right)^{1/n}$				
(3.1) $\lambda_o > \lambda_2$	$\rightarrow +\infty$ for $t \rightarrow +\infty$	> 0 for $t \geq 0$ $\rightarrow 1/\theta$ for $t \rightarrow +\infty$	Series of convex curves	Evolution towards complete stoppage.
(3.2) $\lambda_o = \lambda_2$	$\lambda(t) = \lambda_2$ for $t \geq 0$	0 for $t \geq 0$	Straight line	Constant viscosity fluid.
(3.3) $\lambda_1 < \lambda_o < \lambda_2$	$\rightarrow \lambda_1$ for $t \rightarrow +\infty$	≤ 0 for $t \geq 0$ $\rightarrow 0$ for $t \rightarrow +\infty$	Series of concave curves tending to straight lines	Evolution towards constant viscosity fluid.
(3.4) $\lambda_o = \lambda_1$	$\lambda(t) = \lambda_1$ for $t \geq 0$	0 for $t \geq 0$	Straight line	Constant viscosity fluid.
(3.5) $\lambda_1 < \lambda_o$	$\rightarrow \lambda_1$ for $t \rightarrow +\infty$	≥ 0 for $t \geq 0$ $\rightarrow 0$ for $t \rightarrow +\infty$	Series of convex curves tending to straight lines	Evolution towards constant viscosity fluid.

Note: λ_1, λ_2 : solutions of Equation (2-29) such as $\lambda_1 < \lambda_c < \lambda_2$.

Basically h_c is a characteristic fluid thickness which may be obtained by re-arranging expressions in Table 2-1. Importantly, for $d < h_c$, λ increases monotically along the forward characteristic until fluid stoppage. h_c is a critical fluid thickness below which the fluid flow motion tends to complete stoppage. It is now possible to list four flow situations depending upon the initial degree of fluid jamming λ_o and of the ratio d_o/h_c.

(a) For reservoir depths less than the characteristic fluid thickness (i.e. $d_o < h_c$), $d\lambda/dt$ is positive for $t \geq 0$ on each and every forward characteristic. The degree of jamming of the fluid increases monotically with time along all characteristics until fluid stoppage. The extent of fluid flow is

limited and the flow motion is relatively slow until complete stoppage (Case a). The result is independent of the initial degree of fluid jamming λ_o. In the (x,t) plane, the forward characteristics form a series of convex curves.

(b) For $d_o = h_c$, and $\lambda_o = \lambda_c$, the first forward characteristic is a straight line and all forward characteristics issued from the initial negative characteristic with $d < h_c$ are convex characteristics. Basically, the degree of jamming of the fluid increases monotically with time along each characteristic, but the first initial forward characteristic, until fluid stoppage (Case b1). The extent of fluid flow is limited. For $d_o = h_c$, and $\lambda_o \neq \lambda_c$ (Case b2), $d\lambda/dt$ is positive for $t \geq 0$. The degree of jamming of the fluid increases monotically with time along each characteristic until fluid stoppage. The extent of fluid flow is limited again. Cases a and b are very close. (In fact Cases a and b2 are identical.)

(c) For large initial reservoirs (i.e. $d_o > h_c$), the flow behaviour on each forward characteristic is a function of the initial degree of jamming λ_o and of the flow depth d on the characteristic. Each characteristic may have a different behaviour from adjacent characteristics depending upon the signs of (d_o-h_c), $(\lambda_o-\lambda_1)$ and $(\lambda_o-\lambda_1)$. Note that the solutions λ_1 and λ_2 of Equation (2-29) are functions of the flow depth d itself. That is, λ_1 increases and λ_2 decreases with decreasing flow depth d. At the limit, $\lambda_1 = \lambda_2 = \lambda_c$ for $d = h_c$.
(c1) For $\lambda_o > \lambda_2(d_o)$, $d\lambda/dt$ is positive everywhere along all forward characteristics and λ increases monotically until complete flow stoppage (Case c1). The forward characteristics form a series of convex curves in the (x,t) plane. The extent of flow motion is moderate until fluid stoppage.

(c2) For $\lambda_1 < \lambda_o < \lambda_2(d_o)$ (Case c2), $d\lambda/dt$ is negative along the forward characteristics initially. Along a forward characteristic, the fluid flow tends to a constant viscosity behaviour ($\mu = \mu_o*(1+\lambda_1^n)$) with increasing time towards the wave front. The initial characteristics form a series of concave curves which tend to straight lines. That is, the fluid flow tends to a "pseudo-laminar" flow motion towards the wave front.
(c3) Similarly, for $\lambda_o < \lambda_1(d_o)$ (Case c3), $d\lambda/dt$ is positive initially although it tends to zero with increasing time. On the initial forward characteristics, the fluid flow tends to a constant viscosity or "pseudo-laminar" motion ($\mu = \mu_o*(1+\lambda_1^n)$) towards the shock. The forward characteristics form a series of convex curves which tend to straight lines for large times.

Following the initial backward characteristic, the flow depth decreases with increasing time (Fig. 2-3). On the initial negative characteristic, the flow depth satisfies $h_c < d < d_o$ for $0 < t < t_c$ and $0 < d < h_c$ for $t_c < t < T$ where :

$$t_c = \sqrt{\frac{4 * L}{g * \sin\theta} * \left(1 - \frac{h_c}{d_o}\right)} \qquad (2\text{-}31)$$

and T is the time taken by the initial characteristic C2 to reach the reservoir upstream end (paragraph 2.2.2). Equation (2-31) derives from the trajectory of negative wave characteristic (initial backward characteristic) ([4]). On each forward characteristic issued from the initial negative characteristic at $t > t_c$, the flow depth d is less than the characteristic fluid thickness h_c, and $d\lambda/dt$ is positive everywhere along the forward characteristic. The degree of fluid jamming λ increases

[4]Note that the equation of the initial backward characteristic is derived from the complete Saint Venant equations, while Equations (2-26) and (2-29) are based upon a kinematic wave approximation of the Saint Venant equations. In the initial instants following gate opening, the kinematic wave approximation is inappropriate, and it becomes correct only once the free-surface is parallel to the channel invert.

monotically until complete stoppage. For $d < h_c$, the flow motion is relatively slow and the extent of fluid flow is limited until complete stoppage. The forward characteristics form a series of convex curves in the (x,t) plane (Fig. 2-3).
Basically, Cases c2 and c3 tend to similar flow conditions. For each forward characteristic issued from the initial backward characteristic at $t < t_c$, the flow depth on the forward characteristics satisfies : $d > h_c$. That is, the fluid flow tends to a "pseudo-laminar" (or low viscosity) flow motion towards the wave front. Along the other forward characteristics issued from the initial backward characteristic at $t > t_c$, the flow depths satisfy : $d < h_c$ on these characteristics. The flow motion is relatively slow and the extent of fluid flow is limited until complete stoppage.

(d) For very large initial reservoirs (i.e. $d_o >> h_c$) and initial degree of jamming λ_o such as $\lambda_o << \lambda_2(d_o)$, the fluid flows as a quasi-constant viscosity wave motion (case d). The flow might be laminar or turbulent depending upon the flow Reynolds number. In any case, the flow motion will be relatively rapid and it will stop only when the fluid thickness becomes less than the characteristic fluid thickness h_c.

In summary, several flow regimes may be observed depending upon the initial degree of fluid jamming λ_o and of the ratio d_o/h_c. These flow regimes are: (1) a relatively-rapid flow stoppage for relatively small mass of fluid ($d_o/h_c < 1$) or large initial rest period T_o (i.e. large λ_o) (Cases a, b and c1), (2) a fast flow motion for large mass of fluid ($d_o/h_c >> 1$) (Case d), or (3) an intermediate motion initially rapid before final fluid stoppage for intermediate mass of fluid ($d_o/h_c > 1$) and intermediate initial rest period T_o (i.e. intermediate λ_o) (Cases c2 and c3).

Fig. 2-3 - Dam break wave of thixotropic fluid down a sloping channel - Sketch of characteristic trajectories for $d_o > h_c$

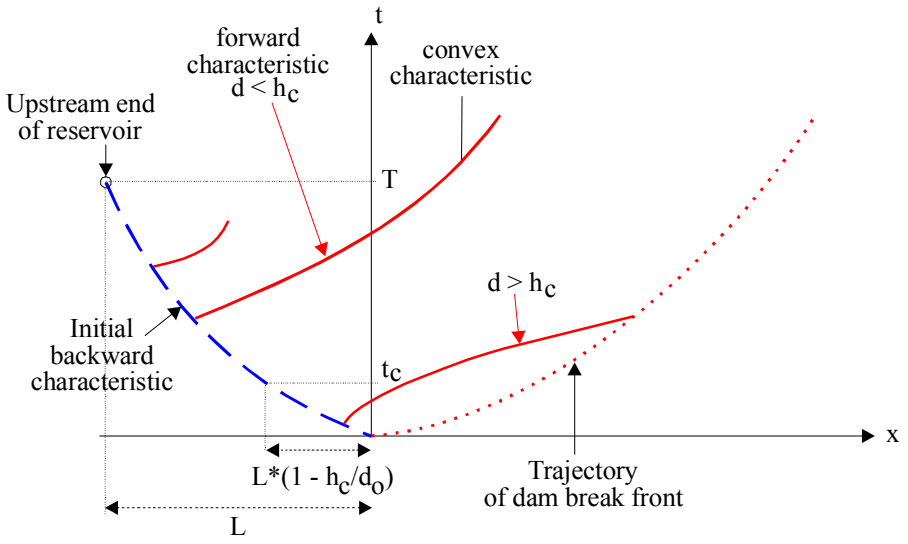

Discussion
For very large initial reservoirs (i.e. $d_o >> h_c$) and relatively-fast flow motion (case d), the maximum extent of the wave front may be deduced from the equation of conservation of mass. Assuming that complete stoppage occurs for $d = h_c$ and that the final fluid thickness remains h_c, the continuity equation yields :

$$\int_{x=-L}^{(X_s)_{end}} h_c * dx = \frac{1}{2} * d_o * L$$

where L is the reservoir length. After transformation, it yields the final wave front position $(X_s)_{end}$:

$$(X_S)_{end} = \frac{1}{2} * \frac{\theta * \alpha * \rho * g * S_o * d_o * L}{\mu_o * (n - 1)^{1/n}} \qquad (2\text{-}32)$$

Equation (2-32) is a crude approximation assuming a two-dimensional flow. But its qualitative trends are coherent with both fluid rheological properties and flow motion equations.

3. THEORETICAL ANALYSIS (1) UNSTEADY BOUNDARY LAYER

3.1 ANALYTICAL SOLUTION OF THE NAVIER-STOKES EQUATIONS

In the previous section, the flow was assumed one-dimensional and the results cannot provide insights into the vertical shear distribution. Considering the front of a dam break wave on a horizontal channel, the boundary layer development at the leading edge of the surge is somehow similar to a startup flow. In the start-up flow, the velocity is independent of the x co-ordinate in the flow direction and the continuity equation yields $V_y = 0$.

For a laminar flow of a Newtonian fluid, the Navier-Stokes equations become :

$$\rho * \frac{\partial V}{\partial t} = - \rho * g * \frac{\partial z}{\partial x} - \frac{\partial P}{\partial x} + \mu * \frac{\partial^2 V}{\partial y^2} \qquad (3\text{-}1a)$$

$$0 = - \rho * g * \frac{\partial z}{\partial y} - \frac{\partial P}{\partial y} \qquad (3\text{-}1b)$$

where ρ and μ are the fluid density and dynamic viscosity respectively, z is the vertical elevation, P is the pressure and V is the x-component of the velocity ($V = V_x$). For a horizontal flow, the gravity force component in the flow direction is zero. The Navier Stokes equations yield :

$$\frac{\partial V}{\partial t} = \nu * \frac{\partial^2 V}{\partial y^2} \qquad (3\text{-}2)$$

where ν is the kinematic viscosity : $\nu = \mu/\rho$. Equation (3-2) is similar to a diffusion equation and a heat conduction equation.

For an advancing dam break wave front, the boundary conditions are : $V = U$ for $y \geq 0$ and $t \leq 0$, and $V(y=0) = 0$ and $V(y \rightarrow +\infty) = U$ for $t > 0$. The celerity U would correspond somehow to the wave front propagation speed C_S. The analytical solution of Equation (3-2) is :

$$\frac{V}{U} = \text{erf}\left(\frac{y}{2 * \sqrt{\nu * t}}\right) \qquad (3\text{-}3)$$

where y is the distance normal to the invert and the function erf is the Gaussian error function defined as :

$$\text{erf}(u) = \frac{2}{\sqrt{\pi}} * \int_0^u \exp(- v^2) * dv \qquad (3\text{-}4)$$

Figure 3-1 presents a sketch of typical velocity distributions with increasing time t. The analytical solution of the Navier-Stokes equations for unsteady plane laminar flows is called the first Stokes problem or Rayleigh problem after STOKES (1856) and RAYLEIGH (1911) respectively (SCHLICHTING and GERSTEN 2000, pp. 126-128). The reasoning may be extended to unsteady turbulent boundary layer flow with constant momentum exchange coefficient (or "eddy viscosity") ν_T and to sloping channel (Appendix C).

3.2 APPLICATION

For a thixotropic fluid, the rheological model of COUSSOT et al. (2002a) gives :

$$\frac{d \lambda}{dt} = \frac{1}{\theta} - \alpha * \frac{\partial V}{\partial y} * \lambda \qquad (3\text{-}5)$$

while the Navier-Stokes equations yield

$$\frac{\partial V}{\partial t} = \frac{\mu_o}{\rho} * (1 + \lambda^n) * \frac{\partial^2 V}{\partial y^2} \qquad (3\text{-}6)$$

Fig. 3-1 - Sketch of velocity distribution in a startup flow

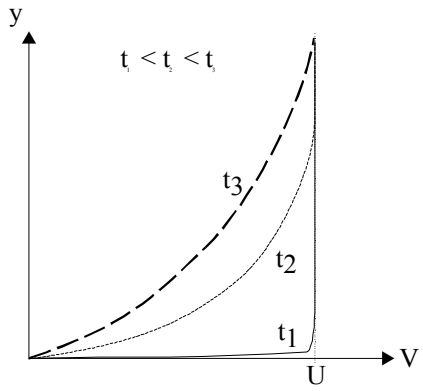

where the local velocity V and the local degree of jamming of the fluid λ are both functions of y and t. The boundary conditions are :

$V = U$ for $y \geq 0$ and $t \leq 0$

$V(y=0) = 0$ and $V(y \rightarrow +\infty) = U$ for $t > 0$

$\lambda = \lambda_o$ for $y \geq 0$ and $t \leq 0$

Equations (3-5) and (3-6) form a non-linear system of two differential equations with two unknowns V and λ. It may be solved numerically. The results may provide some novel insights into the time evolution of the shear region at the leading edge of the dam break wave.

Remark

At startup (t = 0+) and at the boundary (y = 0), the shear rate is infinite and the degree of fluid jamming must be zero :

$\lambda = 0$ for $y = 0$ and $t = 0+$

The time scale of a startup flow may be assumed small compared to the characteristic restructuring time θ. This implies that, during startup, the vertical distribution of apparent fluid viscosity varies from $\mu(y=0) = \mu_o$ at the boundary to $\mu(y \rightarrow +\infty) = \mu_o * (1+\lambda_o^n)$ far away from the boundary.

4. EXPERIMENTAL FACILITIES

4.1 PRESENTATION

New experiments were performed at the Laboratoire des Matériaux et des Structures du Génie Civil (LCPC-ENPC-CNRS, France) (Table 4-1). The main facility was a 2 m long, 0.34 m wide, tilting flume (Fig. 4-1 and 4-2A). The 0.35 m high sidewalls were made of 12 mm thick, 2 m long polycarbonate panels. The floor was a 20 mm thick laminated timber sheet covered with grade 150 sand ([5]) paper to minimise slippage.

Fig. 4-1 - Sketch of the large experimental flume

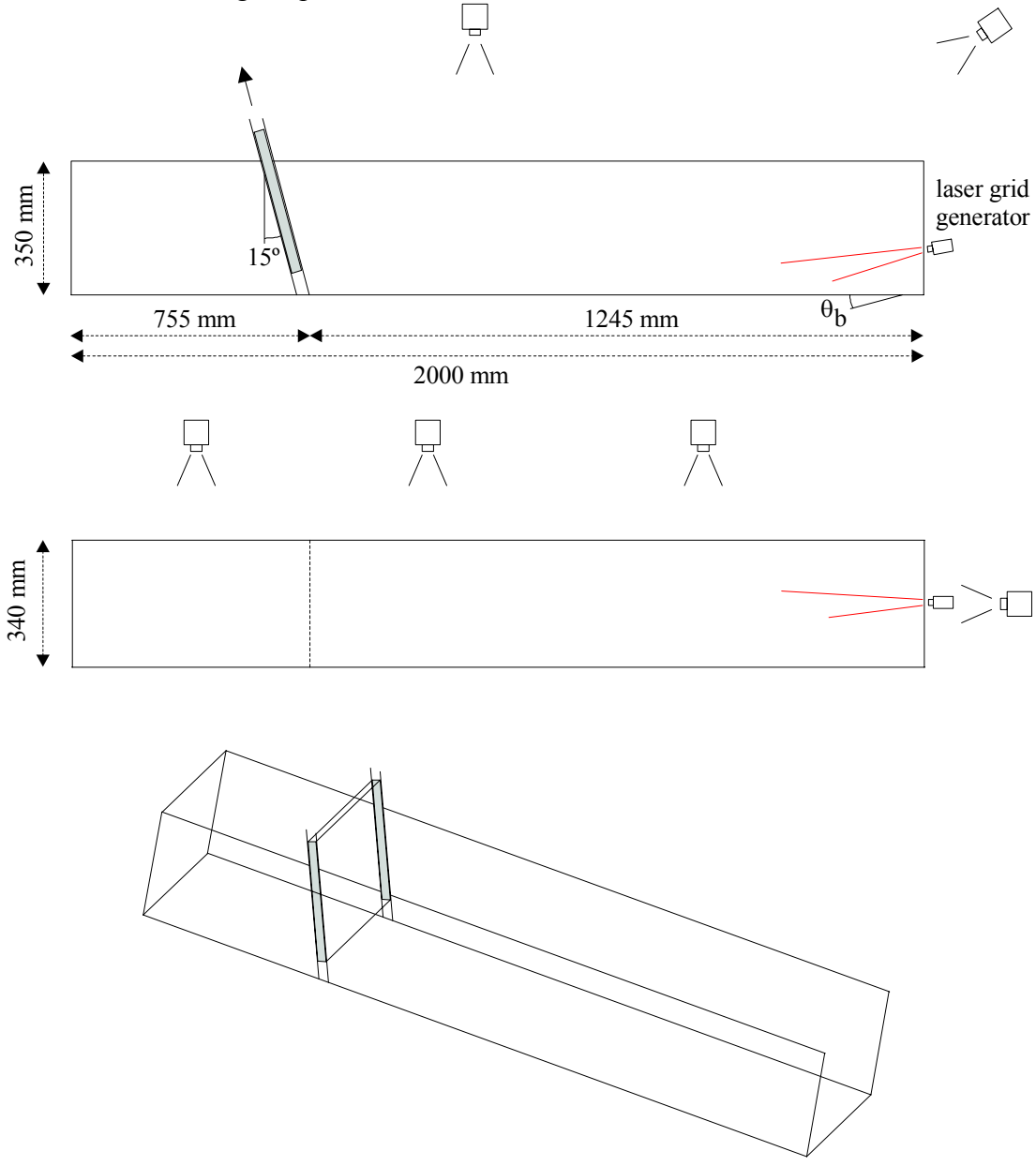

A removable gate was installed. It was made of polycarbonate and tilted 15° with the direction normal to the channel invert. All experiments were conducted with a fixed bed slope θ_b, and most were performed for $\theta_b = 15°$ for which the sluice gate was vertical. The gate was guided by small aluminium U-shaped groves ([6]).

[5]That is, 150 sand grains per cm^2.

[6]The guides were 10 mm wide and protruded less than 3 mm into the channel.

Fig. 4-2 - Photographs of the experimental facilities
(A) Large experimental rig (θ_b = 15º)

In addition, some qualitative experiments were conducted on a smaller inclined plate (0.80 m long, 0.48 m wide) covered with sand paper. On that small plate, the fluid was initially poured in a square mould (0.223 m × 0.223 m) and a cylindrical mould (∅ = 0.1725 m, 0.030 m high) (Fig. 4-2B). The mould was suddenly removed and the flow down the constant slope plane was studied qualitatively.

(B) Small plate (θ_b = 15º) with square mould

(C) Laser grid illumination on the advancing bentonite solution (Test 04)

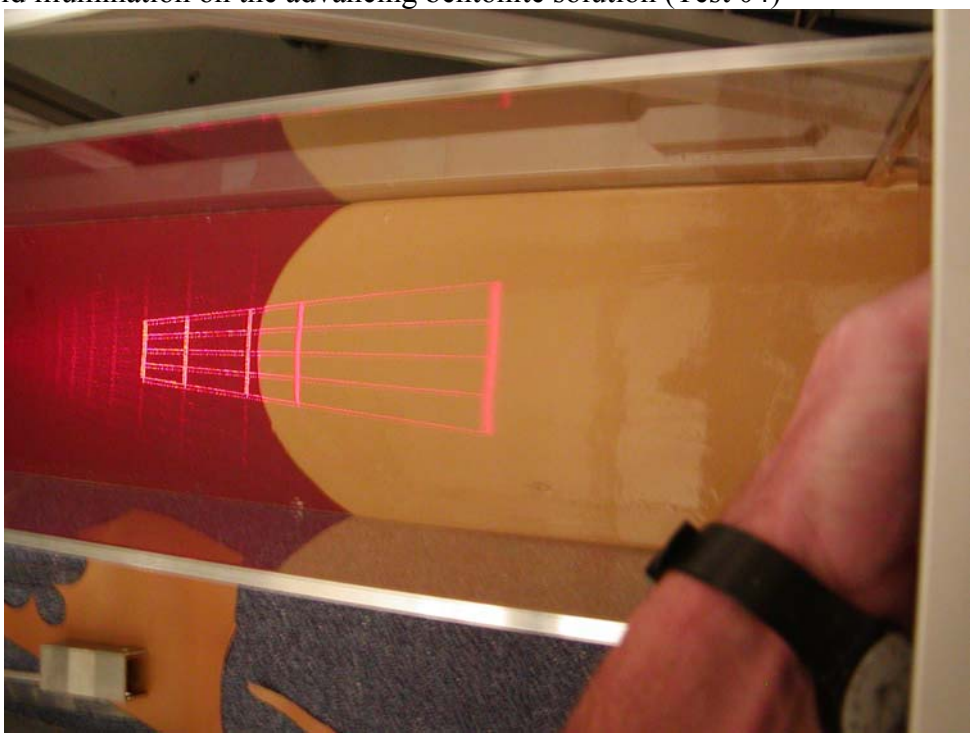

(D) Mixer Perrier™ Labotest GMP Type 32

Table 4-1 - Summary of experimental setups

Facility	Slope θ_b (1)	Bentonite mass concentration C_m(2)	Initial mass M	Rest period T_o (3)	Remarks
	deg.		kg	s	
(1)	(2)	(3)	(4)	(5)	(6)
Large flume	15.0	0.10, 0.13, 0.15, 0.17 & 0.20	1.6 to 4.1	20 sec. to 23 hours	Two-dimensional triangular reservoir. Chute width: 0.340 m
Small plate	15.4 to 24	0.05 to 0.20	--	0 to 30 min.	Cylindrical and square moulds. Chute width: 0.48 m.

Notes : (1) : constant slope experiments; (2) : defined as the ratio of bentonite mass to bentonite & water mass; (3) : measured from the start of suspension pouring into the reservoir/mould.

4.2 INSTRUMENTATION

The channel slope was measured with an electronic inclinometer Digital Protactor™ Pro360 with an accuracy of 0.1°.

For the preparation of the suspensions, the bentonite and water were weighted with a balance Sartorius™ LP3200D with an accuracy of less than 0.01 g. During experiments, the mass of

bentonite suspension was weighted with a balance Metler™ PM16. The range was 50 g to 16 kg, and the error was less than 1 g. The rheological properties of suspensions were measured with a Rheometer Bohlin Instruments™ C-VOR 200 NF, equipped with two rough circular disk (∅ = 40 mm).
Flow visualisations were performed with four digital video-cameras with high-shutter speed : Canon™ MV500i (25 fr/s, shutter: up to 1/8,000 s), Sony™ CDR-TRV950E 3CCD (25 fr/s, shutter: up to 1/10,000 s), Olympus™ Camedia C700 (15 fr/s, shutter: up to 1/1,000 s) and a CCD camera (25 fr/s) connected to a computer system.
Unsteady free-surface elevations were further measured using the CCD camera at the intersection of a series of laser beams (He/Ne 10mW) at low incidence with the free-surface (Fig. 4-2C). The camera recorded 25 frames per second with 256 grey levels at high resolution (1024*1280 pixels). The data were analysed using a Mourier projection method.

4.3 FLUID PREPARATION

Great care taken to prepare systematically and consistently the thixotropic fluid using the procedure described by HUYNH et al. (2001) and COUSSOT et al. (2002b).
Solid mass concentrations of 5 to 20% were used, although most tests were performed with 10, 13, 15 and 17% mass concentration suspensions. The bentonite solution was prepared with distilled water and industrial grade bentonite (Impersol powder, Société Française des Bentonites et Dérivés, France) with no chemical additives. The precision on bentonite mass concentration was less than 0.1‰. The bentonite-water suspension was first agitated continuously for about 3 h to ensure complete homogenisation. (Mixing was performed with a Perrier™ Labotest GMP Type 32 mixer (Fig. 4-2D).) The suspension was then left to rest for at least 48 hours to allow hydration and dispersion of bentonite particles. For completeness, the 13% solution was prepared with a 20% solution diluted accordingly with distilled water. The 17% solution was prepared by combining 10% and 20% solutions with the appropriate quantities.

Remark
The mass concentration C_m is defined as the ratio of mass of bentonite to mass of bentonite plus water.
The bentonite density is about : $\rho_b \approx 2600$ kg/m^3.
The density ρ_s of bentonite suspension is related to the water density ρ_w and bentonite density ρ_b by:

$$\rho_s = \frac{\rho_w * \rho_b}{C_m * \rho_w + (1 - C_m) * \rho_b} \qquad (4\text{-}1)$$

4.4 FLUID PROPERTIES

Basic properties of bentonite suspensions were measured with a rheometer equipped with two rough circular disks separated by a 1 mm gap ([7]). The tests were performed under controlled stress for relatively short durations at constant temperature (25 Celsius).
For each rheological test, a small sample of well-stirred liquid was placed between the plates. The specimen was pre-sheared at constant a shear rate of 500 s^{-1} for 20 sec. It was then rested for a known period T_o before being subjected to a controlled stress loading and unloading of 1 minute each.

[7]The gap was selected to be at least 10 times the mean particle size. Since some very-fine sand particles were detected, the gap was set at 1 mm.

Results provided some information on the apparent yield stress of the fluid, τ_c, and the effective viscosity μ as functions of the bentonite suspension mass concentration C_m and rest time T_o. Remark that a more complete characterization of the rheological behavior of such thixotropic fluids would require the determination of the parameters of a thixotropic model. Such a work was carried out successfully for a suspension bentonite (Roussel et al. 2004). Within the frame of the present work, since no systematic quantitative comparison of theory with experiments have been made, we only proceeded to a more rapid but also more approximate characterization of the materials used. It can be expected that, as the solid fraction changes in such suspensions, these characeristics parameters are mainly the apparent viscosity under given conditions which change while the other parameters of the kinetic equation remain more or less constant. The yield stress and viscosity were estimated during the unloading phase, to be consistent with the inclined plate experiments. Yield stress and viscosity results were derived by fitting the rheometer data with a Herschel-Buckley model :

$$\tau = \tau_c + \mu * \left(\frac{\partial V}{\partial y}\right)^n \qquad (4\text{-}2)$$

Experimental results are presented in Table 4-2 and Figure 4-3. They showed that an increase in yield stress with increasing rest time for a given mass concentration, as well as a marked increase in yield stress with mass concentration for a constant rest period. Viscosity data indicated little effect of mass concentration and rest period. In average over all tests, the apparent viscosity was 0.34 Pa.s for $1 \leq T_o \leq 900$ s and $0.10 \leq C_m \leq 0.17$.

Fig. 4-3 - Bentonite suspension rheometer test
(A) Loading and unloading cycle in the Bohlin Instruments™ C-VOR 200 Rheometer for C_m = 0.13 and T_o = 1 sec.

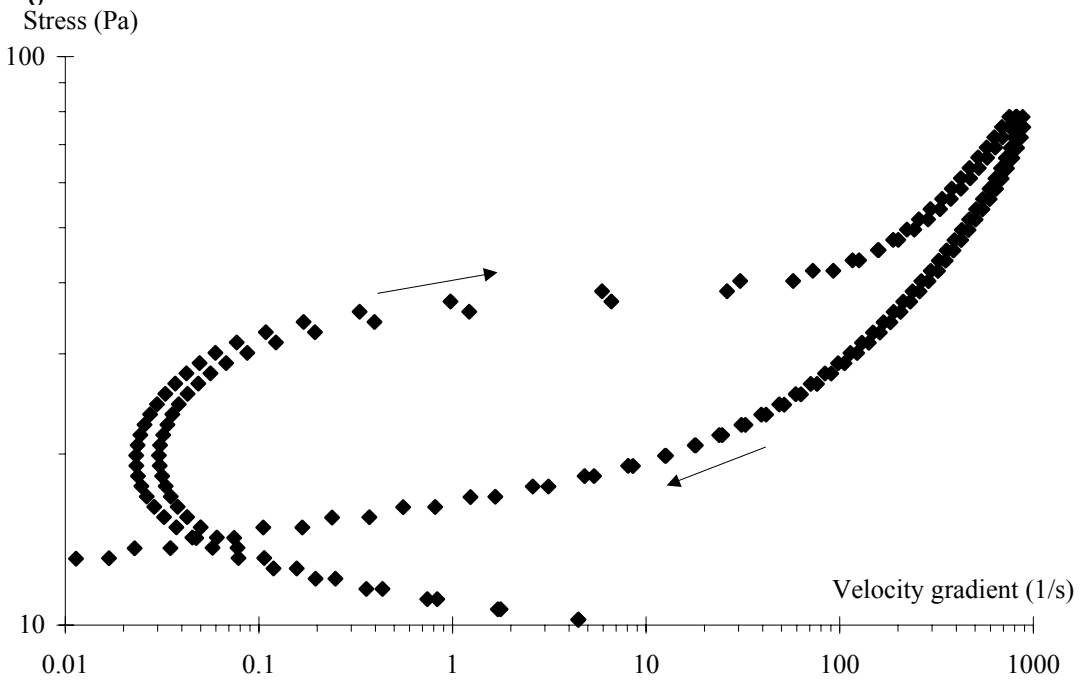

(B) Yield stress and apparent viscosity of bentonite suspensions

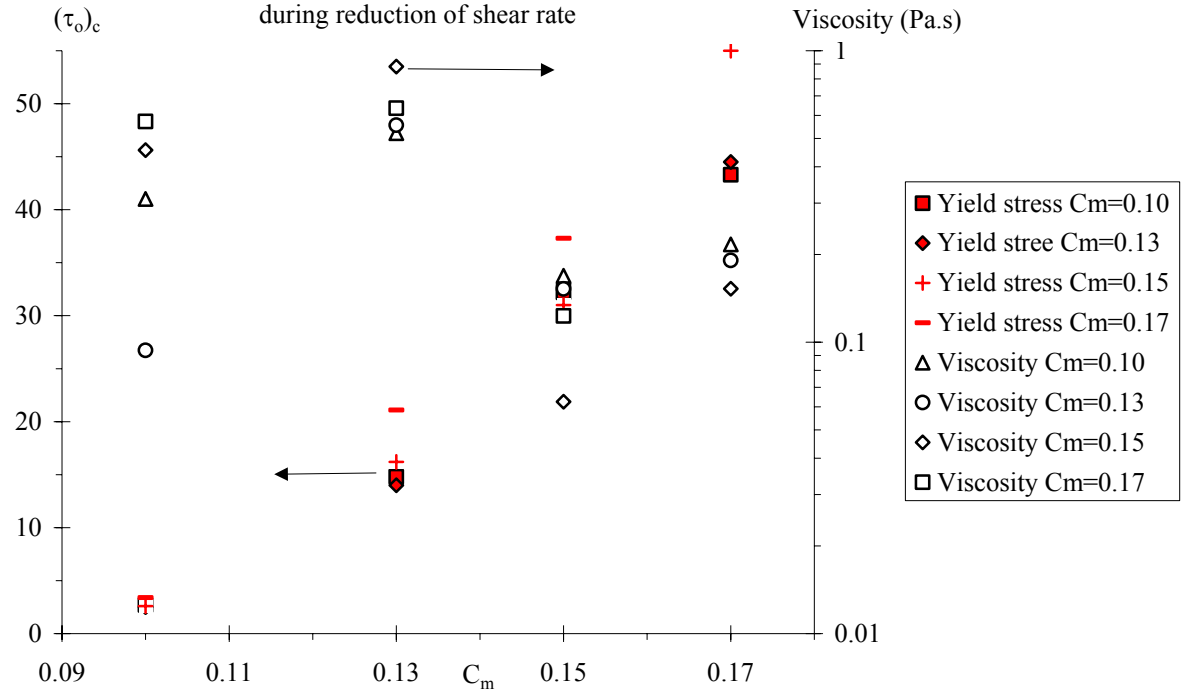

Table 4-2 - Measured properties of bentonite suspensions

C_m	ρ_s	T_o = 1 s		T_o = 60 s		T_o = 300 s		T_o = 900 s	
		τ_c	μ	τ_c	μ	τ_c	μ	τ_c	μ
	kg/m^3	Pa	Pa.s	Pa	Pa.s	Pa	Pa.s	Pa	Pa.s
(1)	(2)	(3)	(4)	(5)	(6)	(7)	(8)	(9)	(10)
0.10	1064	2.7	0.31	2.5	0.0937	2.6	0.4562	3.4	0.572
0.13	1085	14.8	0.5217	14	0.5555	16.2	0.8819	21.1	0.6351
0.15	1100	32.2	0.1689	33	0.1523	31	0.0625	37.3	0.123
0.17	1115	43.3	0.2166	44.5	0.1907	55	0.1525	--	--

Notes : τ_c, μ : yield stress and effective viscosity during unloading phase.

4.5 PREPARATION OF THE EXPERIMENTS

Prior to each test, the bentonite suspension was stirred for about 1 h to ensure that the fluid was de-structured completely. Then the suspension was poured into the reservoir, where it formed a quasi-two-dimensional, triangular reservoir. The free-surface was quasi-horizontal. The bentonite suspension was then rested for a given period of time T_o before the gate was suddenly opened. The gate removal was rapid (less than 0.1 sec.). (In the small plate facility, the same procedure was used. The fluid was poured into a mould, rested for a given period before the mould was suddenly removed.)

All measurements were conducted in ambient conditions (i.e. 20 Celsius).

5. BASIC FLOW PATTERNS

5.1 PRESENTATION

In the large experimental facility, several experiments were conducted systematically on a 15º slope with various masses of fluid, bentonite mass concentrations and rest times (Table 5-1). Details of the experimental flow conditions are summarised in Table 5-1, which lists the mass of fluid M (column 4), the initial reservoir fluid thickness d_o at the gate measured normal to the invert (column 5), the rest period T_o (column 6), the position of the front at end of experiment (column 7) measured from the gate, and the type of flow (column 8). In column 7, the mention N/A indicates that the fluid flowed past the downstream end of the plate.

For the range for investigated flow conditions, the results demonstrated four basic fluid flow patterns along the 2.0 m long plate ([8]). These are illustrated in Figures 5-1 to 5.4 and sketched in Figure 5-5. For small bentonite mass concentrations ($C_m \leq 0.15$) and short relaxation times ($T_o \leq$ 30 s), the fluid flowed rapidly down the constant-slope all along the plate length, and it spilled into the overflow container (Flow Type I). During the initial instants immediately following gate opening, the flow was subjected to a very-rapid acceleration over a short period. Inertial effects were dominant leading to some form of "orifice" flow motion. The flow was basically two-dimensional for $t^*\sqrt{g/d_o} < 4.1$, for the investigated flow configurations. Afterwards, the fluid flowed rapidly down the inclined chute. The suspension appeared to have a very low viscosity (Fig. 5-1).

For intermediate concentrations and rest periods, the suspension flowed rapidly initially (as described above), decelerated relatively suddenly, continued to flow slowly for sometimes and later the flow stopped, often before the plate downstream end (Flow Type II). Observations suggested three distinct flow periods. Immediately after gate opening, the fluid was rapidly accelerated. The flow out of the gate was quasi-two-dimensional and somehow similar to a sudden orifice flow. Then the suspension continued to flow rapidly although sidewall effects started to develop. The latter were associated with a slower front propagation at and next to the walls. Later the fluid decelerated relatively rapidly, and this was followed by a significant period of time during which the suspension continued to flow slowly before stopping ultimately. During and after the fluid deceleration, careful video analysis suggests that the front propagation was subjected to some form of perturbations. That is, the wave front (on centreline) seemed to accelerate and decelerate with periods of about 0.1 to 0.25 s ([9]). In view in elevation, the front exhibited a distinctive quasi-parabolic shape centred around the channel centreline. After stoppage, the fluid had a relatively uniform constant thickness but near the upstream end of the tail (Fig. 5-2).

For large mass concentrations and long rest periods, the mass of fluid stretched down the slope, until the head separated from the tail (Flow Type III, Fig. 5-3). After separation, a thin film of suspension connected the head and tail volumes which could eventually break for long travelling distance of the head (Fig. 5-3B). The head had a crescent ("croissant") shape. For long rest periods (i.e. several hours), several successive packets were sometimes observed (Flow Type IIIb). In flows Type IIIb, the packets of fluid were observed to be about the same mass ([10]), while the second and subsequent packets ran slower than the first packet of fluid. Sometimes a last packet would shear from the reservoir fluid although it did not flow (e.g. Test 20). For each packet, the fluid length (in the streamwise direction) measured on the centreline was typically about $1.5*d_o$ to $2.5*d_o$, independently of mass concentration and rest time.

---

[8]The present classification are based upon observations along the 2 m long plate, and it might be different on a longer plate

[9]Observations were limited by the video-cameras taking pictures at 25 Hz.

[10]For example, in Test 20, the mass of each fluid packet was about 0.8 to 0.95 kg, while the mass of the reservoir "tail" was 1.34 kg.

The last flow pattern (Type IV) corresponded to an absence of flow. That is, for large bentonite concentrations and long rest times, the fluid may not flow at all after the sudden gate opening, even after waiting 30 to 60 minutes.

Table 5-1 - Summary of experimental flow conditions with a constant slope $\theta = 15°$ (Large facility, chute width: 0.34 m)

Mass concentration	Solution density	Test	Mass	Initial height	Rest time	Front end position	Type of flow	Remarks
C_m	ρ		M	d_o	T_o	$(X_s)_{end}$		
	kg/m^3		kg	m	s	m		
(1)	(2)	(3)	(4)	(5)	(6)	(7)	(8)	(9)
0.10	1063.7	Test 11	1.505	0.0472	300	N/A (1)	II	
		Test 10	4.047	0.0774	14220	N/A	I-II	
		Test 09	4.059	0.0776	300	N/A	I	
		Test 27	4.149	0.0784	80880	N/A	III to IIIb	Several packets of gelled fluid after first packet.
0.13	1085.1	Test 25	1.614	0.0484	60	0.643	II	
		Test 24	2.728	0.0629	60	1.215	II	
		Test 23	3.69	0.0732	60	N/A	I	Almost transition between flow types I and II at downstream end.
		Test 21	3.718	0.0735	2400	1.204	II	Possibly close to transition between flow types II and III, with slight "crescent of crust" croissant" at leading edge.
		Test 22	3.72	0.0735	7200	1.089	III	
		Test 20	3.924	0.0755	62160	N/A	IIIb	2 packets plus 1 slide. Mass of first 2 packets: 1.812 kg. Mass of 3rd block (slide): 0.773 kg. Mass reservoir behind 3rd block: 1.339 kg.
		Test 19	3.936	0.0756	900	N/A	II	
		Test 18	3.952	0.0758	300	N/A	II	
0.15	1099.8	Test 04	3.141	0.0671	60	0.72	II	
		Test 03	3.364	0.0694	60	0.805	II	
		Test 02	3.504	0.0709	60	1.007	II	
		Test 07	3.652	0.0723	900	0.51	II to III	
		Test 06	3.686	0.0727	300	0.753	II	
		Test 08	3.689	0.0727	2400	0.565	III	
		Test 05	3.707	0.0729	60	0.958	II	
		Test 01	3.786	0.0737	60	1.055	II	
		Test 26	3.974	0.0755	62100	0.042	IIIb-IV	Sliding of one block without flow motion.
		Test 26b	3.974	0.0755	62100	N/A	Sliding	At end of Test 26, vibration of plate leading to 2D sliding of 1 block.
0.17	1115.0	Test 17	3.461	0.0699	20	0.381	II	
		Test 15	3.532	0.0707	300	0.241	II	
		Test 16	3.579	0.0711	900	0.15	III	
		Test 14	3.65	0.0718	60	0.527	II	
0.20	1138.4	Test 13	3.536	0.0700	30	0.078	II or III	High-speed mixing of suspension for 3 minutes before test.
		Test 12	3.684	0.0714	60	0	IV	No flow.

Notes : C_m : defined as the ratio of bentonite mass to bentonite & water mass; d_o : vertical reservoir height at the gate; T_o : rest time measured from the start of bentonite suspension pouring into the reservoir/mould; ρ : bentonite suspension density; (^{1}) : flow past downstream end of plate.

Transition between flow regimes

The experiments on the large inclined plate showed that the characteristic conditions for the transition between flow regimes were functions of the mass concentration of bentonite suspension C_m, rest time T_o and initial mass of fluid M. A summary of the observations is shown in Figure 5-6 for a fixed mass M, while all the results are given in Table 5-1 (column 8).

Basically the type of flow regime changed from no flow (Type IV) to a rapid flow (Type I) with increasing mass M, decreasing mass concentration C_m and decreasing rest period T_o. Figure 5-6 illustrates the trend in terms of mass concentration and rest period for a given mass of fluid and constant plate slope.

Fig. 5-1 - Photographs of Flow type I at the end of experiment - The fluid ran past the plate downstream end - Large facility (Test 23, $\theta_b = 15^o$, $C_m = 0.13$, rest period: $T_o = 60$ sec.)

Fig. 5-2 - Photographs of Flow type II (photographs taken after stoppage)
(A) Large facility (Test 04, θ_b = 15º, C_m = 0.15, rest period: T_o = 60 sec.)

(B) Small plate with square mould (θ_b = 24º, C_m = 0.20, rest period: 30 min.)

(C) Large facility (Test 05, θ_b = 15º, C_m = 0.15, rest period: T_o = 60 sec.) - View in elevation of the leading edge - Flow direction from top to bottom

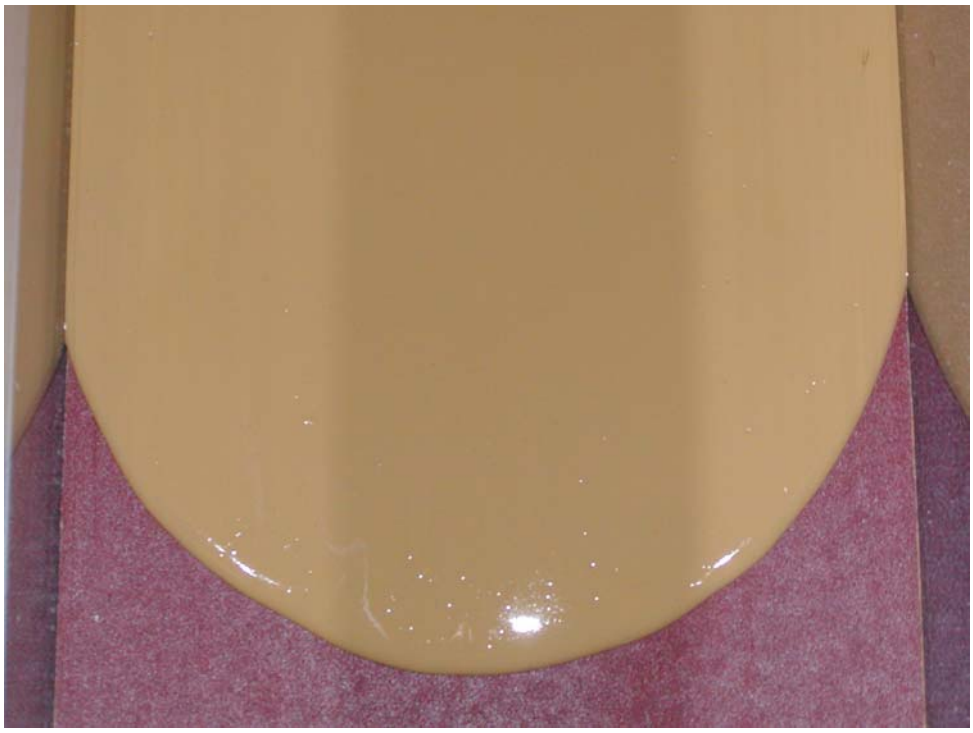

(D) Large facility (Test 05, θ_b = 15º, C_m = 0.15, rest period: T_o = 60 sec.) - Side view - Flow direction from top to bottom

Fig. 5-3 - Photographs of Flow type III (photographs taken after stoppage)
(A) Large facility (Test 08, θ_b = 15º, C_m = 0.15, rest period: T_o = 40 min.) - Flow direction from right to left

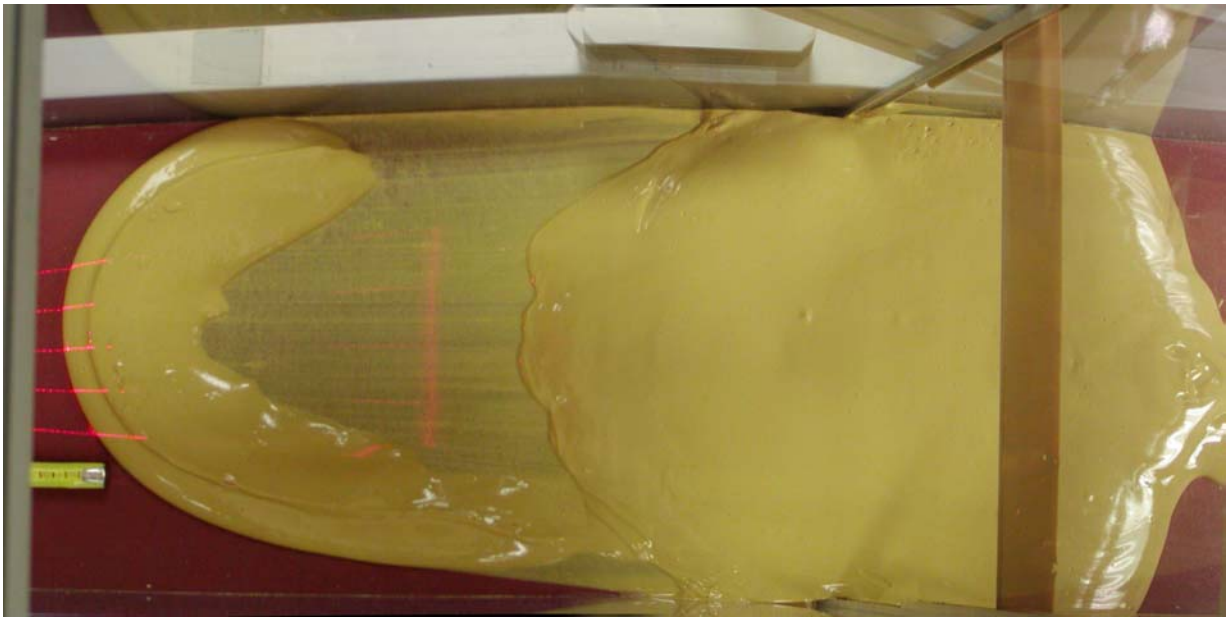

(B) Small plate with cylindrical mould (θ_b = 16.6º, C_m = 0.20, rest period: T_o = 30 sec.)

(C) Large facility (Test 08, θ_b = 15º, C_m = 0.15, rest period: T_o = 40 min.) - Detail of the head volume - Flow direction from top to bottom

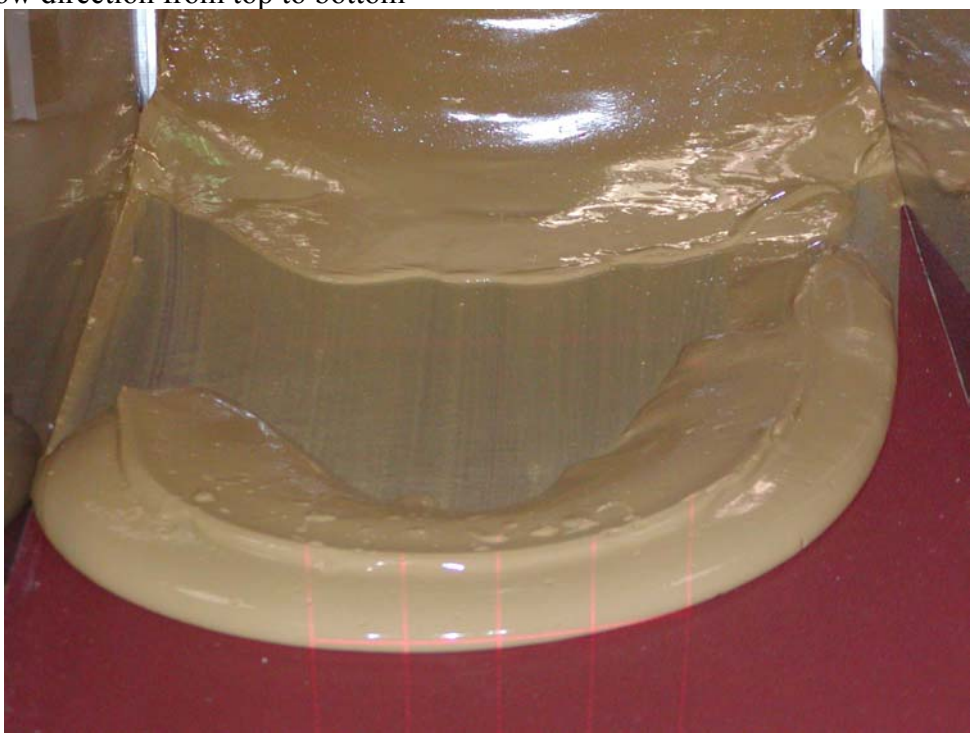

Fig. 5-4 - Photograph after stoppage of an experiment at the transition between Type II and Type III flow regimes - Detail of the head with a crescent of re-structured fluid at the top- Large facility (Run 07, θ_b = 15º, C_m = 0.15, rest period: T_o = 15 min.) - Flow direction from right to left

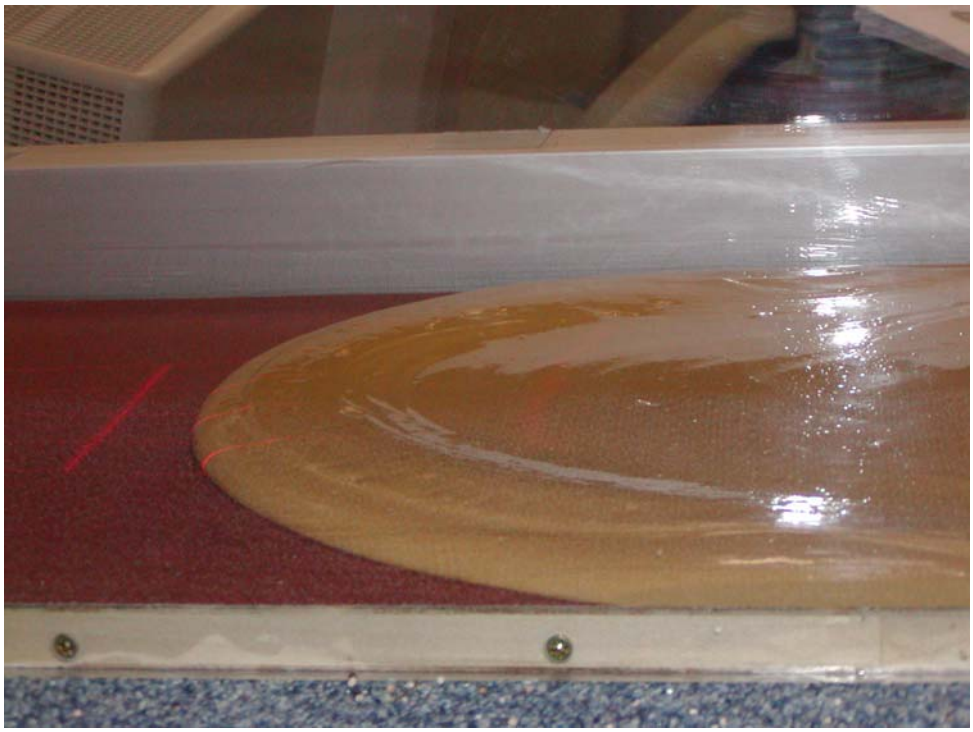

Fig. 5-5 - Sketch of Flow Types II and II
(A) Flow Type II

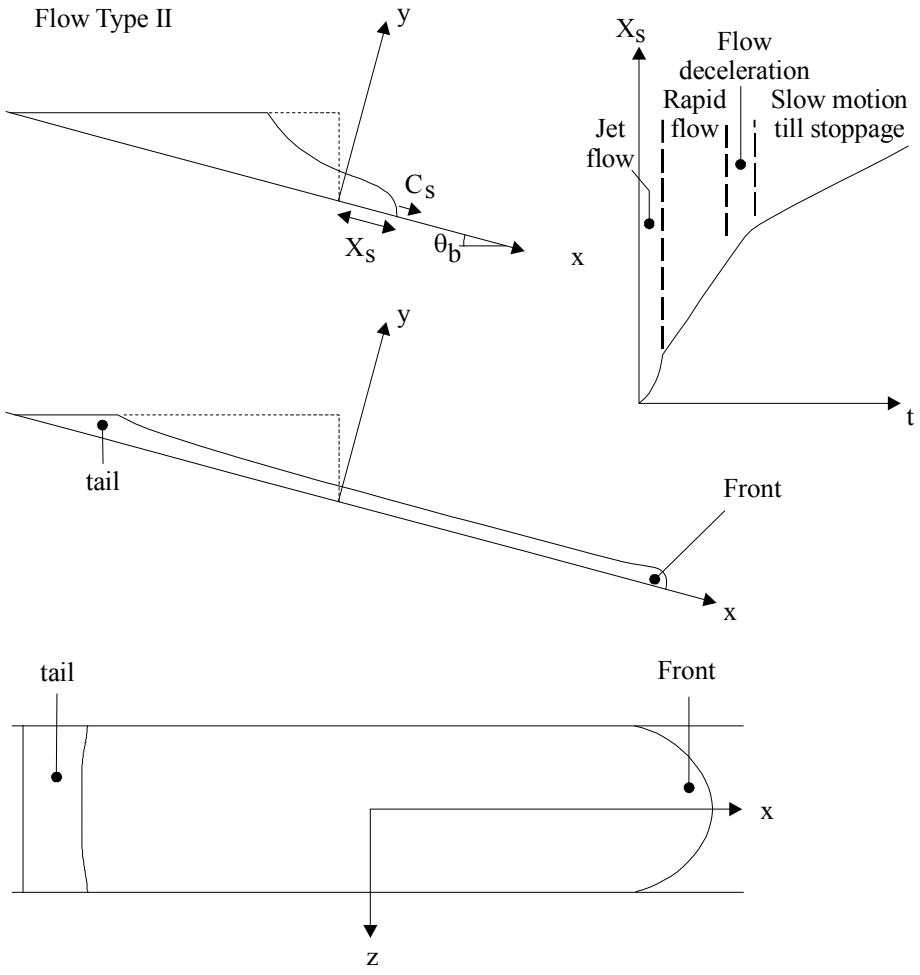

5.2 DISCUSSION

The physical observations of flow regimes were in remarkable agreement with the theoretical considerations developed in paragraph 2.3. Theoretical results are qualitatively similar to the experimental ones. In particular, exactly the same flow regimes can be identified as well as same trends for the effects of the bentonite concentration and rest time. For example, theoretical considerations predict an intermediate motion with initially rapid before final fluid stoppage for intermediate mass of fluid M (i.e. $d_o/h_c > 1$) and intermediate initial rest period T_o, where d_o is the initial reservoir height and h_c is a critical fluid thickness below which the fluid flow motion tends to complete stoppage

$$h_c = \frac{\mu_o * (n - 1)^{1/n}}{\theta * \alpha * \rho * g * S_o} \qquad (2\text{-}30)$$

The theory predicts a more rapid flow stoppage with increasing rest period. Similarly, it shows that an increase in bentonite mass concentration, associated with an increase in the product ($\theta*\alpha$) (paragraph 6.4), yields a faster fluid stoppage with a larger final fluid thickness. A similar comparison between theory and physical experiments may be developed for fast-flowing motion and relatively-rapid flow stoppage situations.

(B) Flow Type III

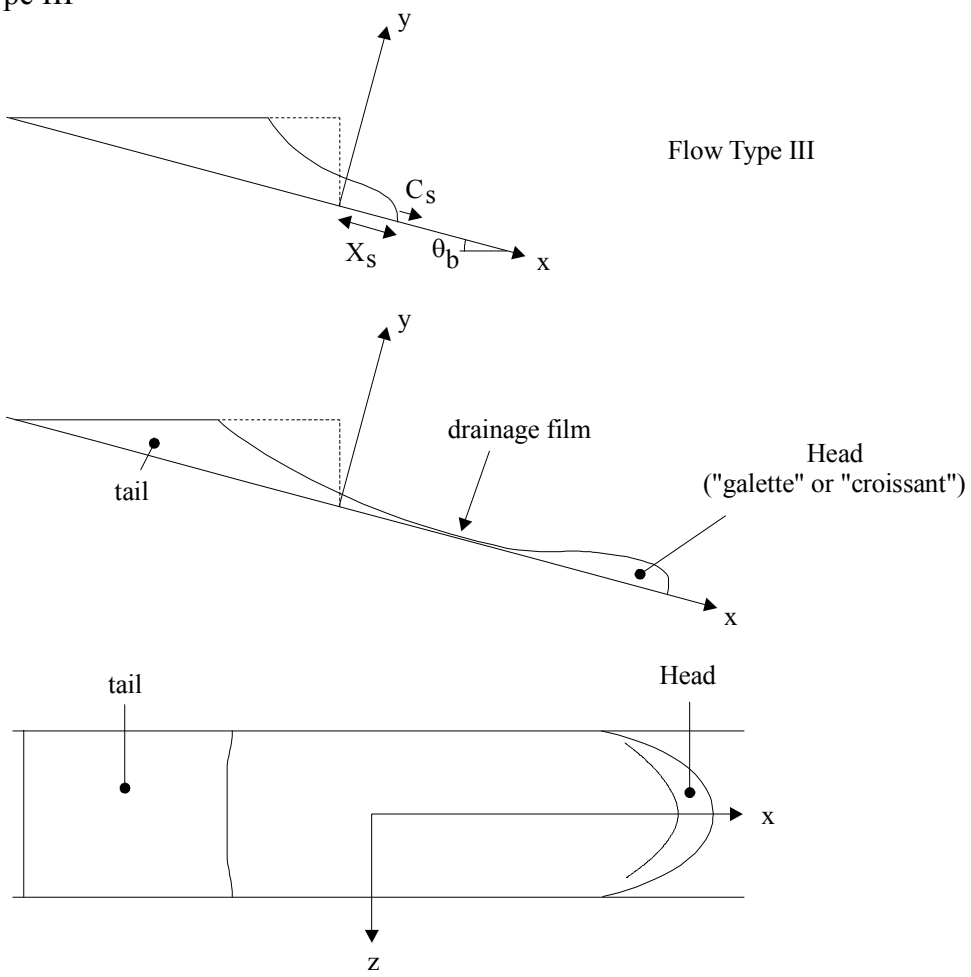

Fig. 5-6 - Chart of flow regimes : rest time T_o as function of the mass concentration C_m for a given mass of fluid (M = 3.7 kg) and fixed slope (θ_b = 15°) - Comparison with experimental flow conditions

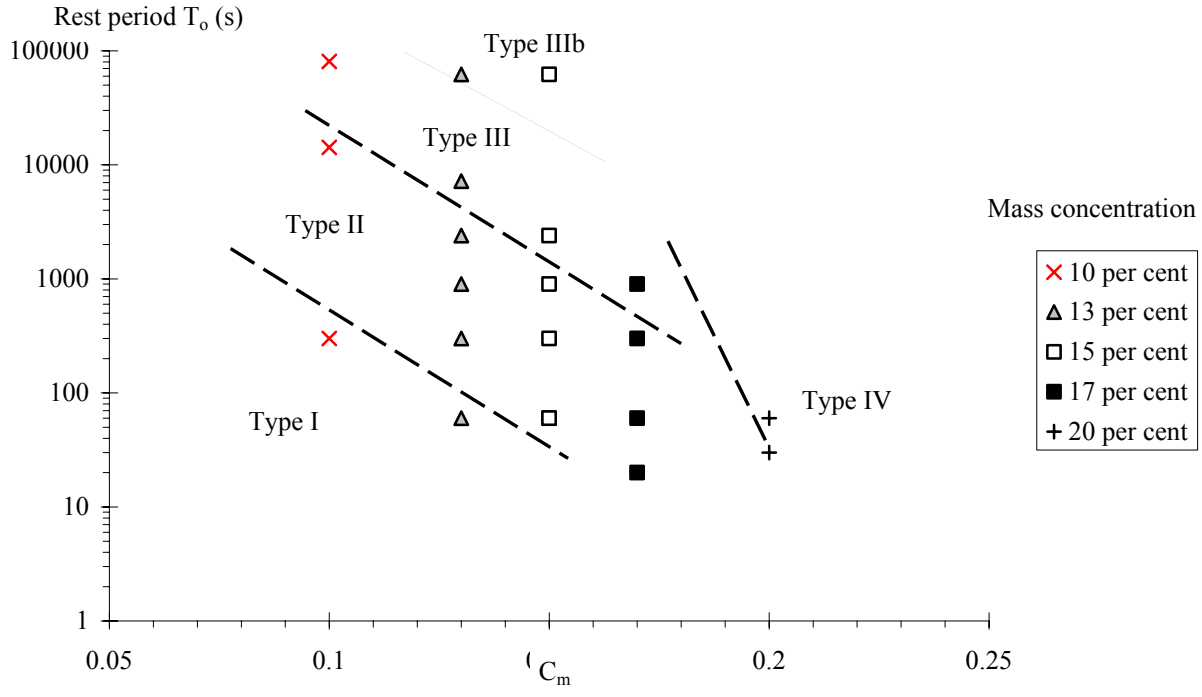

This qualitative agreement between simple theory and reality means that the basic physical ingredients of the rheological model and kinematic wave equations are likely to be at the origin of the observed phenomena. Considering the strongly different flow regimes involving either solid or liquid regions in a complex interplay, this suggests that, in contrast with usual models devoted to a specific field, a model of this type is capable to reproduce the different stages of flow of natural mass movements which turns from solid to liquid or from liquid to solid. In contrast with the usual separation of materials in distinct categories, the apparent behaviour of a jammed material under continuously varying conditions can cover all possible liquid or solid aspects.
Lastly it is interesting to note that the Flow Type III is the only flow pattern not predicted by theoretical considerations. It is believed that this situation reflects simply the limitations of the Saint-Venant equations that are one-dimensional flow equations, and of the kinematic wave approximation that implies a free-surface parallel to the chute invert, hence incompatible with the Type III free-surface pattern.

5.3 REMARKS

The opening of the gate was associated with both a shock propagation downstream (i.e. dam break wave) and a negative wave propagating upstream into the reservoir. The negative wave propagation was associated with a drawdown (emptying) of the reservoir similar to a reservoir drawdown with laminar and turbulent Newtonian fluid. For most flow conditions, no shearing/sliding was observed in the reservoir tail, but in Flow Type IIIb (see paragraph 5.1).
Near the transition between Flow Type II and Type III, the development of a crescent of re-structured fluid at the surface of the fluid next to the front was observed. This is illustrated in Figure 5-4, while the conditions for the transition between types of flow are discussed in paragraph 5.1.

6. EXPERIMENTAL RESULTS

6.1 FRONT CURVATURE

During flow motion, the fluid exhibited a curved front, viewed in elevation for all investigated flow conditions. This is well illustrated in Figures 5-2 (e.g. Fig. 5-2C) and 5-4. Experimental measurements of wave front shape at several instants after gate opening are presented in Figure 6-1 for experiments with Flow Types I, II and III. The results showed that the front curvature increased with time, hence the travelled distance X_S, for a given experiment. Further video-observations demonstrated slower fluid motion next to the sidewalls.

For all experiments, the flow curvature developed rapidly, and it exhibited a power law profile that was best fitted by :

$$\frac{X}{d_o} \propto \left(\frac{Z}{d_o}\right)^{0.4} \qquad (6\text{-}1)$$

where $X = X_S - x$, Z is the transverse distance measured from the centreline, X_S is the coordinate of the front and d_o is the initial reservoir thickness at the gate. Basically X = 0 and Z = 0 at the shock front on the channel centreline. Importantly Equation (6-1) was obtained independently of time t, initial mass M, mass concentration C_m, rest period T_o and flow regime. It is compared with experimental observations in Figure 6-1.

Interestingly HUANG and GARCIA (1998) presented a photograph showing a similar front curvature with kaolinite suspension mud flows, but they did not elaborate on the shock front curvature.

Discussion

Since the polycarbonate panels of sidewalls were much smoother than the invert, it was unlikely that sidewall friction played a preponderant role in the front curvature. Further calculations of sidewall boundary layer development showed that these were thin : i.e., typically a few centimetres at x = 0.5 m ([11]). Hence sidewall boundary layers could not explain the curved profile over distances as short as during the present study. Another possible explanation could be the development of shock waves, or cross-waves, induced by the gate grooves, since cross-waves are always associated with some flow concentration. Shock waves are commonly encountered in supercritical open channel flows (e.g. HENDERSON 1966, CHANSON 2004a). They initiate at a sidewall disturbance and propagate downstream across the channel (IPPEN and HARLEMAN 1956). During the present study, no shock wave was visually observed.

The front curved profile might be caused by interactions between sidewall and bottom boundary layers. Indeed the flow was quasi-two-dimensional as long as flow resistance had little effect on the fluid motion (paragraph 6.2). At present, the marked curvature of the surge front over such short distances is not yet fully understood.

[11] Simplified calculations were conducted assuming either laminar or turbulent boundary layers.

Fig. 6-1 - Curved profiles of the wave front, viewed in elevation of the front

(A) Test 23, θ_b = 15º, C_m = 0.13, M = 3.7 kg, rest period: 60 s, Flow Type I (almost Type II)

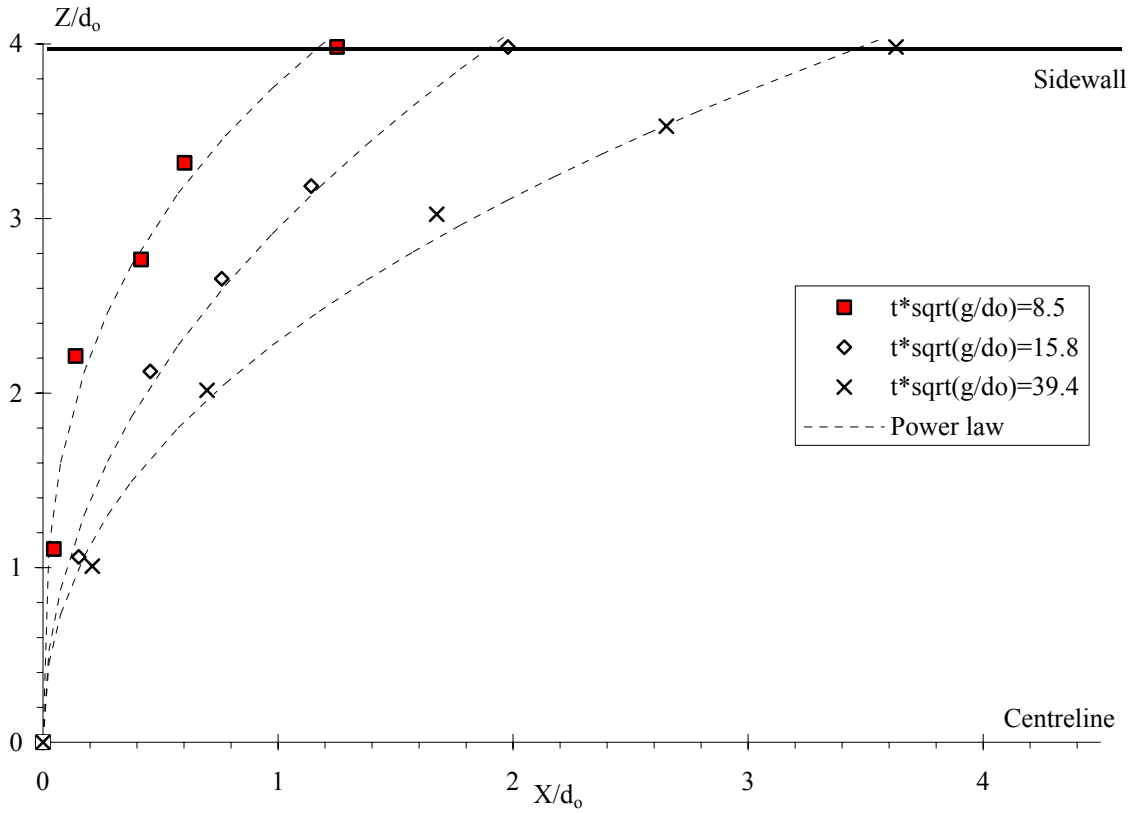

(B) Test 25, θ_b = 15º, C_m = 0.13, M = 1.6 kg, rest period: 60 s, Flow Type II

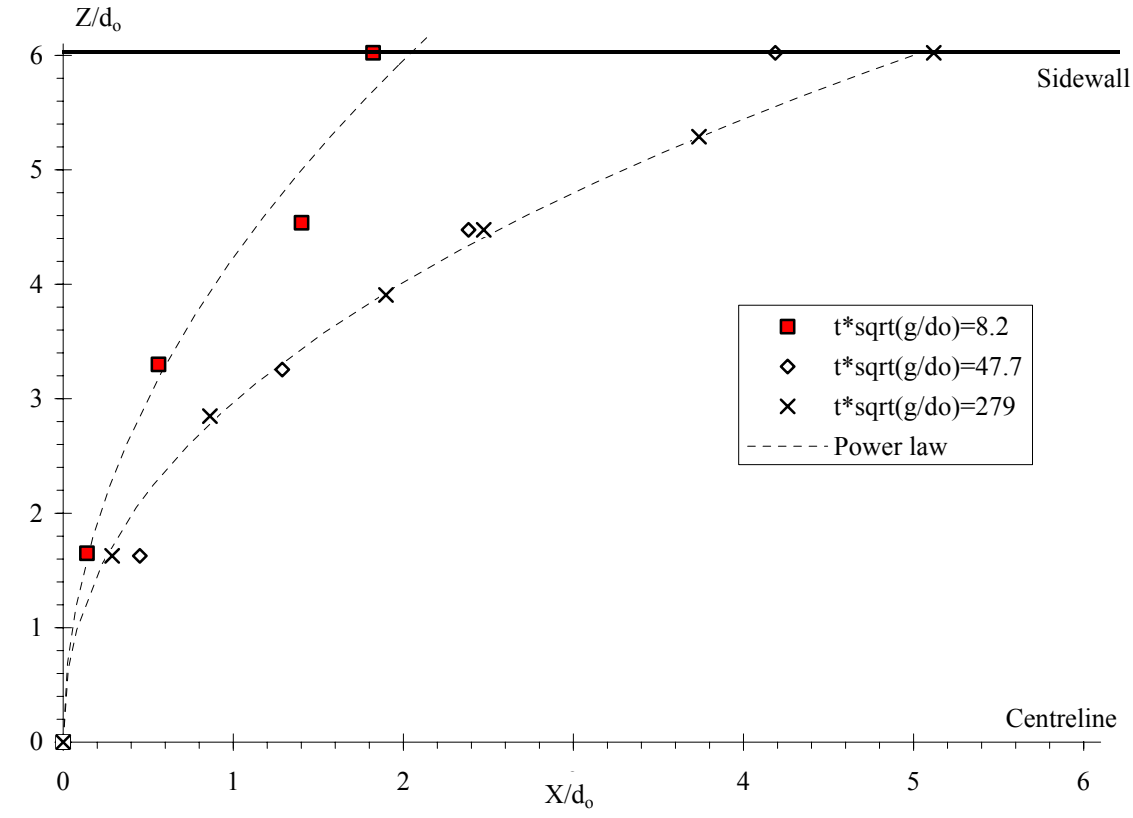

(C) Test 22, θ_b = 15º, C_m = 0.13, M = 3.7 kg, rest period: 7,200 s, Flow Type III

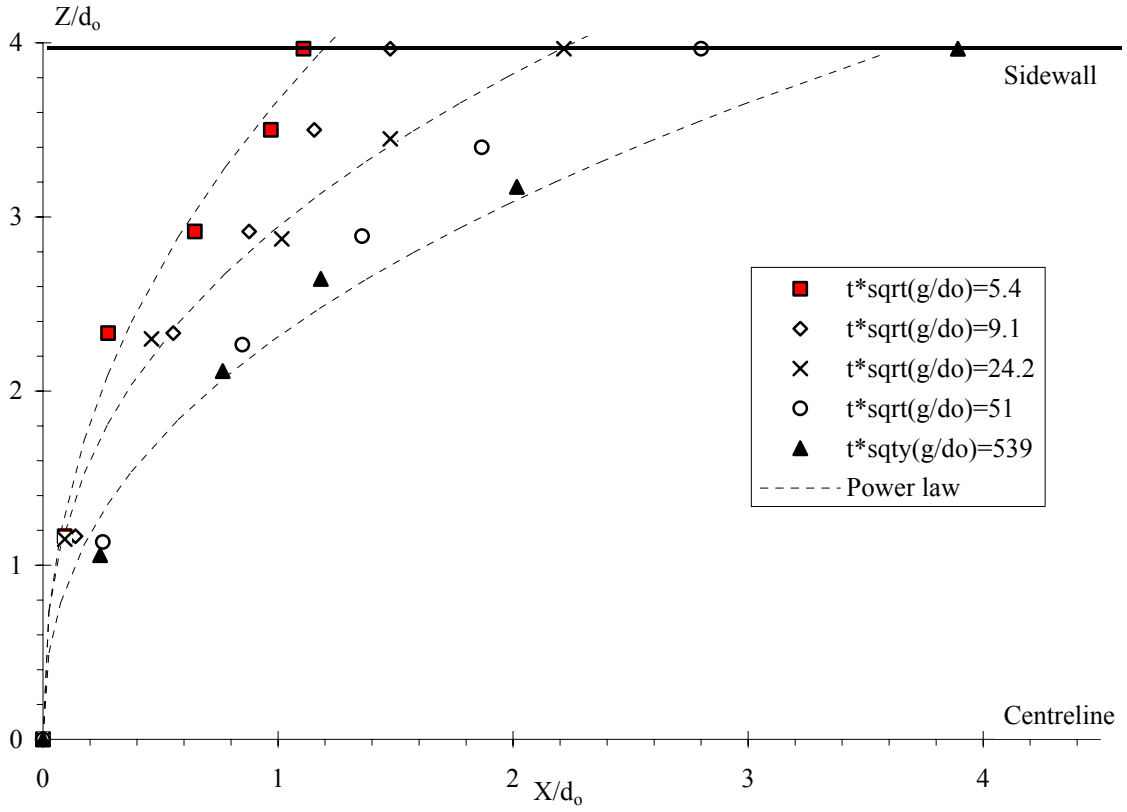

6.2 WAVE FRONT PROPAGATION

The propagation of the wave front was investigated with video-cameras. Typical results are presented in Figures 6-2 and 6-3. Figure 6-2 presents the dimensionless wave front location X_S/d_o as function of the dimensionless time $t^*\sqrt{g/d_o}$, while Figure 6-3 shows the relative shock location $X_S/(X_S)_{end}$ as function of the dimensionless time, where $(X_S)_{end}$ is the final location of the front after stoppage on the plate ([12]). In addition, the dimensionless wave front celerity $C_S/\sqrt{g^*d_o}$ is plotted ([13]). On some graphs, data from several cameras are presented showing good agreement between all data, independently of camera location and type. In addition, a small number of experiments were repeated. The results demonstrated conclusively the repeatibility of the experiments.

Figures 6-2 and 6-3 regroup experimental data for a range of Flow Types, bentonite suspension mass concentrations and rest periods. Note that Figure 6-2C shows data for a Flow Type IIIb, and the data include the propagation of the second packet of fluid behind the main front.

Discussion

For the Flow Type II (and possibly some Flow Types I and III), the extrapolation of present results to an infinitely long inclined plate yields a relationship between wave front location and time, that is sketched on Figure 6-4, with five characteristic periods (before stoppage).

[12]This presentation can only be applied to experiments for which the fluid stopped before the downstream end of the plate : i.e., $(X_S)_{end} < 1.245$ m (Fig. 4-1).

[13]The wave front celerity C_S was calculated simply by linear interpolation.

Fig. 6-2 - Wave front propagation on the channel centreline : X_S/d_o as function of the dimensionless time $t^*\sqrt{g/d_o}$

(A) Flow Type I (almost Type II) - Test 23, $\theta_b = 15°$, $C_m = 0.13$, M = 3.7 kg, rest period: 60 s

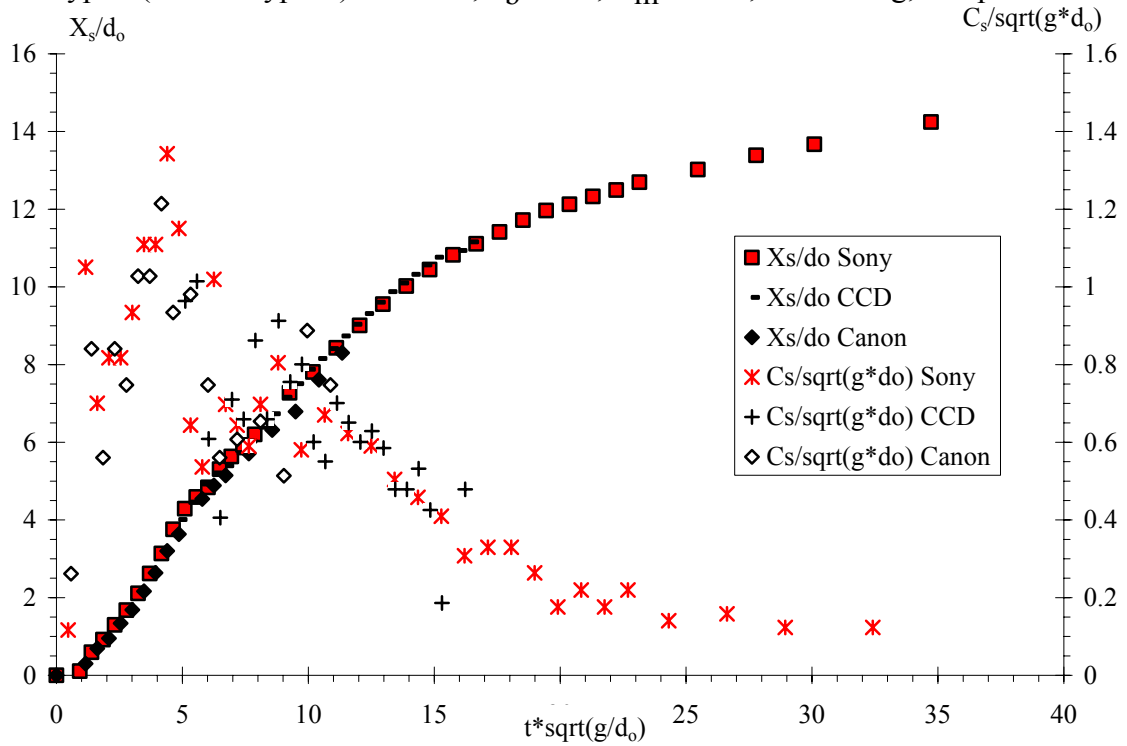

(B) Flow Type II - Test 11, $\theta_b = 15°$, $C_m = 0.10$, M = 4.0 kg, rest period: 14,420 s (3 h 57 min.)

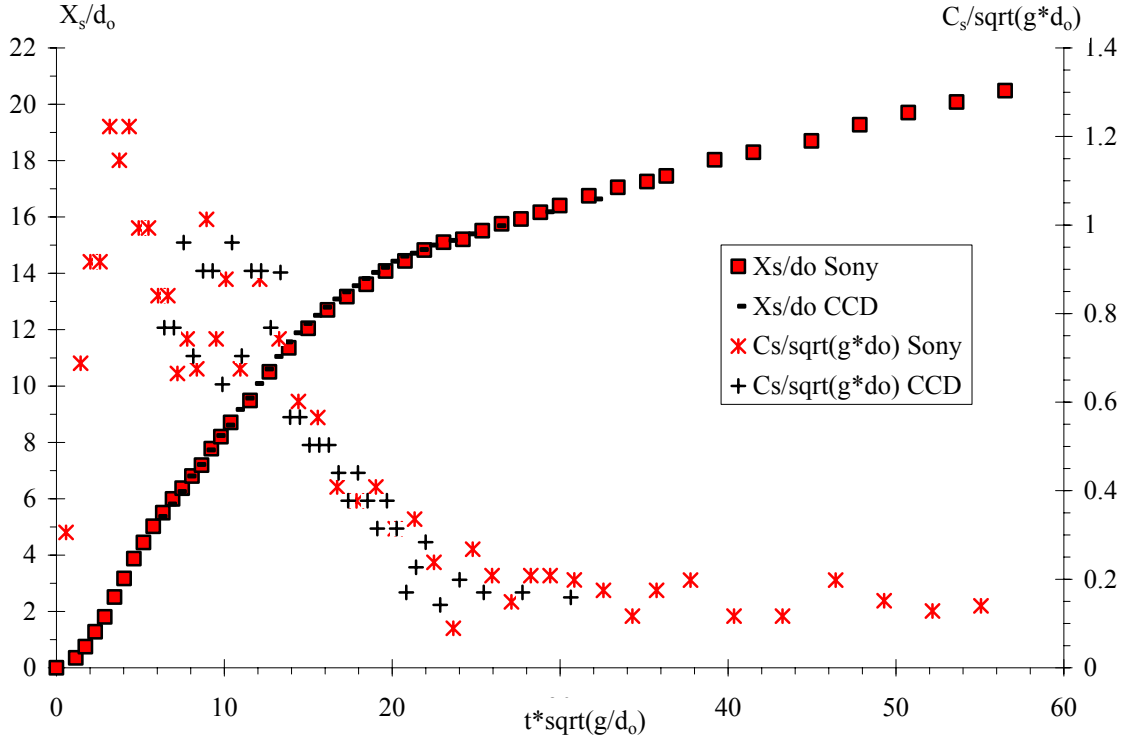

(C) Flow Type IIIb - Test 20, θ_b = 15°, C_m = 0.13, M = 3.9 kg, rest period: 62,160 s (17 h 16 min.)
Note the data for the second packet of fluid

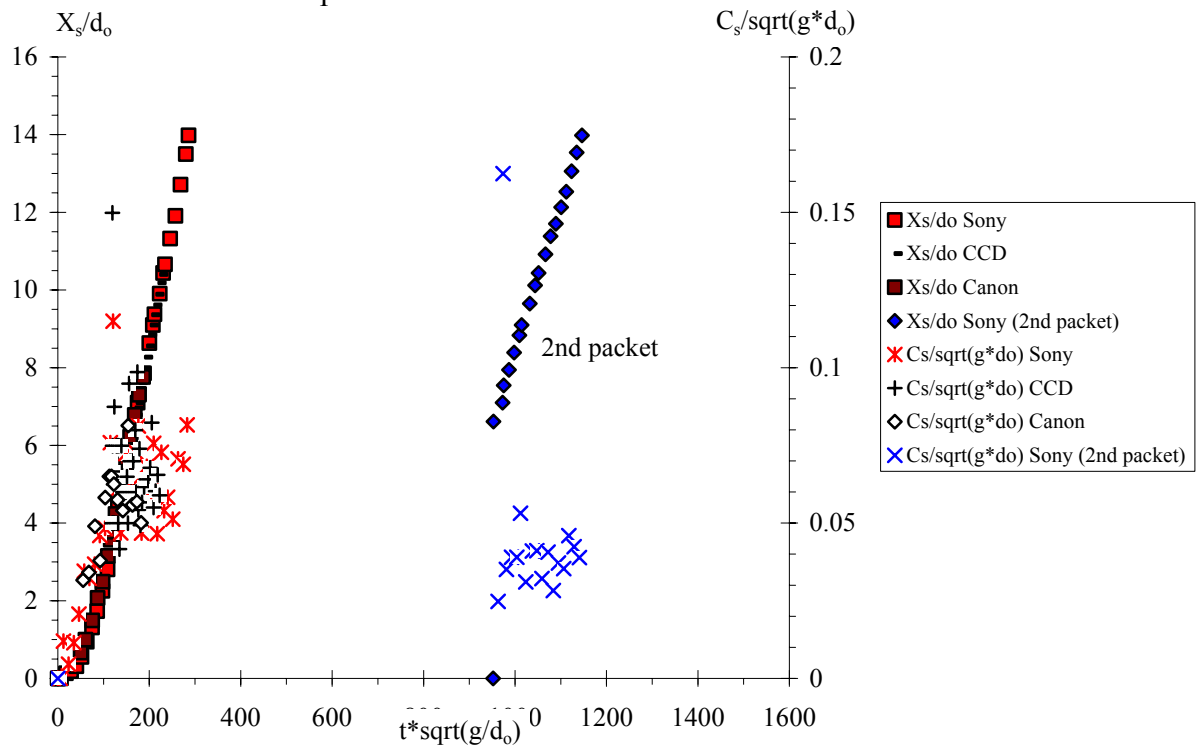

Fig. 6-3 - Wave front propagation on the channel centreline : $X_s/(X_s)_{end}$ as function of the dimensionless time $t^*\sqrt{g/d_o}$

(A) Flow Type II - Test 6, θ_b = 15°, C_m = 0.15, M = 3.7 kg, rest period: 300 s

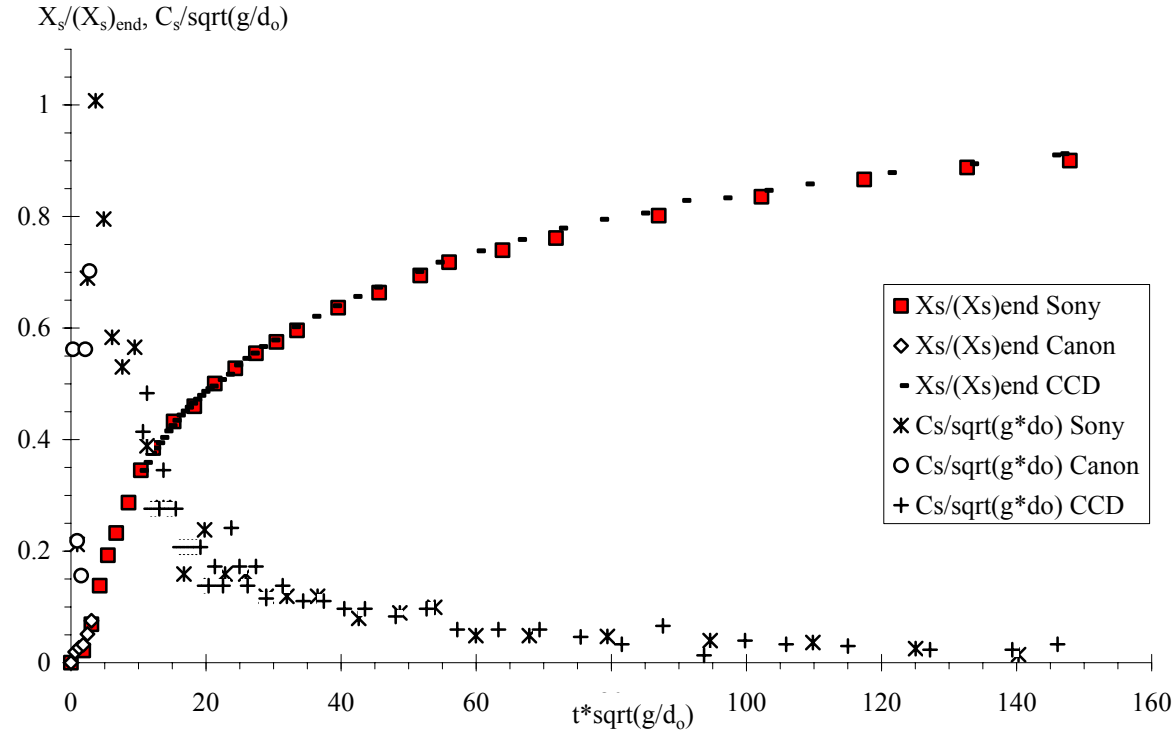

(B) Flow Type III - Test 8, θ_b = 15°, C_m = 0.15, M = 3.7 kg, rest period: 2,400 s (40 min.)
Note the data for the trailing packet of fluid (i.e. the tail)

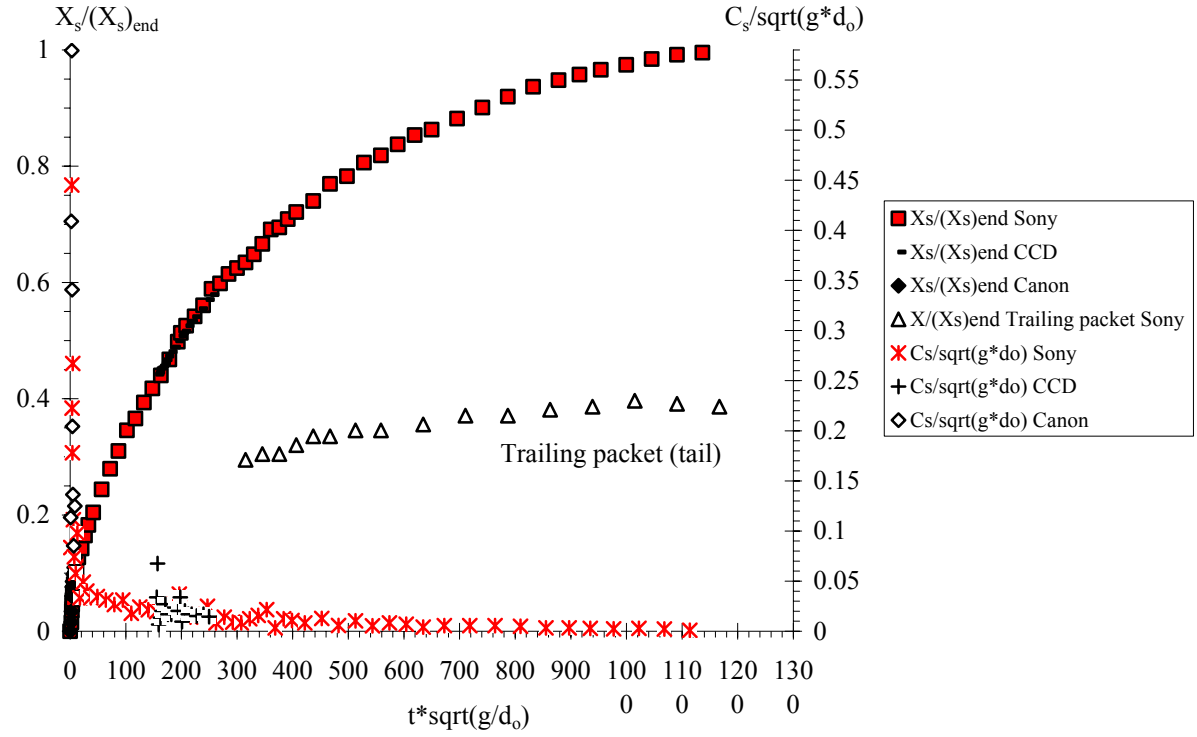

The initial instants following the gate opening are characterised by a very-rapid acceleration of the fluid. The flow is somehow similar to a jet flow motion. The fluid is subjected to an acceleration component parallel to the plate caused by the gravity acceleration component, as well as to an acceleration component normal to the invert as the result of both gravity component and sudden lowering of the reservoir free-surface. Neglecting the acceleration component normal to the invert, the wave front location and celerity in the initial instants after gate opening may be deduced from the motion equation as:

$$\frac{X_s}{d_o} = \frac{1}{2} * \left(t * \sqrt{\frac{g*\sin\theta_b}{d_o}} \right)^2 \qquad (6\text{-}2)$$

$$\frac{C_s}{\sqrt{g * d_o}} = t * \sqrt{\frac{g*\sin\theta_b}{d_o}} \qquad (6\text{-}3)$$

assuming little flow resistance. The latter is reasonable since the fluid starts from zero velocity. Equations (6-2) and (6-3) imply that the flow acceleration derives solely from the gravity force component in the longitudinal direction.

Equations (6-2) and (6-3) are compared with experimental data in Figure 6-5. Basically the comparison is favourable for $t*\sqrt{g/d_o}$ < 4.5 to 6, which corresponds basically to the period for which the wave front is two-dimensional (paragraph 5.1). The result demonstrates that the initial flow motion is somehow similar to a jet flow motion and that it is little affected by bed friction.

When the wave front starts to become three-dimensional (i.e. start to be curved as viewed in elevation), the relationship between front location and time becomes nearly linear, and the flow motion remains rapid (Fig. 6-4). For $t*\sqrt{g/d_o}$ ~ 10 to 20, a relatively strong flow deceleration is observed, which is seen by a sharp change in the slope of the function $C_S(t)$ (e.g. Fig. 6-2A and 6-2B). It is thought that the fluid motion at the wave front is characterised by a shear-dominated region next to the invert, an upper fluid layer and an interfacial zone (Fig. 6-6). In the upper flow

zone, the fluid is subjected to much less stress, it has time to restructure and its apparent viscosity increases significantly.
After the marked flow deceleration, experimental observations show that a relatively slower flow motion, followed by a very-slow flow motion. The latter is nearly a "creeping" motion, until stoppage.

Fig. 6-4 - Sketch of wave front propagation results

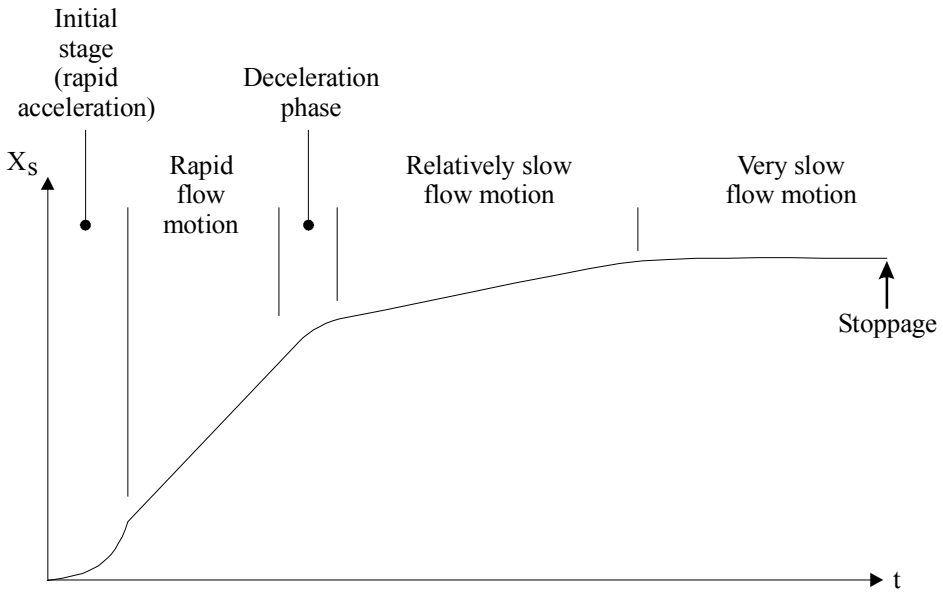

Fig. 6-5 - Wave front propagation immediately after gate opening - Comparison with Equations (6-2) and (6-3)

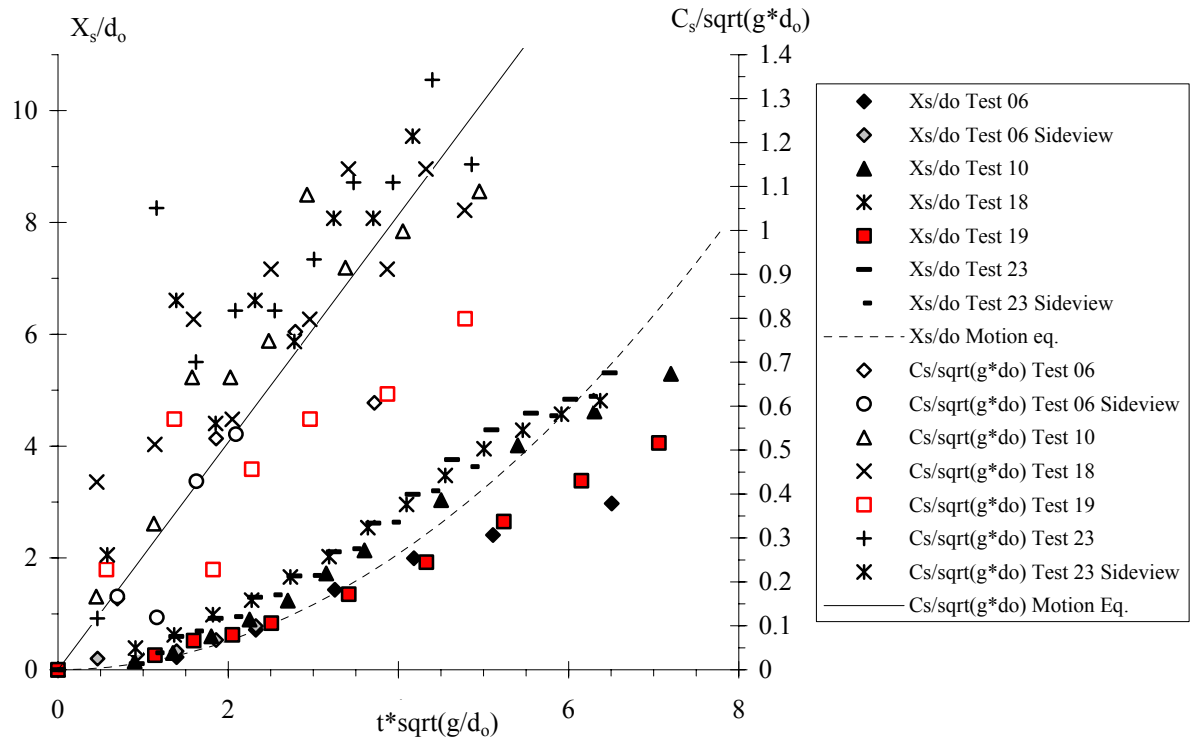

Fig. 6-6 - Sketch of fluid entrainment and recirculation at the wave front

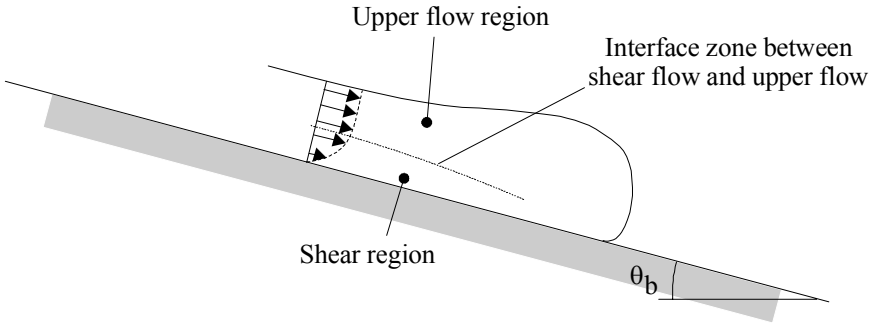

Remark
All experiments showed a strong flow acceleration immediately after gate opening. Observations of maximum shock celerity and corresponding instant are summarised in Table 6-1 (columns 2 and 3). The results were basically dependent primarily upon the Flow Type. Further a Reynolds number was estimated in terms of the maximum shock celerity $(C_S)_{max}$, initial reservoir height d_o and measured fluid properties (Table 4-2). The results are presented in Table 6-1 (column 4).
First the fluid acceleration for $0 < t < t_{max}$ is about $g*\sin\theta$. The result is consistent with the above discussion. Second the lesser maximum shock celerity observed in Flow Types II and III may indicate some incomplete destructuration of the fluid at gate opening. Second the Reynolds number of Flow Type I is significantly high; it is relevant to ask if the flow was turbulent or laminar. Although the transition between laminar and turbulent flows is typically for Re ~ 1,000 to 10,000 in industrial circular pipes, this estimate is based upon relatively smooth-boundaries. Turbulent flows may be observed for much lower Reynolds numbers with large roughness, and it cannot be excluded that turbulent flow motion was experienced during the present study in Flow Type I.

Table 6-1 - Maximum shock celerity $(C_S)_{max}$, instant t_{max} at which it occurs and corresponding flow Reynolds number $\rho*(C_S)_{max}*d_o/\mu$

Flow Type	$\frac{(C_S)_{max}}{\sqrt{g*d_o}}$	$t_{max}*\sqrt{\frac{g}{d_o}}$	$\rho*\frac{(C_S)_{max}*d_o}{\mu}$	Remarks
(1)	(2)	(3)	(4)	(5)
Type I	1.5	4.2	310	3 experiments.
Type II	0.86	3.4	150	13 experiments.
Type III	0.37	2.3	73	5 experiments.

Notes : ρ : fluid density; μ : measured effective viscosity (paragraph 4.4).

6.3 SIDE PROFILES OF THE SURGE FRONT

Visual observations through the sidewalls showed that the surge front has a smooth shape during the flow motion. Typical examples are shown in Figures 6-6 and 6-7. Figure 6-6 presents the longitudinal wave front at a given time. Test conditions and instantaneous flow properties are given in caption with the time t since gate opening, the wave front position X_S on the centreline and the wave front celerity C_S. Figure 6-7 presents time variations of fluid height at a given location. Both centreline and sidewall data are shown.

Fig. 6-6 - Longitudinal wave front profile at a fixed time
(A) Flow Type I-II - Test 10, θ_b = 15º, C_m = 0.10, M = 4.05 kg, rest period: 14,220 s (3 h 57 min.)
Centreline data: t = 0.91 s, X_S = 0.575 m, C_S = 0.56 m/s
Sidewall data : t = 1.03 s, X_S = 0.63 m, $(X_S)_{wall}$ = 0.571 m, C_S = 0.57 m/s

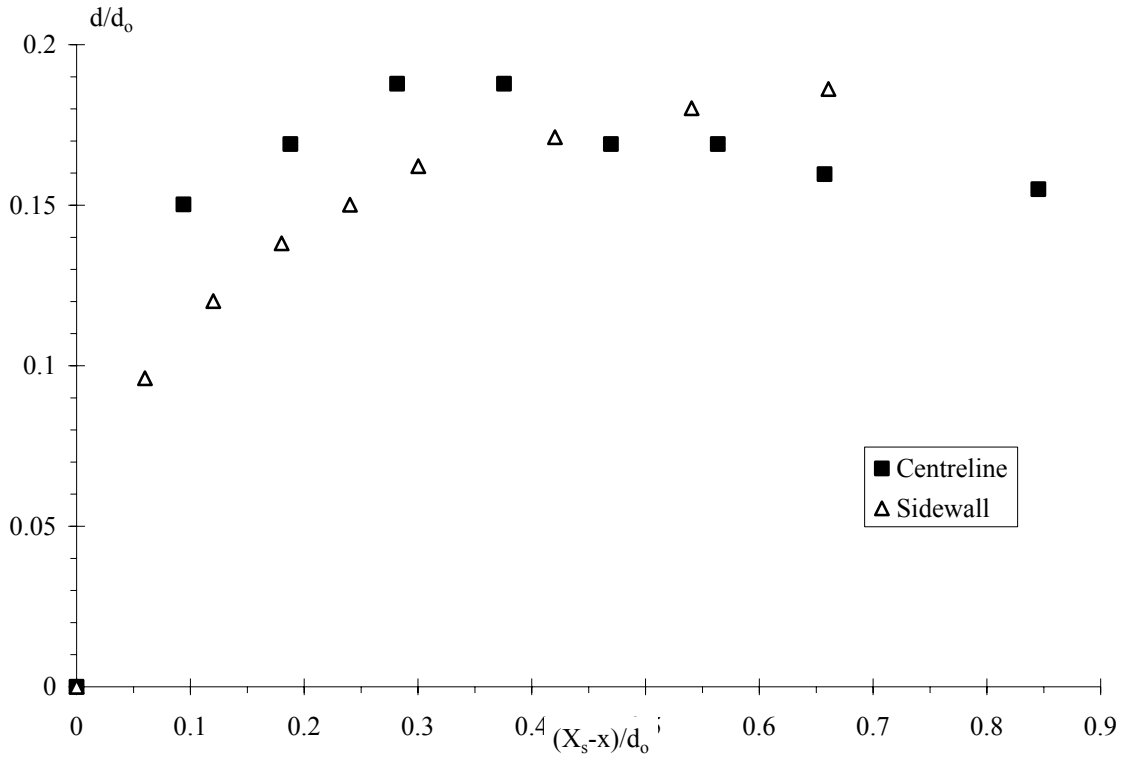

(B) Flow Type II - Test 19, θ_b = 15º, C_m = 0.13, M = 3.93 kg, rest period: 900 s (15 min.)
Centreline data: t = 1.36 s, X_S = 0.630 m, C_S = 0.29 m/s
Sidewall data : t = 1.72 s, X_S = m, $(X_S)_{wall}$ = 0.61 m, C_S = 0.19 m/s

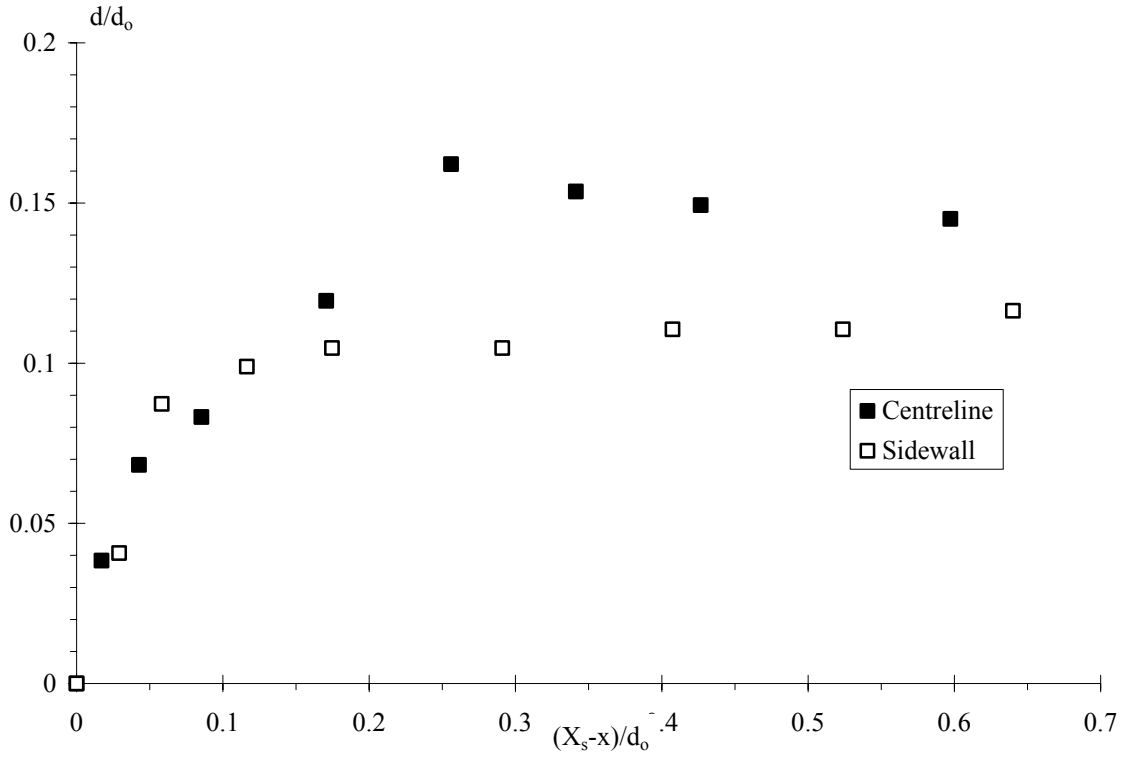

(C) Flow Type III - Test 8, θ_b = 15º, C_m = 0.15, M = 3.69 kg, rest period: 2400 s (40 min.)
Centreline data: t = 0.60 s, X_s = 0.072 m, C_s = 0.041 m/s

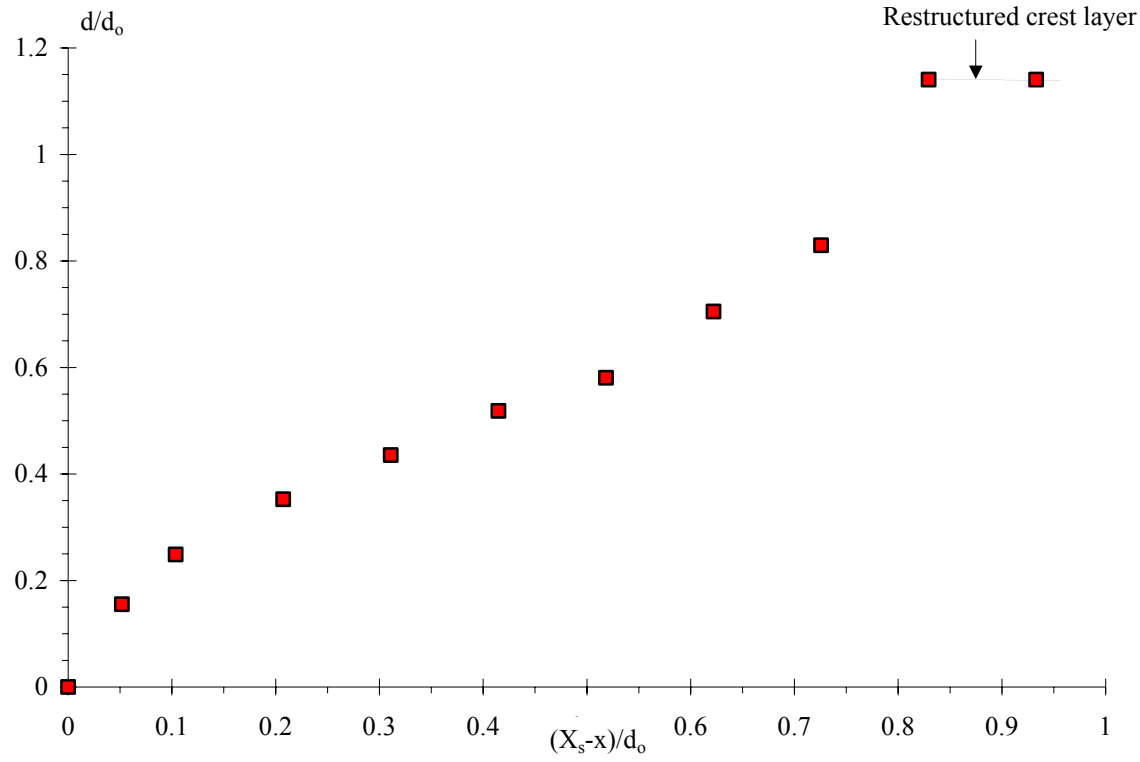

Fig. 6-7 - Time variations of wave front profile at a fixed location (x = 0.541 m)
Flow Type II - Test 5, θ_b = 15º, C_m = 0.15, M = 3.71 kg, rest period: 60 s
Centreline data: t_s = 0.46 s, X_s = 0.541 m
Sidewall data : t_s = 1.38 s, X_s = 0.583 m, $(X_s)_{wall}$ = 0.541 m

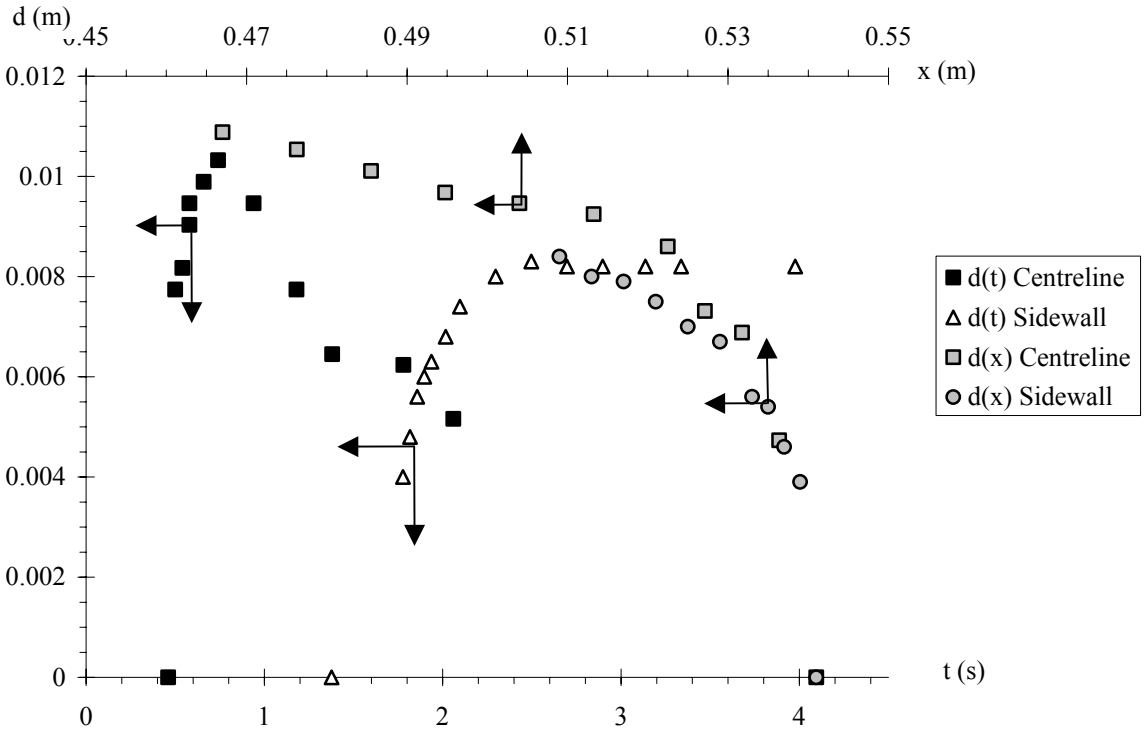

First the experimental data demonstrated a smooth shape. In Flow Type III, however, a cap of restructured fluid was observed shortly after gate opening. This is illustrated in Figure 6-6C. The finding indicates that the restructured fluid next to the reservoir free-surface was not subjected to high shear rate, although it was entrained by the flowing fluid beneath.
Second, in Flow Types I and II, the surge front on the centreline was thicker than the nappe of fluid behind. This is illustrated in Figures 6-6A and 6-6B showing a thicker shock than the fluid behind.
Third, there were consistently differences between centreline and sidewall profiles. This is seen in Figures 6-6 and 6-7.

6.4 FREE-SURFACE PROFILES AFTER STOPPAGE

Detailed free-surface profiles after complete fluid stoppage were measured based upon the deformation of the laser grid illumination. Typical results are presented in Figure 6-8 where $X = X_S - x$ and d_{end} is the measured fluid thickness after complete stoppage. Detailed experimental results are presented in Appendix D for completeness.
For all experiments, the results showed consistently very little transverse variations of the fluid thickness, and a smooth increase in fluid thickness in the downstream direction towards the shock. It is proposed that the wave front decelerated first while the fluid behind might slow slightly faster, yielding a gradual increase in fluid mass toward the shock. This would be also consistent with visual observations showing some fluid motion up to 1 to 2 minutes after the front stoppage.

Discussion

Theoretical fluid motion and rheology considerations yield a characteristic fluid thickness h_c below which the fluid flow motion tends to complete stoppage (paragraph 2.3.2) :

$$h_c = \frac{\mu_o * (n - 1)^{1/n}}{\theta * \alpha * \rho * g * S_o} \qquad (2\text{-}30)$$

where ρ is the bentonite suspension density, g is the gravity acceleration, S_o is the bed slope, and μ_o, n, θ and α are four material parameters (paragraph 1.3). By continuity, and assuming crudely a two-dimensional flow, it yields the final wave front position $(X_S)_{end}$:

$$(X_S)_{end} = \frac{1}{2} * \frac{\theta * \alpha * \rho * g * S_o * d_o * L}{\mu_o * (n - 1)^{1/n}} \qquad (2\text{-}32)$$

The observed fluid thickness after stoppage, and final wave front position, were compared with Equation (2-30), and Equation (2-32) respectively, assuming that μ_o is the apparent viscosity measured under controlled stress for relatively short durations at constant temperature (paragraph 4.4, Table 4.2). The results provide some estimates of the characteristic parameters of the rheological model, namely ($\theta*\alpha$) and n. Results are summarised in Table 6-2. (Note that the product $\theta*\alpha$ may be estimated using either Equations (2-30) or (2-32). The comparison with experiments gave similar results.)
The results show that the product $\theta*\alpha$ must decrease with increasing mass concentration, thus increasing minimum apparent yield stress. The qualitative agreement between theory and experiments suggests that the basic equations of this development (i.e. kinematic wave equation and rheology model) are likely to model correctly both fluid behaviour and flow motion.

Fig. 6-8 - Longitudinal free-surface profile after stoppage (all data)
Flow Type II - Test 5, θ_b = 15º, C_m = 0.15, M = 3.71 kg, rest period: 60 s

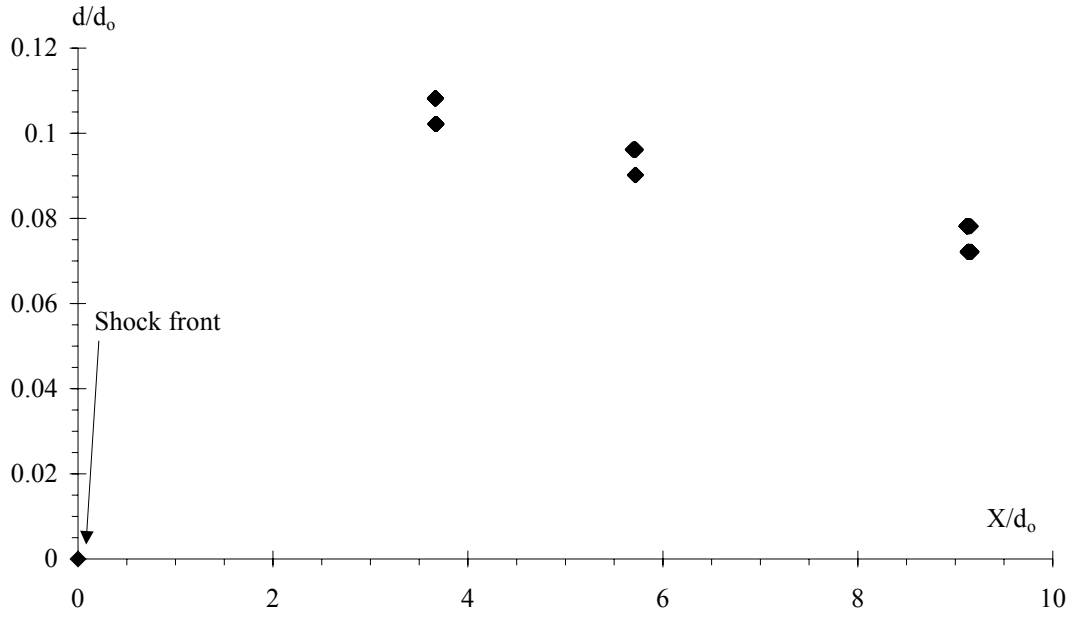

Table 6-2 - Comparison between final fluid thickness and wave front position observations and Equations (2-30) and (2-32) - Values of n and θ*α for best fit

C_m	n	θ*α	Remarks
		s	
(1)	(2)	(3)	(4)
0.10	1.1	0.014	2 experiments (Flow types I & II).
0.13	1.1	0.0032	7 experiments (Flow types I, II & III).
0.15	1.1	0.0017	5 experiments (Flow types II & III).

7. UNUSUAL FLOW PATTERNS AND INSTABILITIES

7.1 PRESENTATION

The experimental facility provided an opportunity for additional observations of unusual flow patterns and instabilities. Figure 7-1 to 7-4 present some photographic evidences, but it must be emphasised that these constituted unusual events that were not representative of the bulk of the experiments.

First the conditions of fluid preparation were found to be important as discussed by COUSSOT et al. (2002b). Figure 7-1 presents an identical experiment with two different fluid preparations. In Figure 7-1A, the fluid was not properly destructured before the start of that experiment, and little flow motion was observed.

Second, some form of "roll waves" were seen during the cleanup of the fluid after fluid stoppage. Figure 7-2 illustrates an example where instabilities developed after pushing the reservoir fluid with a paddle towards the downstream end of chute. Figure 7-2A1 shows the initial development of the waves, while Figures 7-2A2 and 7-2A3 illustrates well-defined instabilities few instants later.

Third, some free-surface anomalies were observed at the end of some experiments after fluid stoppage. Figure 7-3A presents some spots of fluid restructuration at the surface of Flow type II after stoppage. Figure 7-3B shows deformations of the free-surface after a very-small fluid motion.

Fourth, in Flow Type IIIb, several successive packets of fluid were observed with a clear "pause" between each motion. Figure 7-4A shows the second packet of fluid at end of motion, while Figure 7-4B and 7-4C presents the fluid reservoir before and after shearing of a third packet of fluid which did not flow.

Fig. 7-1 - Effect of malaxage on the flow conditions
(A) Experiment on the small plate with sandpaper - Bentonite suspension (θ_b = 17º, C_m = 20%, T_o = 30 s, square mould) - Fluid about 3 minutes after start : no flow as the result of poor and insufficient malaxage

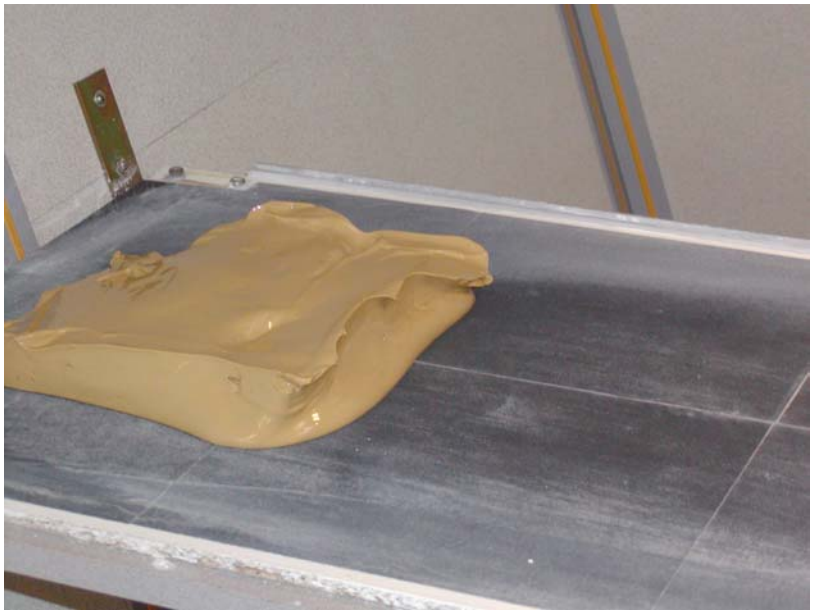

(B) Identical experiment after a better malaxage

Fig. 7-2 - Man-made instabilities induced after stoppage in the large flume
After fluid stoppage during some experiment, free-surface instabilities were sometimes observed during cleanup when the reservoir fluid was pushed over the stopped fluid
(A) Test 05 (θ_b = 15º, C_m = 15%, T_o = 60 s, M = 3.7 kg, Flow Type II)
(A1) Development of kind of "roll waves" during clean up, looking upstream

(A2) Same setup few instants later, looking upstream

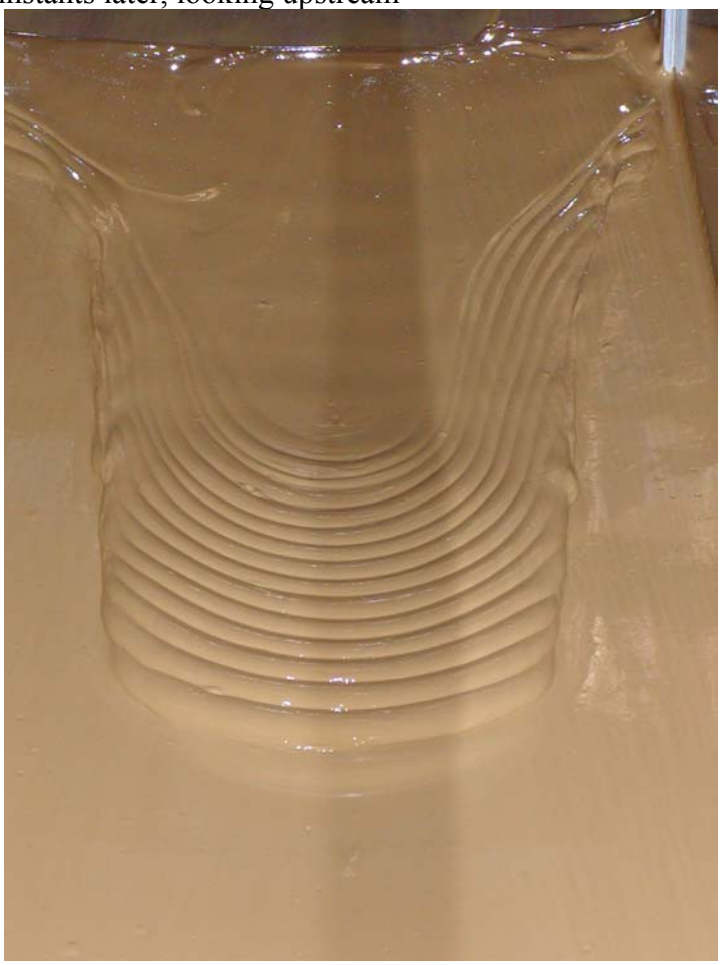

(A3) Same setup few instants later, side view with flow direction from right to left

(B) Test 21 (θ_b = 15º, C_m = 13%, T_o = 40 min., M = 3.7 kg, Flow Type II)
Development of waves during clean up, looking upstream

Fig. 7-3 - Free-surface details after fluid stoppage
(A) Photograph showing spots of fluid restructuration at free-surface - Looking upstream at the stopped fluid - Test 06 (θ_b = 15º, C_m = 15%, T_o = 300 s, M = 3.7 kg, Flow Type II)

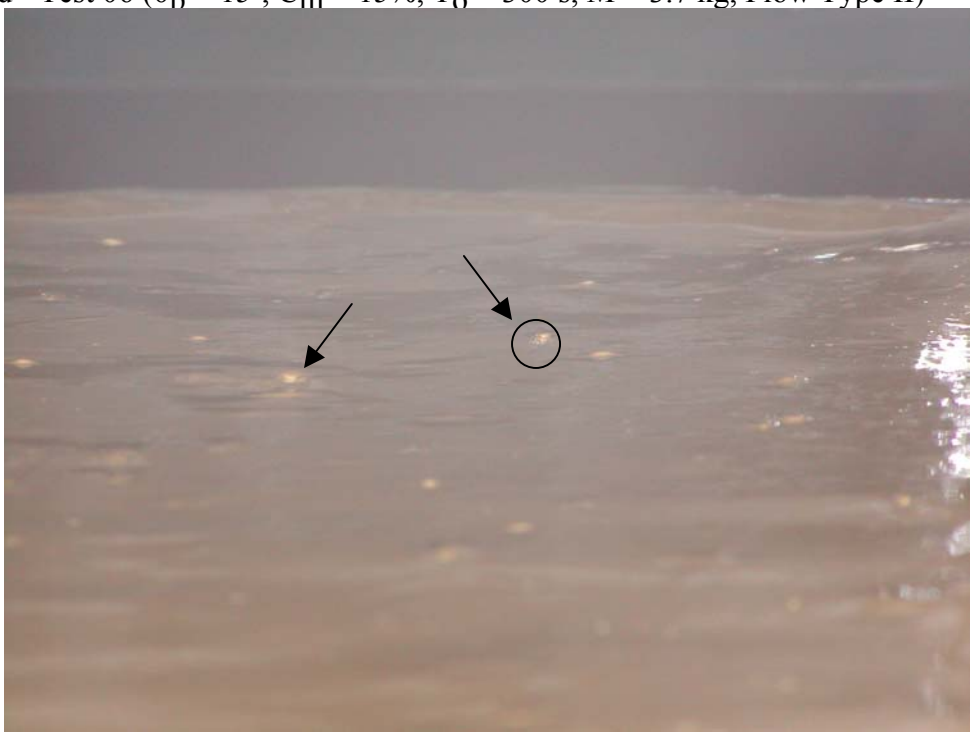

(B) Free-surface deformation after a very short fluid motion - Test 13 (θ_b = 15º, C_m = 20%, T_o = 30 s, M = 3.5 kg, Flow Type III-IV)

Fig. 7-4 - Instantaneous photographs of fluid motion in Flow Type IIIb
Test 20 (θ = 15º, C_m = 13%, T_o = 17 h 16 min., M = 3.9 kg, Flow Type IIIb)
(A) Second fluid packet near the downstream end of flume

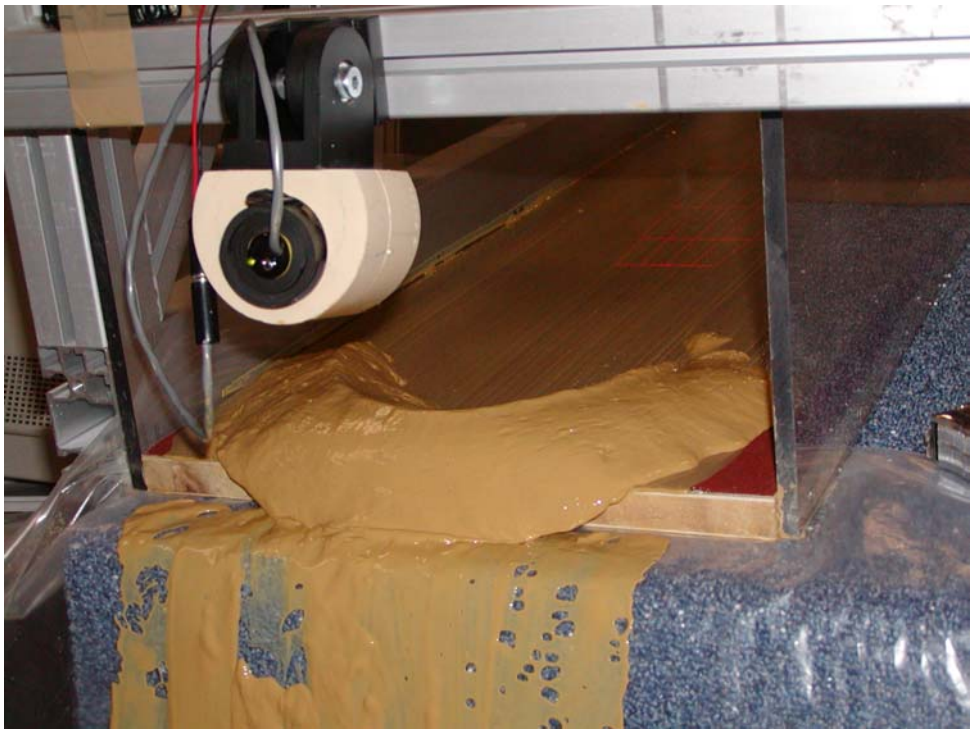

(B) Reservoir of fluid after the motion of the second fluid packet, before shearing of a third block

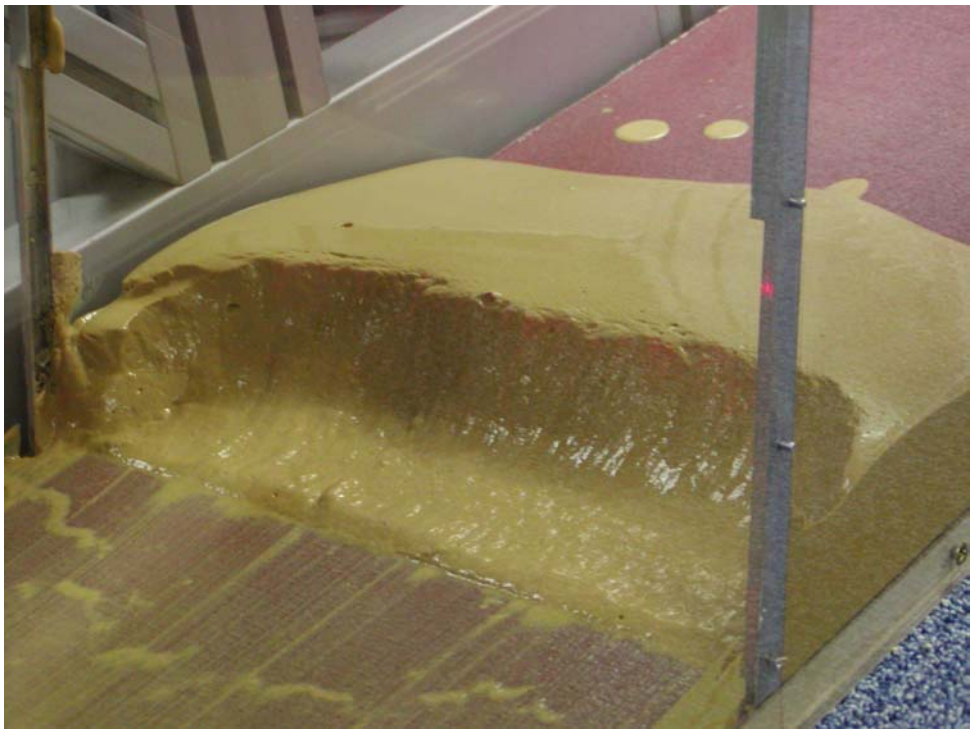

(C) Reservoir of fluid after shearing of a third block of fluid

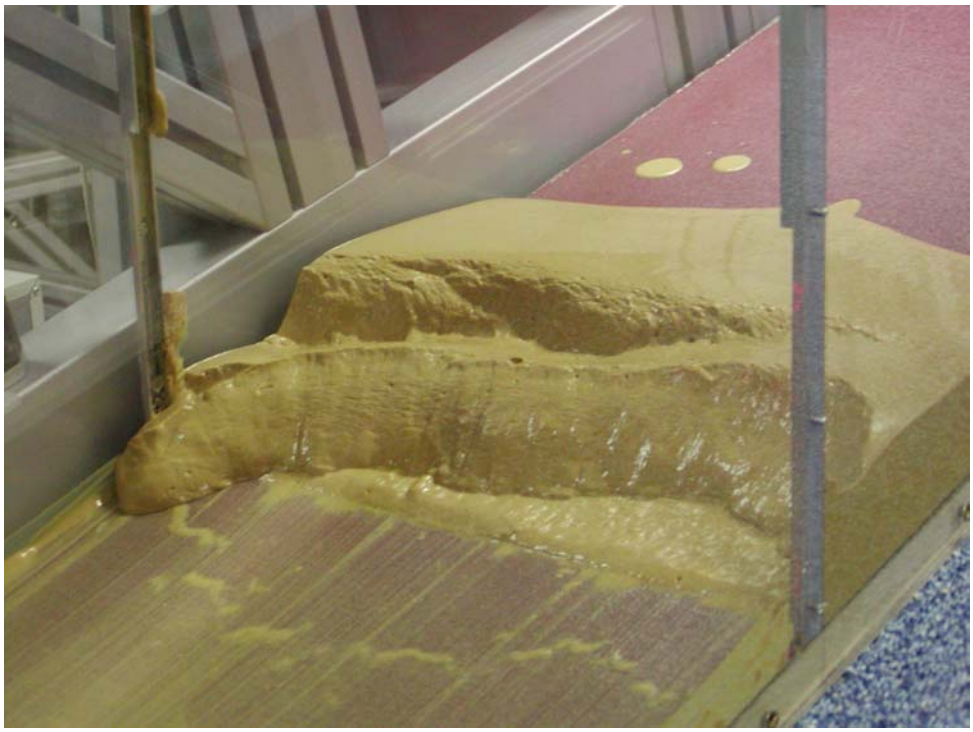

7.2 A PARTICULAR EXPERIMENT: TEST 26B

For one experiment with a long rest period (C_m = 0.15, rest period: 17 hours 15 min., Test 26), no flow was observed after the rapid gate opening. However cracks started to develop at the reservoir free-surface about 15 minutes after opening (Fig. 7-5A). A block of fluid started to slide about 22 minutes after opening, and the sliding motion lasted for about 48 minutes. At the end, the front of

the block was measured at $(X_s)_{end}$ = 42 mm ([14]) downstream of the initial gate position (Fig. 7-5B). No further motion was observed.
Afterwards the inclined plane was vibrated with a shake in the x-direction, using a hammer applied at the downstream end. After a fair amount of hammering, the bentonite suspension block detached from the main reservoir, travelled along the plate, and spilled into the overflow container. During the motion, the block slid over the sand paper in a quasi-two-dimensional manner (Fig. 7-5C). The two-dimensional nature of the block was totally different from observations with Flow Types III and IIIb (paragraphs 5.1 & 6.1). This might suggest that the three-dimensional nature of the shock, including the front curvature, would not be observed in rigid block of fluid (i.e. after a very long time).

Fig. 7-5 - Photographs of Test 26 in the Large facility (Test 26, θ_b = 15°, C_m = 0.15, rest period: 17 hours 15 min.)
(A) Development of cracks at the reservoir surface several minutes (20-25 min.) after gate opening (Test 26)

[14]The downstream distance x was measured from the initial position of the gate downstream face.

(B) Final geometry of sliding block and reservoir about 80 minutes after gate opening (Test 26)

(C) Photograph of bentonite block sliding over the sandpaper after vibrating the invert (Test 26B) - Note that the block shape was quasi-two-dimensional, although it tilted around the centreline

8. SUMMARY AND CONCLUSION

This study is focused on the highly unsteady flow motion of a thixotropic fluid with a free-surface. The phenomenon, called dam break wave, is a shock during which the interactions between flow motion and fluid rheology are very strong, and the fluid is subjected to a continuous transition from a liquid to a solid behaviour.

Theoretical considerations were developed based upon a kinematic wave approximation of the Saint-Venant equations for a thixotropic fluid down a prismatic sloping channel. A simple thixotropic fluid model was used which is based upon a minimum number of parameters, and describes the instantaneous state of fluid structure by a single parameter. The analytical solution of the basic flow motion and rheology equations predict three basic flow regimes depending upon the fluid properties and flow conditions, including the initial degree of jamming of the fluid : (1) a short motion with relatively-rapid flow stoppage for relatively small mass of fluid ($d_o/h_c < 1$), (2) a fast flow motion for a large mass of fluid ($d_o/h_c >> 1$), or (3) an intermediate motion initially rapid before final fluid stoppage for intermediate mass of fluid ($d_o/h_c > 1$) and intermediate initial rest period T_o. This behaviour, unknown to turbulent or laminar fluid motion, is typical of well-known thixotropic fluid flows, such as pasty cement flows, mountain stream flows and subaerial or submarine landslides.

Physical experiments were performed by pouring a given volume of bentonite suspension in a dam reservoir at the top of an inclined channel (slope: 15°, rough surface to avoid slip). This mass of fluid was left at rest for a controlled time T_o before the gate was abruptly lifted. A series of systematic experiments were performed under different times of rest T_o, during which the fluid restructured, for various solid volume fractions C_m, and initial mass of fluid M. Qualitatively, four flow types were observed. For small bentonite mass concentrations C_m and short relaxation times T_o, the fluid flowed rapidly down the slope and spilled into the overflow container (Flow Type I). For intermediate concentrations and rest periods, the suspension flowed rapidly initially, decelerated relatively suddenly, continued to flow slowly for sometimes before complete stoppage (Flow Type II). For large mass concentrations and long rest periods, the mass of fluid stretched down the slope, until the head separated from the tail (Flow Type III). Sometimes a second and third packets followed (Flow Type IIIb). The last flow pattern (Type IV) corresponded to an absence of flow for large bentonite concentrations and long rest times.

Quantitative informations were documented in terms of the final fluid thickness, wave front position, wave front curvature, side profile of the wave front during motion and after stoppage, as well as the flow motion immediately after gate opening. These are detailed in paragraph 6., while some free-surface instabilities are discussed and illustrated in paragraph 7.

It is believed that the present study is the first theoretical analysis combining successfully the basic principles of unsteady flow motion (i.e. the Saint-Venant equations) with a thixotropic fluid model, which was validated with large-size systematic laboratory experiments. It is the belief of the writers that for such complex systems this kind of approach, combining both rheology and fluid dynamics, is necessary to gain new insights of these complicated flow motions.

Further works may include an extension of the theory to three-dimensional flow situations, possibly with some numerical modelling, some high-speed video movies of the flow motion to study wave instabilities during the fluid motion, detailed flow measurements of the interactions between sidewall and bottom boundary layers, detailed study and explanation of peculiar flow instabilities.

ACKNOWLEDGMENTS

The writers thank Dr Nicolas ROUSSEL (Division BCC, LCPC Paris) for his review of the report and his valuable comments. They further acknowledge the technical assistance of the L.M.S.G.C..

APPENDIX A - DAM BREAK WAVE IN A HORIZONTAL INITIALLY-DRY CHANNEL

Considering an ideal dam break surging over a dry river bed, the method of characteristics may be applied to solve completely the wave profile as first proposed by RITTER (1892). The dam break may be idealised by a vertical wall that is suddenly removed (Fig. A-1). After removal of the wall, a negative wave propagates upstream and a dam break wave moves downstream. Although there is considerable vertical acceleration during the initial instants of fluid motion, such acceleration is not taken into account by the method of characteristics and the pressure distributions are assumed hydrostatic.

For an ideal dam break over a dry horizontal channel, the basic equations are those of the simple wave :

$$\frac{D}{Dt}(V + 2 * C) = 0 \qquad \text{forward characteristics (A-1a)}$$

$$\frac{D}{Dt}(V - 2 * C) = 0 \qquad \text{backward characteristics (A-1b)}$$

along :

$$\frac{d x}{dt} = V + C \qquad \text{forward characteristics C1 (A-2a)}$$

$$\frac{d x}{dt} = V - C \qquad \text{backward characteristics C2 (A-2b)}$$

where V is the flow velocity and C is the celerity ($C = \sqrt{g*d}$ for a rectangular channel). The instantaneous dam break creates a negative wave propagating upstream into a fluid at rest with known water depth d_o. In the (x, t) plane, the initial negative wave characteristics has a slope dt/dx = $-1/C_o$ where $C_o = \sqrt{g*d_o}$ assuming a rectangular channel and d_o is the initial reservoir depth (Fig. A-1B). A forward characteristic can be drawn issuing from the initial backward characteristics for t > 0 and intersecting the trajectory of the leading edge of the dam break wave front (Fig. A-1B, trajectory E1-F1). The forward characteristic satisfies :

$$V + 2 * C = V_o + 2 * C_o = 2 * C_o \qquad (A-3)$$

since $V = V_o = 0$ and $C = C_o = \sqrt{g*d_o}$ at the point E1 (Fig. A-1B).

At the leading edge of the dam break wave front, the water depth is zero, hence C = 0, and the propagation speed of the dam break wave front equals :

$$C_S = 2 * C_o = 2 * \sqrt{g * d_o} \qquad \text{ideal dam break (A-4)}$$

Considering any backward characteristic issuing from the dam break wave front (Fig. A-1B, trajectory F1-G1), the C2 characteristic is a straight line because the initial backward characteristics is a straight line. The inverse slope of the backward characteristics is a constant :

$$\frac{d x}{dt} = V - C = 2 * C_o - 3 * C$$

using Equation (A-3). The integration of the inverse slope gives the water surface profile at the intersection of the C2 characteristic with a horizontal line t = constant (Fig. A-1B, point G1). At a given time, the free-surface profile between the leading edge of the negative wave and the wave front is a parabola :

$$\frac{x}{t} = 2 * \sqrt{g * d_o} - 3 * \sqrt{g * d} \qquad \text{for } -\sqrt{g*d_o} \le \frac{x}{t} \le +2*\sqrt{g*d_o} \quad (A-5)$$

At the origin (x = 0), Equation (A-5) predicts a constant water depth :

$$d(x=0) = \frac{4}{9} * d_o \qquad \text{(A-6)}$$

while the velocity at the origin is deduced from Equation (A-3). After dam break, the flow depth and velocity at the origin are both constants, and the water discharge at x = 0 equals :

$$Q(x=0) = \frac{8}{27} * d_o * \sqrt{g * d_o} * W \qquad \text{(A-8)}$$

where W is the channel width.

Fig. A-1 - Sketch of dam break wave in a dry horizontal channel

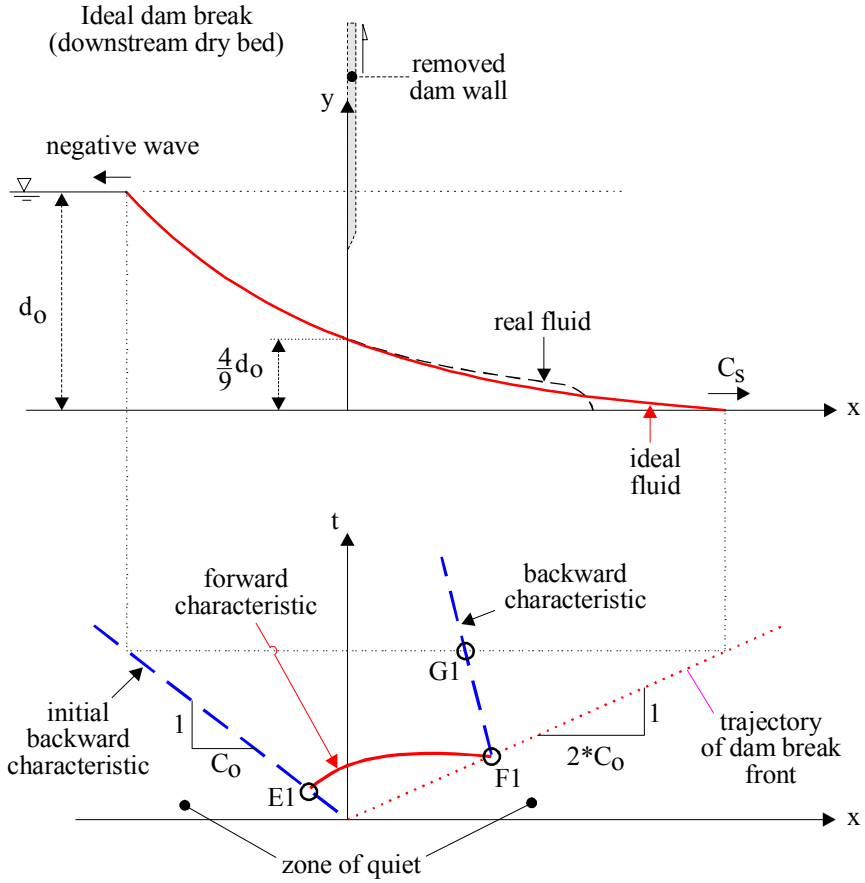

Discussion

The above calculations were performed assuming a smooth rectangular channel, an infinitely long reservoir and for a quasi-horizontal free-surface. That is, bottom friction is zero and the pressure distribution is hydrostatic. Experimental results (e.g. SCHOKLITSCH 1917, FAURE and NAHAS 1961, LAUBER 1997) showed that the assumptions of hydrostatic pressure distributions and zero friction are reasonable, but for the initial instants and at the leading tip of the dam break wave.
Bottom friction affects significantly the propagation of the leading tip. ESCANDE et al. (1961) investigated specifically the effects of bottom roughness on dam break wave in a natural valley. They showed that, with a very-rough bottom, the wave celerity could be about 20 to 30% lower than for a smooth bed. The shape of a real fluid dam break wave front is sketched in Figure A-1A.

Notes

The assumption of hydrostatic pressure distributions has been found to be reasonable, but for the initial instants : i.e., $t < 3*\sqrt{d_o/g}$ (LAUBER 1997).

RITTER's theory implies that the celerity of the initial negative wave characteristics is $-\sqrt{g*d_o}$. Experimental observations suggested however that the real celerity is about $-\sqrt{2}*\sqrt{g*d_o}$ (LAUBER 1997, LEAL et al. 2001). It was suggested that the difference was caused by streamline curvature effects at the leading edge.

Note that the above development was conducted for a semi-infinite reservoir. At a given location $x > 0$, Equation (A-5) predicts an increasing water depth with increasing time :

$$d = \frac{4}{9} * d_o * \left(1 - \frac{3}{2} * \frac{x}{\sqrt{g * d_o} * t}\right)^2 \qquad \text{(A-5b)}$$

At any distance x from the dam site, the water depth d tends to $d = 4/9*d_o$ for $t = +\infty$ (for a semi-infinite reservoir).

APPENDIX B - APPLICATION OF THE METHOD OF CHARACTERISTICS TO DAM BREAK WAVE OF THIXOTROPIC FLUID

B.1 PRESENTATION

B1.1 Basic equations

HUNT (1982) developed a kinematic wave solution for turbulent dam break wave down a sloping, prismatic, two-dimensional channel (Fig. 2-1, paragraph 2.2). Considering a kinematic wave, the Saint-Venant equations give :

$$\frac{D\,d}{Dt} = 0 \qquad \text{(B-1a)}$$

along the forward characteristic trajectory :

$$\frac{d\,x}{dt} = \frac{3}{2} * \sqrt{\frac{8 * g}{f} * S_o * d} \qquad \text{characteristic trajectory (B-1b)}$$

where S_o is the bed slope ($S_o = \sin\theta_b$) and the Darcy friction factor f becomes a function of time and space because of the thixotropic nature of the fluid. f is defined as :

$$f = \frac{8 * \tau_o}{\rho * V^2} \qquad \text{(B-2)}$$

For a thixotropic fluid, the rheological equations ([1]) may be simplified into :

$$\tau_o \approx \mu * \frac{V}{d} \qquad \text{(B-3)}$$

$$\mu = \mu_o * (1 + \lambda^n) \qquad \text{(B-4)}$$

$$\frac{d\,\lambda}{dt} \approx \frac{1}{\theta} - \alpha * \frac{V}{d} * \lambda \qquad \text{(B-5)}$$

assuming that $\partial V/\partial y \approx V/d$ where V is the depth-averaged velocity and d is the flow depth (or fluid thickness) measured normal to the flow direction.
The kinematic wave approximation ($S_o = S_f$) yields :

$$V = \frac{\rho * g * S_o * d^2}{\mu_o * (1 + \lambda^n)} \qquad \text{Kinematic wave approximation (B-6)}$$

That is, along the characteristic trajectory, the degree of jamming of the material satisfies :

$$\frac{d\,\lambda}{dt} + \alpha * \frac{\rho * g * d * S_o}{\mu_o} * \frac{\lambda}{1 + \lambda^n} = \frac{1}{\theta} \qquad \text{(B-7)}$$

with d = constant along the forward characteristic.
Combining Equations (B-1) and (B-6), the equation of the characteristic becomes :

$$\frac{d\,x}{dt} = \frac{3}{2} * \frac{\rho * g * S_o * d^2}{\mu_o * (1 + \lambda^n)} \qquad \text{forward characteristic trajectory (B-8)}$$

The trajectory is not a straight line since λ is a function of time and space (Fig. B-1).

Discussion

Along a forward trajectory where Dd/Dt = 0, the boundary shear stress equals :

$$\tau_o = \rho * g * d * S_o$$

[1] Model of COUSSOT et al. (2002a).

The result derives from the kinematic wave approximation for a wide channel. It is independent of the initial degree of jamming.
The above development is based upon a kinematic wave approximation. For turbulent flows, HUNT (1982) showed that the assumption is valid once the wave front has travelled approximately four lengths of reservoir downstream of the dam site : i.e., $X_S/L > 4$ where X_S is the wave front location and L is the reservoir length. The assumption is not valid in the initial instants after dam break nor until the free-surface becomes parallel to the chute invert. HUNT (1984) commented however that his approach could be adapted for $X_S/L < 4$: "*it is possible that an approach similar [...] could be used to route the flood downstream and that the result might be valid even for relatively small distance downstream*".
At any time t (t > 0), the location of the dam break wave front is deduced from the equation of conservation of mass :

$$\int_{x=-L}^{X_S} d * dx = \frac{1}{2} * d_o * L \qquad \text{(B-9)}$$

B1.2 Initial negative wave characteristic

The sudden gate removal is associated with the dam break wave propagating down the chute as well as a backward characteristic C2 propagating upstream into the reservoir initially at rest (Fig. 2-1B). Since the propagation of the initial negative (backward) wave is relatively rapid, the kinematic wave approximation is improper and the complete equations of St Venant (i.e. dynamic wave equation) must be considered.
The Saint-Venant equations (Eq. (2-1) & (2-2)) may be transformed to yield a characteristic system of equations :

$$\frac{D}{Dt}(V + 2 * C) = - g * (S_f - S_o) \qquad \text{forward characteristic C1}$$

$$\frac{D}{Dt}(V - 2 * C) = - g * (S_f - S_o) \qquad \text{backward characteristic C2}$$

along :

$$\frac{d x}{dt} = V + C \qquad \text{forward characteristic C1}$$

$$\frac{d x}{dt} = V - C \qquad \text{backward characteristic C2}$$

where C is celerity of a small disturbance for an observer travelling with the flow: $C = \sqrt{g*d}$ where d is the local reservoir depth (e.g. HENDERSON 1966, MONTES 1988, CHANSON 2004a,b). The initial backward characteristic propagates in a fluid at rest (V = 0) and its equations are :

$$\frac{D}{Dt}C = -\frac{g}{2} * S_o \qquad \text{initial backward characteristic}$$

along :

$$\frac{d x}{dt} = - C \qquad \text{initial backward characteristic}$$

The upstream extent of the negative wave is :

$$x_{C2} = -\frac{1}{4} * g * \sin\theta_b * t^2$$

where t is the time from dam removal. For a rectangular reservoir, the initial characteristic C2 reaches the reservoir upstream end for :

$$T = \sqrt{\frac{4 * L}{g * \sin\theta_b}}$$

where L is the reservoir length (Fig. 2-1).

B.2 ANALYTICAL SOLUTIONS. (1) PARTICULAR CASES

B.2.1 Particular case: $\mu = \mu_o * \lambda^n$ with $\theta \rightarrow +\infty$

Assuming that the fluid viscosity tends to zero for an infinity high shear rate :

$$\mu = \mu_o * \lambda^n \qquad \text{(B-10)}$$

Equation (B-7) becomes :

$$\frac{d\lambda}{dt} + \alpha * \frac{\rho * g * d * S_o}{\mu_o} * \frac{1}{\lambda^{n-1}} = \frac{1}{\theta} \qquad \text{(B-11)}$$

since n is typically greater than unity for real thixotropic fluids.
For $\theta \rightarrow +\infty$ the analytical solution of Equation (B-11) is :

$$\lambda^n = \lambda_o^n - n * \alpha * \frac{\rho * g * d * S_o}{\mu_o} * t \qquad \text{(B-12)}$$

with d = constant along the characteristic and λ_o is the initial degree of jamming of the fluid. The result shows that λ tends monotically to zero with increasing time along the trajectory equation (i.e. toward the shock).
In a general case ($\theta > 0$), simple analytical solutions of Equation (B-7) exist for integer values of n.

Fig. B-1 - Dam break wave of thixotropic fluid down a sloping channel for $\mu = \mu_o * \lambda^n$: characteristics and dam break wave front path in the (x, t) plane (Convex characteristics, Flow category III)

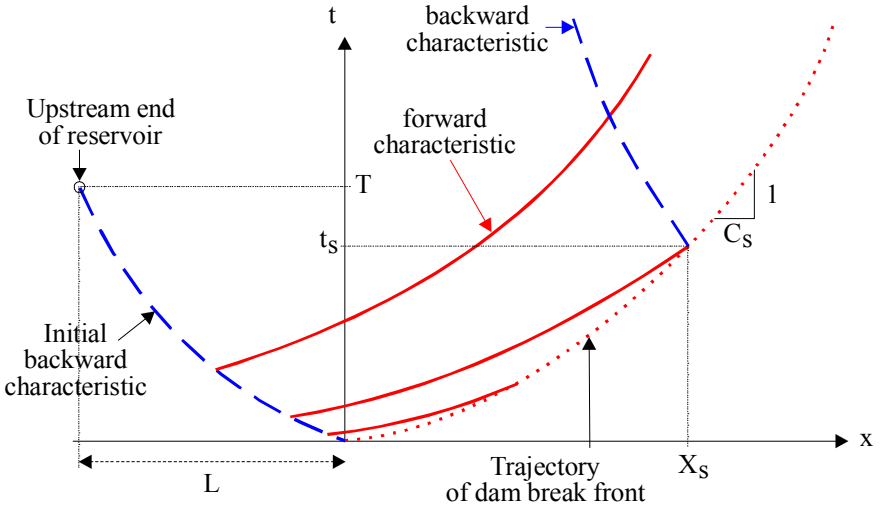

B.2.2 Particular case: $\mu = \mu_o * \lambda^n$

The fluid viscosity is assumed to tend to zero for an infinitely high shear rate :

$$\mu = \mu_o * \lambda^n \qquad \text{(B-10)}$$

Equation (B-7) becomes :

$$\frac{d\lambda}{dt} = \frac{1}{\theta} - \alpha * \frac{\rho * g * d * S_o}{\mu_o} * \frac{1}{\lambda^{n-1}} \qquad \text{(B-11)}$$

and the trajectory of the forward characteristic is :

$$\frac{dx}{dt} = \frac{3}{2} * \frac{\rho * g * S_o * d^2}{\mu_o * \lambda^n} \qquad \text{forward characteristic trajectory (B-13)}$$

Considering a fluid with an initial degree of jamming $\lambda(t=0) = \lambda_o$ and assuming $n > 1$, two different behaviours may be observed depending upon the sign of the term :

$$\frac{1}{\theta} - \alpha * \frac{\rho * g * d * S_o}{\mu_o} * \frac{1}{\lambda_o^{n-1}}$$

Initially ($t = 0$), $d\lambda/dt$ is positive if

$$\frac{1}{\theta} - \alpha * \frac{\rho * g * d * S_o}{\mu_o} * \frac{1}{\lambda_o^{n-1}} > 0$$

and $\lambda(t) > \lambda(t=0) = \lambda_o$. For $t = 0 + \delta t$, it yields :

$$\frac{1}{\theta} - \alpha * \frac{\rho * g * d * S_o}{\mu_o} * \frac{1}{(\lambda(t=0+\delta t))^{n-1}} > 0$$

and $d\lambda/dt$ is positive 0.
By extension, Equation (B-11) predicts that $d\lambda/dt > 0$ everywhere along the characteristic trajectory if

$$\frac{1}{\theta} - \alpha * \frac{\rho * g * d * S_o}{\mu_o} * \frac{1}{\lambda_o^{n-1}} > 0$$

That is, λ increases monotically for $\lambda_o > \lambda_c$ where λ_c is a characteristic degree of jamming of the fluid defined as :

$$\lambda_c = \left(\theta * \alpha * \frac{\rho * g * d * S_o}{\mu_o}\right)^{\frac{1}{n-1}} \qquad \text{(B-14)}$$

with d = constant along the forward characteristic. Hence $\lambda(t>0) > \lambda_o > \lambda_c$. The forward characteristic (Eq. (B-8)) is a convex curve in the (x,t) plane since $d^2x/dt^2 < 0$ ([2]). Figure B-1 illustrates a series of convex characteristics. Physically, for $\lambda_o > \lambda_c$, the fluid viscosity increases with increasing time along the trajectory towards the shock. The flow resistance increases toward the wave front since λ and μ increase, and the velocity decreases :

$$f = \frac{8 * \mu_o * \lambda^n}{\rho * d * V} \qquad \text{(B-15)}$$

Conversely λ decreases monotically along the characteristic trajectory for $\lambda_o < \lambda_c$ (i.e. toward the wave front) and $0 < \lambda(t) < \lambda_o < \lambda_c$. The forward characteristic is a concave curve in the (x,t) plane since $d^2x/dt^2 > 0$. Along a characteristic trajectory, the fluid behaviour is a function of the initial degree of jamming, the fluid thickness (or water depth), bed slope and characteristic time of restructuration.

[2]In the (x,t) plane, the slope of the characteristics is dt/dx (Fig. B-1).

In summary, along a forward characteristic trajectory, the fluid evolves either towards complete stoppage for $\lambda > \lambda_c$, or towards a quasi-steady flow motion ($\lambda < \lambda_c$) in which the flow resistance counter-balances exactly the gravity force component in the flow direction ([3]). For $\lambda_o = \lambda_c$, the degree of jamming becomes of constant along a forward characteristic : $\lambda(t >0) = \lambda_o = \lambda_c$. The characteristic is a straight line.

Application

The above development was performed along a forward characteristic on which the flow depth d was a constant (Eq. (B-1)). Let us consider a series of forward characteristics issued from the reservoir with different water depths d which must satisfy : $0 \leq d \leq d_o = H_{dam}*\cos\theta$ where H_{dam} is the vertical reservoir height at gate (Fig. B-1). The characteristic degree of jamming of the fluid (Eq. (B-14)) may be associated with a characteristic fluid thickness h_c :

$$h_c = \frac{\mu_o * \lambda_o^{n-1}}{\theta * \alpha * \rho * g * S_o} \qquad \text{(B-16)}$$

For flow depths less than the characteristic fluid thickness (i.e. $d < h_c$), Equation (B-10) predicts $d\lambda/dt > 0$, and the degree of jamming of the fluid increases monotically with time. Conversely, the degree of jamming of the fluid decreases monotically with time for $d > h_c$.

Three flow situations may occur depending upon the ratio d_o/h_c : i.e., Category I for $d_o/h_c >> 1$, Category II for $d_o/h_c > 1$ and Category III for $d_o/h_c < 1$.

(1) For $d_o/h_c >> 1$ (Flow Category I), nearly all forward characteristics issued from the reservoir are characterised by $d/h_c > 1$. That is, each forward characteristic is associated with some destructuration of the fluid and a decrease in fluid viscosity with time. The fluid flows fast down the sloping plane. It is gradually accelerated with time since the flow resistance decreases with increasing time. The forward characteristics are a series of concave curves in the (x,t) plane. Figure B-2 illustrates an example.

(2) For $d_o/h_c < 1$ (Flow Category III), all characteristics are issued from the reservoir for a flow depth $d/h_c < 1$. After dam break ($t > 0$), the degree of jamming of all fluid increases (everywhere) monotically with time and the fluid must stop ultimately. The fluid flow (Category III) must be slow and the maximum extent of the dam break wave front is relatively small. Figure B-1 illustrates a series of characteristics. Considering the convex forward characteristics issued from the initial backward characteristic, the flow depth on each characteristic decreases with increasing starting time until $d = 0$ at the upstream end of the reservoir (i.e. $t = T$). That is, the convexity of each curve increases with decreasing reservoir depth since $d^2x/dt^2 < 0$. Along each forward characteristic, the degree of jamming of the fluid increases with increasing time until fluid stoppage.

(3) For $d_o/h_c > 1$ (Flow Category II), the fluid flow is characterised by two different behaviours with increasing time. Initially, all characteristics are issued from the reservoir with $d/h_c > 1$ and they are characterised by some destructuration of the fluid and a decrease in fluid viscosity with time. This behaviour occurs for the forward characteristics issued from the initial backward characteristic with $0 \leq t < t_c$ where :

$$t_c = \sqrt{\frac{4 * L}{g * \tan\theta} * \left(1 - \frac{h_c}{d_o}\right)} \qquad \text{(B-17)}$$

Equation (B-16) derives from the equation of negative wave characteristic (initial backward characteristic) (paragraph 2.2) ([4]). Afterwards, the forward characteristics issued from the reservoir

---

[3]Note however that the flow resistance tends to zero, since the viscosity is zero (i.e. ideal fluid) for $\lambda = 0$.

[4]For a flat slope, and a two-dimensional triangular reservoir, the equation of the initial backward characteristic is

with $t > t_c$ are characterised by $d/h_c < 1$. Then the fluid flow propagates with an increasing viscosity with time until fluid stoppage. Two different families of characteristic curves may be observed (Fig. B-3). Considering the forward characteristics issued from the initial negative characteristic with $0 \le t < t_c$, the characteristics form a series of concave curves, while they are a series of convex curves if they are issued from the reservoir with $t_c < t$. The forward characteristic intersecting the initial backward characteristic at $t = t_c$ is a straight line and its equation is :

$$x = \frac{3}{2} * \frac{\lambda_o^{n-1}}{\theta^2 * \alpha^2 * \rho * g * S_o} * (t - t_c) - L * \left(1 - \frac{h_c}{d_o}\right) \qquad t = t_c$$

Fig. B-2 - Dam break wave of thixotropic fluid down a sloping channel for $\mu = \mu_o * \lambda^n$: Flow category I

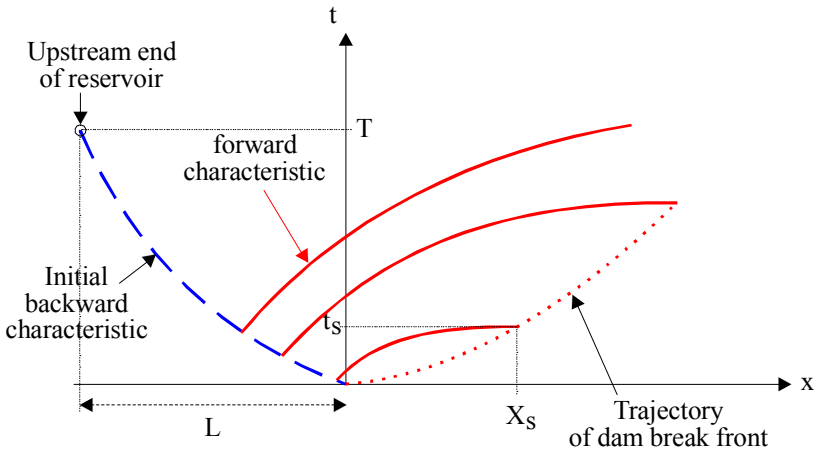

Fig. B-3 - Dam break wave of thixotropic fluid down a sloping channel for $\mu = \mu_o * \lambda^n$: Flow category II

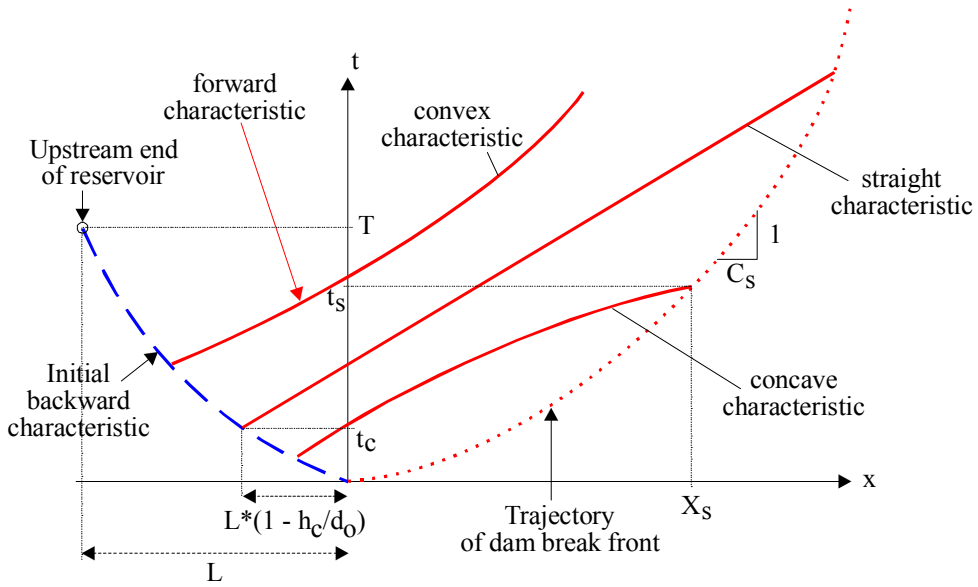

$$x = -\frac{1}{4} * g * \tan\theta * t^2$$

where t is the time from dam removal. It is basically independent of the initial degree of jamming of the fluid since the fluid in the reservoir is initially at rest.

Considering the forward characteristics issued from the initial negative characteristic with $0 \le t \le t_c$, each forward characteristic extends from the initial backward characteristic until the dam break wave front (Fig. B-3). Each forward characteristic issued from the reservoir at $t > t_c$ extends from the initial backward characteristic until the dam break wave front or until complete stoppage for large values of the degree of fluid jamming λ.

Discussion
In Flow Category II, it is conceivable, although not likely, that some convex characteristics intersect the dam break wave front curve. However a rough estimate from the maximum extent of the dam break wave may be deduced from the intersection of the forward characteristic issued from the initial negative characteristic for $d = h_c$ and $t = t_c$, with the dam break wave front curve.

B.3 ANALYTICAL SOLUTIONS. (2) GENERAL CASES

B.3.1 General case with $\theta \to +\infty$

For $\theta \to +\infty$, the analytical solution of Equation (B-7) is :

$$\frac{\lambda^n}{n} + \mathrm{Ln}(\lambda) = \frac{\lambda_o{}^n}{n} + \mathrm{Ln}(\lambda_o) - \alpha * \frac{\rho * g * d * S_o}{\mu_o} * t \qquad \text{(B-18)}$$

where λ_o is the initial degree of jamming of the fluid. For $\theta \to +\infty$, the result implies that λ tends monotically to zero with increasing time along the trajectory equation (i.e. toward the shock).

B.3.2 General case with n integer

Case n = 1
For n = 1, the analytical solution of Equation (B-7) is:

$$t = \theta * \lambda + \alpha * \frac{\rho * g * d * S_o}{\mu_o} * \theta^2 * \lambda * \mathrm{Ln}\left(\left(\alpha * \frac{\rho * g * d * S_o}{\mu_o} - \frac{1}{\theta}\right) * \lambda - \frac{1}{\theta}\right)$$
$$- \left(\theta * \lambda_o + \alpha * \frac{\rho * g * d * S_o}{\mu_o} * \theta^2 * \lambda_o * \mathrm{Ln}\left(\left(\alpha * \frac{\rho * g * d * S_o}{\mu_o} - \frac{1}{\theta}\right) * \lambda_o - \frac{1}{\theta}\right)\right) \qquad \text{(B-19)}$$

It may be rewritten in dimensionless form :

$$\frac{t}{\theta} = \lambda + a * \lambda * (\mathrm{Ln}((a - 1)*\lambda - 1) - \mathrm{Ln}\theta) - (\lambda_o + a * \lambda_o * (\mathrm{Ln}((a - 1)*\lambda_o - 1) - \mathrm{Ln}\theta)) \qquad \text{(B-19B)}$$

where :

$$a = \alpha * \frac{\rho * g * d * S_o}{\mu_o} * \theta$$

must be positive and greater than unity.

Case n = 2
For n = 2, the analytical solution of Equation (B-7) is:

$$t = \theta * \lambda + \alpha * \frac{\rho * g * d * S_o}{\mu_o} * \lambda * \frac{\mathrm{ArcTan}\left(\frac{\lambda}{\sqrt{1 - \alpha * \frac{\rho * g * d * S_o}{\mu_o} * \theta * \lambda}}\right)}{\sqrt{\frac{1}{\theta^4} - \alpha * \frac{\rho * g * d * S_o}{\mu_o} * \lambda}} - t_o \qquad \text{(B-20)}$$

where ArcTan is the inverse tangent function and t_o is a characteristic time.
Further analytical solutions may be obtained for positive integer values of n assuming that all other parameters, but λ, are independent of x and t.

B.3.3 General case (n > 1)

Equation (B-7) may be rewritten as :

$$\frac{d\lambda}{dt} = \frac{1}{\theta} - \alpha * \frac{\rho * g * d * S_o}{\mu_o} * \frac{\lambda}{1 + \lambda^n} \qquad \text{(B-7)}$$

and the trajectory of the forward characteristic is :

$$\frac{dx}{dt} = \frac{3}{2} * \frac{\rho * g * S_o * d^2}{\mu_o * (1 + \lambda^n)} \qquad \text{forward characteristic trajectory (B-8)}$$

Further differentiations with respect to time yield :

$$\frac{d^2\lambda}{dt^2} = \alpha * \frac{\rho * g * d * S_o}{\mu_o} * \frac{1 - (n - 1) * \lambda^n}{(1 + \lambda^n)^2} * \frac{d\lambda}{dt}$$

$$\frac{d^2x}{dt^2} = -\frac{3}{2} * \frac{\rho * g * S_o * d^2}{\mu_o} * \frac{n * \lambda^{n-1}}{(1 + \lambda^n)^2} * \frac{d\lambda}{dt}$$

First note that $d^2\lambda/dt^2$ is zero for $\lambda = \lambda_c$, where

$$\lambda_c = \left(\frac{1}{n - 1}\right)^{1/n}$$

Second, the function $\lambda/(1+\lambda^n)$ tends to zero for $\lambda \to 0$ and $\lambda \to +\infty$ (for n > 1). The function has a maximum for $\lambda = \lambda_c$ and its maximum value is:

$$\frac{(n - 1)^{(n-1)/n}}{n}$$

The function $\lambda/(1+\lambda^n)$ is sketched in Figure B-4. Considering now the case $d\lambda/dt = 0$:

$$0 = \frac{1}{\theta} - \alpha * \frac{\rho * g * d * S_o}{\mu_o} * \frac{\lambda}{1 + \lambda^n} \qquad \text{(B-21)}$$

Equation (B-21) has zero solution, one solution λ_c or two solutions λ_1 and λ_2 (Table B-1, Fig. B-4). Table B-1 summarises the three situations.

Fig. B-4 - Sketch of the function $f(\lambda) = \lambda/(1+\lambda^n)$

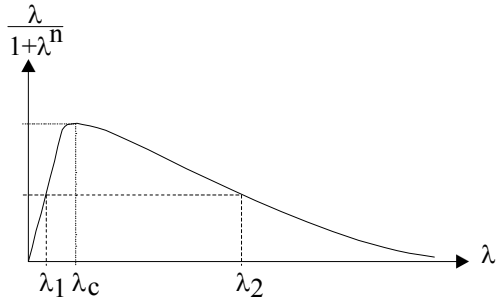

Table B-1 - Summary of Equation's (B-21) solutions

Condition (1)	Solution(s) of Equation (B-21) (2)	Remarks (3)
$\frac{\mu_o}{\theta * \alpha * \rho * g * d * S_o} > \left(\frac{1}{n-1}\right)^{1/n}$	zero solution	
$\frac{\mu_o}{\theta * \alpha * \rho * g * d * S_o} = \left(\frac{1}{n-1}\right)^{1/n}$	one solution $\lambda = \lambda_c$	
$\frac{\mu_o}{\theta * \alpha * \rho * g * d * S_o} < \left(\frac{1}{n-1}\right)^{1/n}$	two solutions λ_1, λ_2	$0 < \lambda_1 < \lambda_c < \lambda_2$

Third, considering a fluid with an initial degree of jamming $\lambda(t=0) = \lambda_o$ and assuming $n > 1$, Equation (B-7) predicts different behaviours along a forward characteristic depending upon the sign of $d\lambda/dt$. At the time origin ($t = 0$), Equation (B-7) may be rewritten :

$$\left(\frac{d\lambda}{dt}\right)_{t=0} = \alpha * \frac{\rho * g * d * S_o}{\mu_o} * \left(\frac{\mu_o}{\theta * \alpha * \rho * g * d * S_o} - \frac{\lambda_o}{1 + \lambda_o{}^n}\right)$$

along a forward characteristic.
Considering the flow situation :

$$\frac{\mu_o}{\theta * \alpha * \rho * g * d * S_o} > \left(\frac{1}{n-1}\right)^{1/n} \qquad \text{(Case 1)}$$

Initially ($t = 0$), $d\lambda/dt$ is positive and $\lambda(t=0+) > \lambda(t=0) = \lambda_o$. More generally, for $t \geq 0$, $d\lambda/dt > 0$ everywhere along the characteristic trajectory and λ increases monotically towards the wave front. For large times ($t >> 1$), $d\lambda/dt$ tends to $1/\theta$ and the degree of jamming λ tends to an infinite value. That is, complete stoppage. Note that the result is independent of the initial degree of jamming λ_o. The forward characteristics form a series of convex curves in the (x,t) plane ([5]).
Considering the flow situation :

$$\frac{\mu_o}{\theta * \alpha * \rho * g * d * S_o} = \left(\frac{1}{n-1}\right)^{1/n} \qquad \text{(Case 2)}$$

three flow situations may occur depending upon the sign of $(\lambda_o - \lambda_c)$. For $\lambda_o > \lambda_c$ (Case 2.1), $d\lambda/dt$ is positive for $t \geq 0$ everywhere along the characteristic trajectory and λ increases monotically. The fluid flow tends to complete stoppage. The forward characteristics form a series of convex curves. For $\lambda_o = \lambda_c$ (Case 2.2), $d\lambda/dt$ is zero and $\lambda(t) = \lambda_c$ everywhere along the forward characteristic which is a straight line. The fluid flow has constant viscosity $\mu = \mu_o * (1+\lambda_c{}^n)$. For $\lambda_o < \lambda_c$ (Case 2.3), $d\lambda/dt$ is positive initially. The degree of jamming tends to $\lambda = \lambda_c$ for large times, and the fluid flow tends to a constant viscosity fluid behaviour for large times t. In the (x,t) plane, the forward characteristics form a series of convex curves which tend to straight lines for large times t.

[5]Remember. In the (x,t) plane, the slope of the characteristics is dt/dx.

Table B-2 - Summary of possible flow situations along a forward characteristic

Condition	λ	$\frac{d\lambda}{dt}$	Forward characteristics	Remarks
(1)	(2)	(3)	(4)	(5)
(1) $\frac{\mu_o}{\theta * \alpha * \rho * g * d * S_o} > \left(\frac{1}{n-1}\right)^{1/n}$	$\rightarrow +\infty$ for $t \rightarrow +\infty$	> 0 for $t \geq 0$	Series of convex curves	Evolution towards complete stoppage.
(2) $\frac{\mu_o}{\theta * \alpha * \rho * g * d * S_o} = \left(\frac{1}{n-1}\right)^{1/n}$				
(2.1) $\lambda_o > \lambda_c$	$\rightarrow +\infty$ for $t \rightarrow +\infty$	> 0 for $t \geq 0$ $\rightarrow 1/\theta$ for $t \rightarrow +\infty$	Series of convex curves	Evolution towards complete stoppage.
(2.2) $\lambda_o = \lambda_c$	$\lambda(t) = \lambda_c$ for $t \geq 0$	0 for $t \geq 0$	Straight line	Constant viscosity fluid.
(2.3) $\lambda_o < \lambda_c$	$\rightarrow \lambda_c$ for $t \rightarrow +\infty$	≥ 0 for $t \geq 0$ $\rightarrow 0$ for $t \rightarrow +\infty$	Series of convex curves tending to straight lines	Evolution towards constant viscosity fluid.
(3) $\frac{\mu_o}{\theta * \alpha * \rho * g * d * S_o} < \left(\frac{1}{n-1}\right)^{1/n}$				
(3.1) $\lambda_o > \lambda_2$	$\rightarrow +\infty$ for $t \rightarrow +\infty$	> 0 for $t \geq 0$ $\rightarrow 1/\theta$ for $t \rightarrow +\infty$	Series of convex curves	Evolution towards complete stoppage.
(3.2) $\lambda_o = \lambda_2$	$\lambda(t) = \lambda_2$ for $t \geq 0$	0 for $t \geq 0$	Straight line	Constant viscosity fluid.
(3.3) $\lambda_1 < \lambda_o < \lambda_2$	$\rightarrow \lambda_1$ for $t \rightarrow +\infty$	≤ 0 for $t \geq 0$ $\rightarrow 0$ for $t \rightarrow +\infty$	Series of concave curves tending to straight lines	Evolution towards constant viscosity fluid.
(3.4) $\lambda_o = \lambda_1$	$\lambda(t) = \lambda_1$ for $t \geq 0$	0 for $t \geq 0$	Straight line	Constant viscosity fluid.
(3.5) $\lambda_1 < \lambda_o$	$\rightarrow \lambda_1$ for $t \rightarrow +\infty$	≥ 0 for $t \geq 0$ $\rightarrow 0$ for $t \rightarrow +\infty$	Series of convex curves tending to straight lines	Evolution towards constant viscosity fluid.

Note: λ_1, λ_2 : solutions of Equation (B-21) such as $\lambda_1 < \lambda_c < \lambda_2$.

Lastly, considering the flow condition :

$$\frac{\mu_o}{\theta * \alpha * \rho * g * d * S_o} < \left(\frac{1}{n-1}\right)^{1/n} \qquad \text{(Case 3)}$$

five flow situations may occur depending upon the signs of $(\lambda_o - \lambda_1)$ and $(\lambda_o - \lambda_2)$, where λ_1 and λ_2 are the solutions of Equation (B-21) ([6]). For $(\lambda_o > \lambda_2)$ (Case 3.1), $d\lambda/dt$ is positive at $t = 0$ and

[6]For very small values of $\lambda/(1+\lambda^n)$, it can be shown that :

$\lambda(t=0+) > \lambda_o$. More generally, for $t \geq 0$, $d\lambda/dt$ is positive everywhere along the characteristic trajectory and λ increases monotically until complete flow stoppage. The forward characteristics form a series of convex curves in the (x,t) plane. For ($\lambda_o = \lambda_2$) (Case 3.2), $d\lambda/dt$ is zero and $\lambda(t) = \lambda_2$ everywhere along the forward characteristic which is a straight line. The fluid flow has constant viscosity $\mu = \mu_o*(1+\lambda_2^n)$. For ($\lambda_1 < \lambda_o < \lambda_2$) (Case 3.3), $d\lambda/dt < 0$ at $t = 0$. More generally, $d\lambda/dt \leq 0$ at $t \geq 0$, although $d\lambda/dt$ tends to zero and λ tends to λ_1 for large times ($t >> 1$). Along a forward characteristic, the fluid flow tends to a constant viscosity behaviour ($\mu = \mu_o*(1+\lambda_1^n)$). The forward characteristics form a series of concave curves which tend to straight lines for large times t. For ($\lambda_o = \lambda_1$) (Case 3.4), $d\lambda/dt$ is zero and $\lambda(t) = \lambda_1$ everywhere along a forward characteristic which is a straight line. The fluid flow has a constant viscosity. For ($\lambda_o < \lambda_1$) (Case 3.5), $d\lambda/dt > 0$ initially. More generally, $d\lambda/dt \geq 0$ at $t \geq 0$. $d\lambda/dt$ tends to zero and λ tends to λ_1 for large times ($t >> 1$). The fluid flow tends to a constant viscosity fluid behaviour ($\mu = \mu_o*(1+\lambda_1^n)$). The forward characteristics form a series of convex curves which tend to straight lines for large times.
All the trends are summarised in Table B-2.

Application to a dam break wave down a sloping channel
The above development was performed along a forward characteristic on which the flow depth d was a constant (Eq. (B-1)). It may be extended to a series of characteristics issued from the initial negative characteristic with different flow depths. For a dam break wave down a sloping channel (Fig. 2-1, paragraph 2.2), the flow depths d must satisfy : $0 \leq d \leq d_o = H_{dam}*\cos\theta$ where H_{dam} is the vertical reservoir height at gate (e.g. Fig. B-1 and B-5).
Let us define a characteristic flow depth h_c:

$$h_c = \frac{\mu_o * (n - 1)^{1/n}}{\theta * \alpha * \rho * g * S_o} \qquad \text{(B-22)}$$

Basically h_c is a characteristic fluid thickness (Table B-2). For $d < h_c$, λ increases monotically along the forward characteristic until fluid stoppage.
It is now possible to list four flow situations depending upon the initial degree of fluid jamming λ_o and of the ratio d_o/h_c.

(a) For reservoir depths less than the characteristic fluid thickness (i.e. $d_o < h_c$), $d\lambda/dt$ is positive for $t \geq 0$ on each forward characteristic. The degree of jamming of the fluid increases monotically with time along each characteristic until fluid stoppage. The extent of fluid flow is limited and the flow motion is relatively slow until complete stoppage (case a). Note that the result is independent of the initial degree of fluid jamming λ_o. In the (x,t) plane, the forward characteristics form a series of convex curves.

(b) For $d_o = h_c$, and $\lambda_o = \lambda_c$, the first forward characteristic is a straight line and all forward characteristics issued from the initial negative characteristic with $d < h_c$ are convex characteristics. Basically, the degree of jamming of the fluid increases monotically with time along each characteristic, but the first initial forward characteristic, until fluid stoppage (case b1). The extent of

---

$$\lambda_1 \approx \frac{1 + \sqrt{1 - 4 * n * \frac{\mu_o}{\theta * \alpha * \rho * g * d * S_o}}}{2 * n}$$

$$\lambda_2 \approx \left(\frac{\theta * \alpha * \rho * g * d * S_o}{\mu_o}\right)^{1/(n-1)}$$

fluid flow is limited. For $d_o = h_c$, and $\lambda_o \neq \lambda_c$ (case b2), $d\lambda/dt$ is positive for $t \geq 0$. The degree of jamming of the fluid increases monotically with time along each characteristic until fluid stoppage. The extent of fluid flow is limited again. (Cases b2 and a are basically identical.)

(c) For large initial reservoirs (i.e. $d_o > h_c$), the flow behaviour on each forward characteristic is a function of the initial degree of jamming λ_o and of the flow depth d on the characteristic.
(c1) For $\lambda_o > \lambda_2(d_o)$ ([7]), $d\lambda/dt$ is positive everywhere along all forward characteristics and λ increases monotically until complete flow stoppage (case c1). The forward characteristics form a series of convex curves in the (x,t) plane. The extent of flow motion is moderate until fluid stoppage.

(c2) For $\lambda_1 < \lambda_o < \lambda_2(d_o)$ (case c2), $d\lambda/dt$ is negative along the forward characteristics initially. Along a forward characteristic, the fluid flow tends to a constant viscosity behaviour ($\mu = \mu_o*(1+\lambda_1^n)$) with increasing time towards the wave front. The initial characteristics form a series of concave curves which tend to straight lines. That is, the fluid flow tends to a "pseudo-laminar" flow motion towards the wave front.
(c3) Similarly, for $\lambda_o < \lambda_1(d_o)$ (case c3), $d\lambda/dt$ is positive initially although it tends to zero with increasing time. On the initial forward characteristics, the fluid flow tends to a constant viscosity or "pseudo-laminar" motion ($\mu = \mu_o*(1+\lambda_1^n)$) towards with the shock. The forward characteristics form a series of convex curves which tend to straight lines for large times.

Following the initial backward characteristic, the flow depth decreases with increasing time (Fig. B-5). On the initial negative characteristic, the flow depth satisfies $0 < d < h_c$ for $t_c < t < T$ where :

$$t_c = \sqrt{\frac{4 * L}{g * \sin\theta} * \left(1 - \frac{h_c}{d_o}\right)} \qquad \text{(B-23)}$$

and T is the time taken by the initial characteristic C2 to reach the reservoir upstream end (paragraph B1.2). Equation (B-23) derives from the equation of negative wave characteristic (initial backward characteristic) ([8]). On each forward characteristic issued from the initial negative characteristic for $t > t_c$, the flow depth d is less than the characteristic fluid thickness h_c, and $d\lambda/dt$ is positive everywhere along the forward characteristic. The degree of fluid jamming λ increases monotically until complete stoppage. For $d < h_c$, the flow motion is relatively slow and the extent of fluid flow is limited until complete stoppage. The forward characteristics form a series of convex curves in the (x,t) plane (Fig. B-5).
Basically, Cases c2 and c3 tend to similar flow conditions. For each forward characteristic issued from the initial backward characteristic for $t < t_c$, the flow depth on the forward characteristics satisfies : $d > h_c$. That is, the fluid flow tends to a "pseudo-laminar" (or low viscosity) flow motion towards the wave front. Along the other forward characteristics issued from the initial backward characteristic for $t > t_c$, the flow depths satisfy : $d < h_c$. The flow motion is relatively slow and the extent of fluid flow is limited until complete stoppage.

---

[7]The solutions λ_1 and λ_2 of Equation (B-21) are functions of the flow depth d. λ_1 decreases and λ_2 increases with increasing flow depth d.
[8]Note that the equation of the initial backward characteristic is derived from the complete Saint Venant equations, while Equations (B-7) and (B-8) are based upon a kinematic wave approximation of the Saint Venant equations. In the initial instants following gate opening, the kinematic wave approximation is inappropriate, and it becomes correct only once the free-surface is parallel to the channel invert.

(d) For very large initial reservoirs (i.e. $d_o >> h_c$) and initial degree of jamming λ_o such as $\lambda_o << \lambda_2(d_o)$, the fluid flows as a quasi-constant viscosity wave motion (case d). The flow might be laminar or turbulent depending upon the flow Reynolds number. In any case, the flow motion will be relatively rapid and it will stop only when the fluid thickness becomes less than the characteristic fluid thickness h_c.

In summary, several flow regimes may be observed : relatively-rapid flow stoppage (cases a, b and c1), a fast flow motion (case d), or an intermediate motion initially rapid before final stoppage (cases c2 and c3).

Fig. B-5 - Dam break wave of thixotropic fluid down a sloping channel - Sketch of characteristic trajectories for $d_o > h_c$

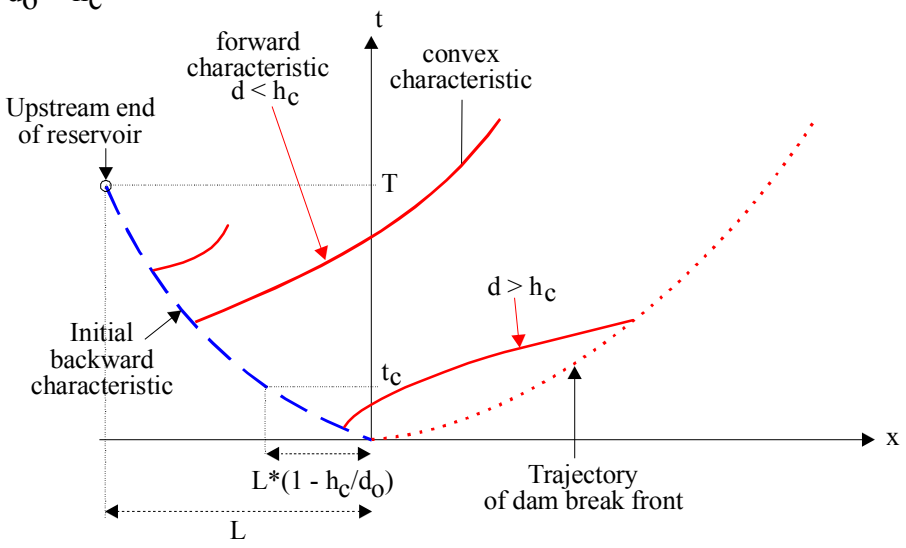

Discussion

In the above development, the equation of the initial backward characteristic is calculated from the complete Saint-Venant equations. But the trajectory of the forward characteristics was derived from a kinematic wave approximation of the same equations that is valid only away from the reservoir (paragraph B.1.1). Therefore, there is some "transition region" in the characteristic diagram (x,t) (e.g. Fig. B-5) between the initial negative characteristic and the start of each forward characteristic.

For very large initial reservoirs (i.e. $d_o >> h_c$) and relatively-fast flow motion (case d), the maximum extent of the wave front may be deduced from the equation of conservation of mass assuming that the final fluid thickness is h_c :

$$\int_{x=-L}^{X_s} h_c * dx = \frac{1}{2} * d_o * L$$

After transformation, it yields :

$$(X_s)_{end} = \frac{1}{2} * \frac{\theta * \alpha * \rho * g * S_o * d_o * L}{\mu_o * (n - 1)^{1/n}} \qquad \text{(B-24)}$$

Note that Equation (B-24) is a crude approximation assuming a two-dimensional flow.

APPENDIX C - THEORETICAL ANALYSIS OF UNSTEADY BOUNDARY LAYER

C.1 ANALYTICAL SOLUTIONS OF THE NAVIER-STOKES EQUATIONS

For a startup flow. The analytical solution of the Navier-Stokes equations for unsteady plane laminar flows is called the first Stokes problem or Rayleigh problem after STOKES (1856) and RAYLEIGH (1911) respectively (SCHLICHTING and GERSTEN 2000, pp. 126-128). In the start-up flow, the velocity is independent of the x co-ordinate in the flow direction and the continuity equation yields $V_y = 0$. For a laminar flow, the Navier-Stokes equations become :

$$\rho * \frac{\partial V_x}{\partial t} = - \rho * g * \frac{\partial z}{\partial x} - \frac{\partial P}{\partial x} + \mu * \frac{\partial^2 V_x}{\partial y^2} \quad \text{(C-1a)}$$

$$0 = - \rho * g * \frac{\partial z}{\partial y} - \frac{\partial P}{\partial y} \quad \text{(C-1b)}$$

where ρ and μ are the fluid density and dynamic viscosity respectively, z is the vertical elevation and P is the pressure. For a horizontal flow, the gravity force component in the flow direction is zero. The Navier Stokes equations yield :

$$\frac{\partial V_x}{\partial t} = \nu * \frac{\partial^2 V_x}{\partial y^2} \quad \text{(C-2)}$$

where ν is the kinematic viscosity. Equation (C-2) is similar to a diffusion equation and a heat conduction equation. Mathematical solutions of diffusion and heat equations were addressed in two classical references (CARSLAW and JAEGER 1959, CRANK 1956).

For an advancing surge flow, the boundary conditions are : $V_x = U$ for $y \geq 0$ and $t \leq 0$, and $V_x(y=0) = 0$ and $V_x(y \rightarrow +\infty) = U$ for $t > 0$. The analytical solution of Equation (C-2) is :

$$\frac{V_x}{U} = \text{erf}\left(\frac{y}{2 * \sqrt{\nu * t}}\right) \quad \text{(C-3)}$$

where y is the distance normal to the invert and the function erf is the Gaussian error function defined as :

$$\text{erf}(u) = \frac{2}{\sqrt{\pi}} * \int_0^u \exp(- v^2) * dv \quad \text{(C-4)}$$

The reasoning may be extended to unsteady turbulent boundary layer flow with constant momentum exchange coefficient (or "eddy viscosity") ν_T. The analytical solution of the Navier-Stokes equations becomes :

$$\frac{V_x}{U} = \text{erf}\left(\frac{y}{2 * \sqrt{\nu_T * t}}\right) \quad \text{(C-5)}$$

Equation (C-5) was successfully applied to turbulent flows in wave runup and dam break wave (MANO 1984, CHANSON 2004c).

Fig. C-1 - Sketch of velocity distribution in a startup flow

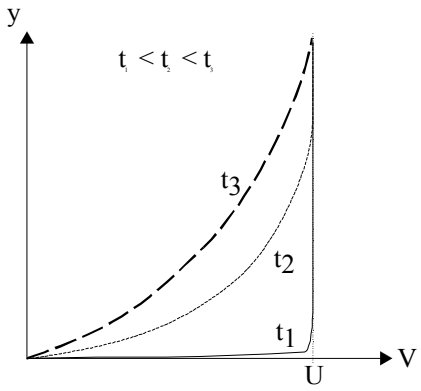

Discussion: Application to a sloping channel

In the start-up flow down a sloping channel with slope θ_b constant, the gravity force component in the flow direction is a constant. In first approximation, the Navier-Stokes equations for the first Stokes problem become :

$$\rho * \frac{\partial V_x}{\partial t} = - \rho * g * \sin\theta_b - \frac{\partial P}{\partial x} + \mu * \frac{\partial^2 V_x}{\partial y^2} \qquad \text{(C-6a)}$$

$$0 = - \rho * g * \cos\theta_b - \frac{\partial P}{\partial y} \qquad \text{(C-6b)}$$

where ρ and μ are the fluid density and dynamic viscosity respectively, z is the vertical elevation and P is the pressure. The Navier Stokes equations yield :

$$\frac{\partial V_x}{\partial t} = \nu * \frac{\partial^2 V_x}{\partial y^2} + g * \sin\theta_b \qquad \text{(C-7)}$$

where ν is the kinematic viscosity. In Equation (C-7), the gravity force component is a source term added to the diffusion equation. Note that Equation (C-7) assumes that both velocity and pressure independent of the x-coordinate (i.e. flow direction).

C.2 APPLICATION TO THIXOTROPIC FLUID ON A HORIZONTAL CHANNEL

For a thixotropic fluid, the rheological equation of COUSSOT et al. (2002a) are :

$$\tau = \mu * \frac{\partial V}{\partial y} \qquad \text{(C-8)}$$

$$\mu = \mu_o * (1 + \lambda^n) \qquad \text{(C-9)}$$

$$\frac{d\lambda}{dt} = \frac{1}{\theta} - \alpha * \frac{\partial V}{\partial y} * \lambda \qquad \text{(C-10)}$$

where the local velocity V and the local degree of jamming of the fluid λ are both functions of y and t. The Navier Stokes equations yield :

$$\frac{\partial V}{\partial t} = \frac{\mu_o}{\rho} * (1 + \lambda^n) * \frac{\partial^2 V}{\partial y^2} \qquad \text{(C-11)}$$

For an advancing surge flow, the boundary conditions are :

$V = U$ for $y \geq 0$ and $t \leq 0$

$V(y=0) = 0$ and $V_x(y \rightarrow +\infty) = U$ for $t > 0$

$\lambda = \lambda_o$ for $y \geq 0$ and $t \leq 0$

Equations (C-10) and (C-11) form a non-linear system of two differential equations with two unknowns V and λ. It may be solved numerically.

Discussion

At startup at t = 0+ and at the boundary (y = 0), the shear rate is infinite and the degree of fluid jamming must be zero :

$\lambda = 0$ for $y = 0$ and $t = 0+$

The time scale of a startup flow may be assumed small compared to the characteristic restructuring time θ. This implies that, during startup, the vertical distribution of fluid viscosity varies from μ_o at the boundary to $\mu_o*(1+\lambda_o^n)$ far away from the boundary.

If the fluid is initially destructured everywhere ($\lambda_o = 0$), the analytical solution of the Navier-Stokes equations is :

$$\frac{V}{U} = \text{erf}\left(\frac{y}{2 * \sqrt{\frac{\mu_o}{\rho} * t}}\right) \quad \text{for } \lambda_o = 0$$

assuming small variations of U and λ during the study period t.

APPENDIX D - FREE-SURFACE MEASUREMENTS AFTER FLUID STOPPAGE

Free-surface elevations were measured after fluid stoppage using the CCD camera at the intersection of a series of laser beams (He/Ne 10mW) with the free-surface (Fig. D-1). The camera recorded 256 grey levels at high resolution (1024*1280 pixels), and the data were analysed using a Mourier projection method. Detailed free-surface profiles were deduced from the deformation of the laser grid illumination (Fig. D-2).

For all experiments, the results showed consistently very little transverse variations of the final fluid thickness.Typical results are presented in Table D-1 showing the transverse average fluid thickness at each laser grid line and the standard deviation of the fluid thickness (after stoppage) across each line. Note that the results are transverse averages along the width of the laser grid lines only.

Fig. D-1 - Photograph of the grid laser illuminations in the dry channel

Fig. D-2 - Photographs of grid laser illuminations after fluid stoppage
(A) Test 02 (θ_b = 15º, C_m = 15%, T_o = 60 s, M = 3.5 kg, Flow Type II)

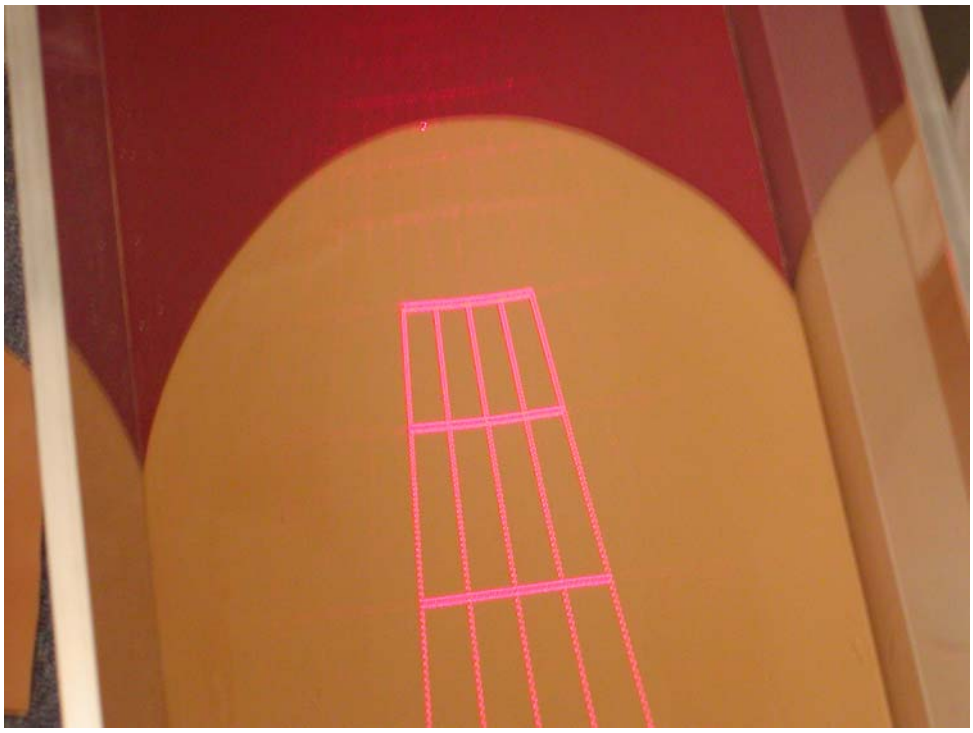

(B) Test 14 (θ_b = 15º, C_m = 17%, T_o = 60 s, M = 3.7 kg, Flow Type II)

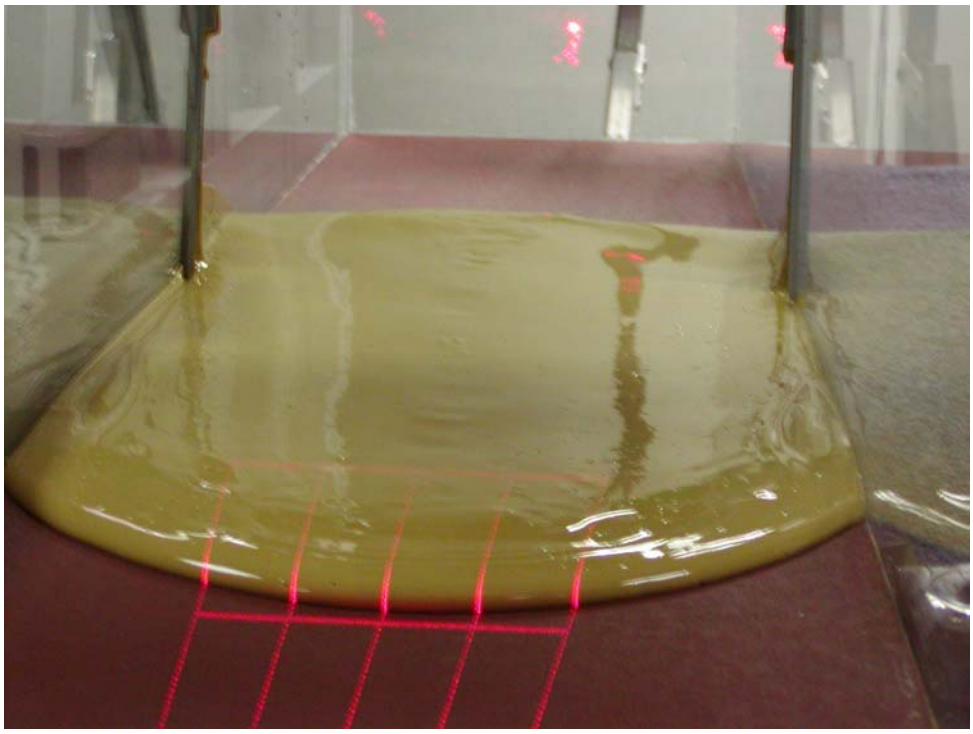

Table D-1 - Experimental results of final fluid thickness after complete stoppage

Run	C_m	M	T	$(X_s)_{end}$	d_o	Flow Type	x	Mean (d)	Std (d)	Remarks
		kg	s		m		m	mm	mm	
(1)	(2)	(3)	(4)	(5)	(6)	(7)	(8)	(9)	(10)	(11)
Test 02	0.15	3.504	60	1.007	0.0709	II	0.29	4.83	0.052	
							0.541	6.57	9.3E-8	
							0.691	7.45	0	
Test 04	0.15	3.141	60	0.72	0.0671	II	0.29	6.04	0.181	
							0.541	8.64	0.196	
Test 05	0.15	3.707	60	0.958	0.0729	II	0.29	5.47	0.286	
							0.541	6.96	0.143	
							0.69	7.69	0.220	
Test 06	0.15	3.686	300	0.7535	0.0727	II	0.29	6.99	0.273	2 first laser lines.
							0.541	9.65	0.221	
Test 07	0.15	3.652	900	0.51	0.0723	II-III	0.29	8.03	0.349	1st laser line only.
Test 09	0.1	4.059	300	Overflow	0.0776	I	0.29	--	--	2 last laser lines.
							0.54	1.12	0.219	
							0.6905	1.30	0.066	
Test 11	0.1	1.505	300	Overflow	0.0472	II	0.29	0.876	2E-08	
							0.54	0.984	0.190	
							0.6905	1.314	0	
Test 18	0.13	3.952	300	Overflow	0.0758	II	0.29	2.924	0.2074	
							0.54	3.504	0	
							0.6905	3.504	0	
Test 19	0.13	3.936	900	Overflow	0.0756	II	0.29	3.07	0	
							0.54	3.89	0.146	
							0.6905	3.94	7.3E-8	
Test 21	0.13	3.718	2400	1.204	0.0735	II	0.285	--	--	2 last laser lines.
							0.536	5.26	0	
							0.687	5.70	0	
Test 22	0.13	3.72	7200	1.089	0.0735	III	0.285	3.96	0.217	
							0.536	4.32	0.270	
							0.687	5.49	0.241	
Test 23	0.13	3.69	60	Overflow	0.0732	I	0.285	3.51	0	
							0.536	3.96	0.082	
							0.687	4.09	0.209	
Test 24	0.13	2.728	60	1.215	0.0629	II	0.285	3.51	0	
							0.536	4.30	0.176	
							0.687	4.38	1.3E-7	
Test 25	0.13	1.614	60	0.643	0.0484	II	0.285	3.84	0.186	2 first laser lines.
							0.536	4.82	0	

Notes : Mean(d) : average fluid thickness across the laserline; Overflow: fluid spill at downstream end of plate; Std(d) : standard deviation of the fluid thickness across the laserline.

REFERENCES

BESQ, A. (2000). "Ecoulement Laminaire de Suspensions de Bentonites Industrielles. Caractérisation Rhéométrique. Ecoulements en Conduites Axisymmétriques. Applications aux Activités du Génie Civil." *Ph.D. thesis*, University of Poitiers, France, 224 pages.

CHANSON, H. (2004a). "The Hydraulics of Open Channel Flows : An Introduction." *Butterworth-Heinemann*, Oxford, UK, 2nd edition (ISBN 0 7506 5978 5).

CHANSON, H. (2004b). "Environmental Hydraulics of Open Channel Flows." *Elsevier*, Oxford, UK (ISBN 0 7506 6165 8).

CHANSON, H. (2004c). "Unsteady Two-Phase Flow Measurements in Surges and Dam Break Waves." *Proc. 5th Intl Conf. on Multiphase Flow*, Yokohama, Japan, Paper 103, 14 pages.

COUSSOT, P. (1997). "Mudflow Rheology and Dynamics." *IAHR Monograph*, Balkema, The Netherlands.

COUSSOT, P., NGUYEN, A.D., HUYNH, H.T., and BONN, D. (2002a). "Avalanche Behavior in Yield Stress Fluids." *Physics Review Letters*, Vol. 88, p. 175501

COUSSOT, P., NGUYEN, A.D., HUYNH, H.T., and BONN, D. (2002b). "Viscosity Bifurcation in Thixotropic, Yielding Fluids." *Jl of Rheology*, Vol. 46, pp. 573-589.

ESCANDE, L., NOUGARO, J., CASTEX, L., and BARTHET, H. (1961). "Influence de Quelques Paramètres sur une Onde de Crue Subite à l'Aval d'un Barrage." ('The Influence of certain Parameters on a Sudden Flood Wave Downstream from a Dam.') *Jl La Houille Blanche*, No. 5, pp. 565-575.

FAURE, J., and NAHAS, N. (1961). "Etude Numérique et Expérimentale d'Intumescences à Forte Courbure du Front." ('A Numerical and Experimental Study of Steep-Fronted Solitary Waves.') *Jl La Houille Blanche*, No. 5, pp. 576-586. Discussion: No. 5, p. 587.

FERROIR, T., HUYNH, H.T., CHATEAU, X., and COUSSOT, P. (2004). "Motion of a Solid Object Through Pasty (Thixotropic) Fluid." *Physics of Fluids*, Vol. 16, No. 3, pp. 594-601.

HENDERSON, F.M. (1966). "Open Channel Flow." *MacMillan Company*, New York, USA.

HUANG, X., and GARCIA, M. (1998). "A Herschel-Bulkley Model for Mud Flow Down a Slope." *Jl of Fluid Mech.*, Vo. 374, pp. 305-333.

HUNT, B. (1982). "Asymptotic Solution for Dam-Break Problems." *Jl of Hyd. Div.*, Proceedings, ASCE, Vol. 108, No. HY1, pp. 115-126.

HUNT, B. (1984). "Perturbation Solution for Dam Break Floods." *Jl of Hyd. Engrg.*, ASCE, Vol. 110, No. 8, pp. 1058-1071.

HUNT, B. (1988). "An Asymptotic Solution for Dam Break Floods in Sloping Channels." in "Civil Engineering Practice", *Technomic Publ.*, Editors P.N. CHEREMISINOFF, N.P. CHEREMISINOFF and S.L. CHENG, Lancaster Pen., USA, Lancaster, USA, Vol. 2, Section 1, Chapter 1, pp. 3-11.

HUNT, B. (1994). "Newtonian Fluid Mechanics Treatment of Debris Flows and Avalanches." *Jl of Hyd. Engrg.*, ASCE, Vol. 120, No. 12, pp. 1350-1363.

HUYNH, H.T., BONN, D., and COUSSOT, P. (2001). "Caratérisation de la Thixotropie de Fluides Pâteux." ('Thixotropic Characteristics of Pastes.') *Proc. 36th Colloque Annuel du Groupe Français de Rhéologie GFR*, Marne-la-Vallée, France, pp. 72-77.

IPPEN, A.T., and HARLEMAN, R.F. (1956). "Verification of Theory for Oblique Standing Waves." *Transactions*, ASCE, Vol. 121, pp. 678-694.

JULIEN, P.Y. (1995). "Erosion and Sedimentation." *Cambridge University Press*, Cambridge, UK, 280 pages.

LAUBER, G. (1997). "Experimente zur Talsperrenbruchwelle im glatten geneigten Rechteckkanal." ('Dam Break Wave Experiments in Rectangular Channels.') *Ph.D. thesis*, VAW-ETH, Zürich, Switzerland (in German). (also *Mitteilungen der Versuchsanstalt fur Wasserbau, Hydrologie und Glaziologie*, ETH-Zurich, Switzerland, No. 152).

LEAL, J.G.A.B., FERREIRA, R.M.L., FRANCO, A.B., and CARDOSO, A.H. (2001). "Dam-Break Waves over Movable Bed Channels. Experimental Study." *Proc. 29th IAHR Congress*, Beijing, China, Theme C, Tsinghua University Press, Beijing, G. LI Ed., pp. 232-239.
MANO, A. (1994). "Boundary Layer Developed near Surging Front." *Coastal Engineering in Japan*, Vol. 37, No. 1, pp. 23-39.
MEWIS, J. (1979). "Thixotropy - A General Review." *Jl of Non-Newtonian Fluid Mech.*, Vol. 6, p. 1.
MONTES, J.S. (1998). "Hydraulics of Open Channel Flow." *ASCE Press*, New-York, USA, 697 pages.
RAYLEIGH, Lord (1911). "On the Motion of Solid Bodies through Viscous Liquids." *Phil.. Mag.*, Vol. 21, pp. 697-711.
RITTER, A. (1892). "Die Fortpflanzung der Wasserwellen." *Vereine Deutscher Ingenieure Zeitswchrift*, Vol. 36, No. 2, 33, 13 Aug., pp. 947-954 (in German).
ROUSSEL, N., LE ROY, R., and COUSSOT, P. (2004). "Thixotropy Modelling at Local and Macroscopic Scales." *Jl of Non-Newtonian Fluid Mech.*, Vol. 117, No. 2-3, pp. 85-95.
SCHLICHTING, H., and GERSTEN, K. (2000). "Boundary Layer Theory." *Springer Verlag*, Berlin, Germany, 8th edition., 707 pages.
SCHOKLITSCH, A. (1917). Über Dambruchwellen." *Sitzungberichten der Königliche Akademie der Wissenschaften, Vienna*, Vol. 126, Part IIa, pp. 1489-1514.
STOKES, G.G. (1856). "On the Effect of Internal Friction of Fluids on the Motion of Pendulums." *Trans. Camb. Phil. Soc.*, Vol. 9, Part II, pp. 8-106.
TABUTEAU, H., BAUDEZ, J.C., BERTRAND, F., and COUSSOT, P. (2004). "Mechanical Characteristics and Origin of Wall Slip in Pasty Biosolids." *Rheol. Acta*, Vol. 43, pp. 168-174.
TOORMAN, E.A. (1997). "Modelling the Thixotropic Behavior of Dense Cohesive Sediment Suspensions." *Rheol. Acta*, Vol. 36, p. 56.
USUI, H. (1995). "A Thixotropy Model for Coal-Water Mixtures." *Jl of Non-Newtonian Fluid Mech.*, Vol. 60, p. 259.
WAN, Zhaohui, and WANG, Zhaoyin (1994). "Hyperconcentrated Flow." *Balkema*, IAHR Monograph, Rotterdam, The Netherlands, 290 pages.
WILSON, S.D.R., and BURGESS, S.L. (1998). "The Steady, Speading Flow of a Rivulat of Mud." *Jl Non-Newtonian Fluid Mech.*, Vol. 79, pp. 77-85.

INTERNET REFERENCES

URL	Description
{http://images.usace.army.mil/advsearch.html} Seach for [Project/Title] Mt St Helen, Mt Pinatubo	Photographs of Mt St Helen debris and mud flows
{http://www.uq.edu.au/~e2hchans/photo.html - Check_dams}	Photographs of check dams and debrid dams
{http://www.uq.edu.au/~e2hchans/sabo.html}	Sabo check dams in Japan
{http://www.hrr.mlit.go.jp/yuzawa/gaiyou/english/gaiyou.htm}	Yuzawa Sabo works office

BIBLIOGRAPHIC REFERENCE OF THE REPORT CH54/04

The Hydraulic Model research report series CH is a refereed publication published by the Department of Civil Engineering at the University of Queensland, Brisbane, Australia.

The bibliographic reference of the present report is :

CHANSON, H., COUSSOT, P., JARNY, S., and TOQUER, L. (2004). "A Study of Dam Break Wave of Thixotropic Fluid: Bentonite Surges down an Inclined plane." *Report No. CH54/04*, Dept. of Civil Engineering, The University of Queensland, Brisbane, Australia, June (ISBN 1864997710).

The Report CH54/04 is available, in the present form, as a series of .PDF files on the Internet at the following address :

http://www.uq.edu.au/~e2hchans/reprints/ch5404.zip

The .zip file contains the following files :

0_lcpc04.pdf	Title page, abstract, table of contents, list of symbols, contributors' biography
1_lcpc04.pdf	Chap. 1. Introduction Chap. 2. Theoretical analysis (1) Dam break wave Chap. 3. Theoretical analysis (1) Unsteady boundary layer Chap. 4. Experimental facilities Chap. 5. Basic flow patterns Chap. 6. Experimental results Chap. 7. Unusual flow patterns and instabilities Chap. 8. Summary and conclusion Acknowledgments
a_lcpc04.pdf	Appendices. App. A - Dam break wave in a horizontal initially-dry channel App. B - Application of the method of characteristics to dam break wave of thixotropic fluid App. C - Theoretical analysis of unsteady boundary layer App. D - Free-surface measurements after fluid stoppage
referenc.pdf	References Internet references Bibliographic reference of the Report CH54/04